Towards a Gigabit-Class Visible Light Communication

by
Muhammad Towfiqur Rahman

SUBMITTED IN TOTAL FULFILMENT OF THE REQUIREMENTS FOR THE DEGREE OF

DOCTOR OF PHILOSOPHY

Electrical and Computer System Engineering
School of Engineering
Monash University
2021

Copyright notice

ABSTRACT

Visible Light Communication (VLC) has become a viable option for optical wireless communication. Light emitting diode (LED) is one of the possible sources in VLC to be used as transmitter, because it can provide white light for illumination and simultaneously be used for high speed data communication. Potential applications of VLC system are vehicle to vehicle communication, robot communication in hospitals, Internet of Things (IoT) applications, underwater communication, information display on signboards and indoor communication. Present researchers are investigating the possibility of increasing the data rate of VLC system to integrate with 5G network. There are some techniques to increase the data rate of VLC system, such as utilizing wavelength Division Multiplexing (WDM), high order modulation schemes, MultiInput Multi Output (MIMO)-OFDM modulation, special pre and post equalization schemes and µLED arrays. The aim of this research is to investigate and develop methods to achieve gigabit class VLC. Initially, WDM system has designed and experimentally verified with different modulation scheme using Red, Green, Blue, Yellow (RGBY) LED. NRZ-OOK and 16 QAM based WDM-VLC system was simulated and experimentally demonstrated, which could operate at a maximum speed of 260 Mb/s using OOK and 1.04 Gb/s using 16QAM in the experiment. In contrast, a simulation model was designed to validate the experimental results and maximum data rate achieved 290 Mb/s by OOK and 1.16 Gb/s by 16 QAM. We proposed for the first time coarse wavelength division multiplexing (CWDM)-visible-light communication (VLC) system (channel spacing of 20 nm or 2.5THz within 400 nm visible range) to increase the number of channels for high speed VLC and explored the possibility of using narrow band LEDs with 7.85 GHz modulation bandwidth in CWDM-VLC grid. Therefore, InGaN/GaN-based multiple quantum well (MQW) LEDs coupled with and without nano-lens structure was designed and investigated all of its optical properties to fit for the CWDM grid using its fixed HWHM. In this simulation, the achievable modulation bandwidth is up to 7.85 GHz for 510nm and this concept extends to 530nm and 550nm LEDs to establish the general method for implementing CWDM-VLC. Finally, we developed a hybrid Radio over VLC (RoF-VLC) communication model combined with 5G-mmWave and CWDM-VLC for multi user gigabit class transmission in simulation environment. This model can help to implement 5G mmWave-RoF backhaul in hybrid VLC network to improve its uplink data rate. Maximum data rate 2.64 Gb/s and 6.58 Gb/s by 10 and 20 channels off the shelf LED using 16 QAM and VLC uplink data rate 2.5 Gb/s fully recovered at CO through mmW based RoF backhaul successfully. For reducing uplink complexity of indoor VLC system, this mmW used to achieve high-speed full-duplex communication and which makes more compatible to each other in 5G network deployments.

This thesis is an original work of my research and contains no material which has been accepted for the award of any other degree or diploma at any university or equivalent institution and that, to the best of my knowledge and belief, this thesis contains no material previously published or written by another person, except where due reference is made in the text of the thesis.

Signature: ……………………

Print Name: ……Muhammad Towfiqur Rahman

Date: …………16/03/2021

Acknoledgements

First and foremost, I would like to thank my mother, for her unconditional love, countless sacrifices and unremitting motivation. I would like to express my sincere gratitude and respect to my supervisor Professor Rajendran Parthiban and Dr. Masuduzzaman Bakaul for offering their valuable time and knowledge. Without their help it is really impossible for me to submit this thesis. Especially I am grateful to Dr. Vineetha Kalavally, for her insightful feedback and support. I would like to pay my thanks to the ECSE Department and laboratory staff - Hasnan, Suresh, Manan and Rozidah for their hardware assistance. Thanks all of my friends and colleagues from Monash, it would have been difficult without you all. Some persons, who collaborated with me, specially Prem kumar, Dr Baki Billah, Dr Afzal Hoq, your efforts and support had helped me in understanding as much as I have taught.

Finally, I wish to express my love and gratitude to my beloved family members, my sisters, brothers, and uncle especially brother in law for their understanding, continuous encourage and support me throughout the study periods. Besides, I would like to acknowledge people in Post Graduate office and Monash research centre who have helped and encourage me a lot during the period of my studies. Their encouragement and support have helped me a lot in increasing my self-confidence and all sort of challenge I encountered seemed bearable.

Last, but not the least, I would like to thank my better half, Tahera Sultana, for her endless encouragement, relentless support and continual tolerance of me and my kids; thank you for coming to my life.

Contents

Chapter One : Introduction

Chapter Two : Techniques to achieve hi-data rate VLC

Chapter Seven : Conclusion

List of Figures

List of Tables

Acronyms

ANSI	American National Standards Institute
ANN	Artificial neural network
APD	Avalanche Photodiode
AWG	Arbitrary Waveform Generator
ACO-OFDM	Asymmetrically Clipped Optical Orthogonal Frequency Division Multiplexing
AOI	Angle of Incidence
BER	Bit Error Rate
CAP	Carrier less amplitude and phase
CCR	Constant Current Reduction
CCT	Correlated Color Temperature
CDMA	Code division multiple access
CFL	Compact Fluorescent Lamp
CIE	International Commission on Illumination
CMOS	Complementary Metal Oxide Semiconductor
CMMA	Cascade multi-mode algorithm
CPFM	Constant Pulse Frequency Modulation
CP	Cyclic Prefix
CO	Central office
CRI	Color Rendering Index
CSK	Color Shift Keying
CT	Color Temperature
CU	Customer unit
CWDM	Course Wavelength Division Multiplexing
DCO-OFDM	DC Offset Orthogonal Frequency Division Multiplexing
DMT	Discrete Multi-Tone
DSL	Digital Subscriber Line

DC	Direct Current
DD	Direct Detection
DFE	Discreet Feedback Equalization
DWDM	Dense Wavelength Division Multiplexing
EM	Electro Magnetic
EMI	Electromagnetic Interference
E-O-E	Electrical Optical Electrical
HB-LED	High Brightness Light Emitting Diode
FDTD	Finite-difference time-domain
FWHM	Full width half maximum
FEC	Forward Error Correction
FM	Frequency Modulation
GaN	Gallium Nitride
ICI	Inter-carrier interference
IEEE	Institute of Electrical and Electronics Engineers
IM	Intensity Modulation
InGaN	Indium Gallium Nitride
IoT	Internet of Things
IR	Infra-Red
IrDA	Infra-Red Data Association
ISI	Inter Symbol Interference
IFFT	Inverse Fast Fourier Transform
ITU	International Telecommunications Union
ITS	Intelligent transport system
JEITA	Japan Electronics and Information Technology Industries Association
LD	Laser Diode
LD-VLC	LD-based VLC Li-Fi Light Fidelity
LED	Light Emitting Diode
LEE	Light extraction efficiency
LPF	Low pass filter
LMS	Least Mean Squares
LOS	Line of Sight

LVI	Luminous Flux - Forward Voltage - Forward Current
MATLAB	Matrix Laboratory
µ-LED	Micro Light Emitting Diode
MQW	Multiple quantum well
MIMO	Multiple Input Multiple Output
NLOS	Non Line of Sight
NRZ-OOK	Non-Return to Zero On-Off-Keying
OBPF	Optical band pass filter
OFDM	Orthogonal Frequency Division Multiplexing
OF	Optical fiber
OLED	Organic Light Emitting Diodes
OOK	On-Off Keying
OWC	Optical Wireless Communication
PAM	Pulse Amplitude Modulation
PAPR	Peak to Average Power Ratio
Pc-LED	Phosphor Converted Light Emitting Diode
PD	Photo Diode
PML	Perfectly matched layer
POF	Plastic Optical Fiber
PON	Passive optical network
PPM	Pulse Position Modulation
PSD	Power Spectral Density
PS	Phase-shifted
PSK	Phase Shift Keying
PWM	Pulse Width Modulation
QAM	Quadrature Amplitude Modulation
QD-LD	Quantum dash-laser diode
QCSE	Quantum confined stark effect
RAGB	Red, Amber, Green, Blue
RC-LED	Resonant Cavity Light Emitting Diode
RCWA	Rigorous coupled-wave analysis
RF	Radio Frequency

RGB	Red, Green, Blue
RoF	Radio over fiber
RPO-OFDM	Reverse Polarity OFDM
RRGBY	Red, Red, Green, Blue, Yellow
SDVLC	Software Defined Visble Light Communication
SER	Symbol error rate
SCFDE	Single-carrier frequency-domain equalisation
SLM	Spatial Light Modulator
SNR	Signal to Noise Ratio
SPD	Spectral Power Density
SSL	Solid State Lighting
TEC	Thermoelectric Cooler
TIA	Trans Impedance Amplifier
TE	Transverse Electric
TM	Transverse Magnetic
U-OFDM	Unipolar OFDM
UV	Ultra Violet
VAP	VLC access point
VLC	Visible Light Communication
VLCC	Visible Light Communications Consortium
VLP	Visible light positioning
VPPM	Variable Pulse Position Modulation
WDM	Wavelength Division Multiplexing
W-FOV	Wide Field of View

CHAPTER ONE

INTRODUCTION

1.1 Introduction

Visible Light Communication (VLC) has become a viable option for optical wireless communication after the first time introduced in 1999. Light Emitting Diode (LED) is one of the possible sources in VLC to be used as a transmitter because it can provide white light for illumination and simultaneously be used for high-speed data communication. Recently, there is an increased interest in the LED-based VLC system due to the energy efficiency and durability of LEDs, and high security and high modulation bandwidth provided by VLC systems (Rajbhandari et al., 2017). A VLC system is enabled by modulating LEDs and transmitting the signal through the visible light frequency range. At the receiver, the data is recovered by photodiodes (PDs). The VLC system's potential applications are vehicle to vehicle communication, robot communication in hospitals, Internet of Things (IoT) applications, underwater communication, information display on signboards and indoor communication.

Researchers are investigating the possibility of increasing the data rate of VLC to 10 Gb/s or beyond to integrate this with 5G network. There are some techniques to increase the data rate of the VLC system such as utilizing wavelength division multiplexing (WDM), high order modulation schemes, multiple-input multiple-output (MIMO) modulation, special pre and post equalization schemes, and µLED arrays. The aim of this research is to investigate and develop methods to achieve gigabit-class VLC

1.2 Evaluation of Visible Light Communication

Rapid development of fibers based optical communication has started in the early 1970 and high-speed semiconductor lasers and Light Emitting Diodes (LED) based VLC introduced after two decades in 1999 (Rajbhandari et al., 2017). The optical fiber came to replace the present copper wires and changed the concept of data communication using the speed of light. With the increasing demand of optical fiber, the research is ongoing to increase the data rate and the new transmission concept, the wavelength division multiplexing (WDM) technique, has been introduced. To compete with the fiber-based communication structure, the wireless communications system (RF) is upgrading itself to represent user-friendly, high-speed communication technology. The next step revolution came in the middle of the 90s when Nakamura et al. (Nakamura et al., 1994) produced high brightness blue LED for the first time. In the following years, phosphor-coated blue LED was introduced to convert the blue spectrum to the longer visible wavelengths as white light. After that, the LED revolt influenced the whole lighting industry worldwide and took over exiting the business opportunity of incandescent and fluorescent lamps (Dhoble & Nair, 2020). The LED modulates the light intensity based on the electric signal amplitude level determined by the bias tee. The transmitted light signal from LED propagate in the visible light free space channel, and it is received by a suitable photo receiver known as photodiode (PD). Optical color filters, lenses and amplifiers are used to improve the signal quality when it strikes the PD, which converts the light signal to an electric signal. Lastly, the demodulation of the received signal or offline process is performed to extract the actual transmitted data bit. For the first time white LED-based VLC was introduced to transfer audio data through LEDs by Pang et al. (Pang et al., 2002).

More recently, due to single-channel LED's fundamental limitations, Multiple Input Multiple Output (MIMO) and Wavelength Division Multiplexing (WDM) system have been introduced. These technologies mostly use in Radio Frequency (RF) communication and Optical Fiber (OF) communication, and now use into VLC. MIMO systems in VLC employ several LEDs as transmitters where each LED transmits independent information, while an array of receivers are used to de-correlate and isolate individual transmitters (C.-Y. Chen et al., 2013). WDM systems typically employ red, green and blue LEDs, which appears white if each individual average intensity is controlled appropriately. Up to date, the highest data rates in VLC have been demonstrated using WDM systems, with data rates exceeding 15.73 Gb/s reported (Bian et al., 2019). Early VLC systems typically employed simple single carrier modulation schemes such as On-Off Keying (OOK) or Pulse Position

Modulation (PPM), which allow for limited system capacity due to low spectral efficiency. Orthogonal Frequency Division Multiplexing (OFDM) has been shown to have high spectral efficiency due to orthogonal subcarrier spacing in the frequency domain (Zhou et al., 2019).

Li-Fi was the best invention by the Time Magazine in 2011 introduced by Harold Haas at a TED Talk event (BBC, 2015). In 2015, Li-Fi enabled light bulb, which was claimed that it could transmit 100 times faster data than the traditional wireless fidelity (Wi-Fi). The fundamental aspects of Li-Fi technology are built around VLC by considering link-level algorithms, networking protocols, and data security (Haas et al., 2016). At present, VLC has become one of the most important communication media in optical wireless communication due to its high bandwidth capacity. Moreover, as a common transmitter of VLC, LEDs are used for data communication regardless of illumination. With the increasing demand for VLC applications, such as LiFi (light fidelity), robotics, intelligent lighting system, intelligent transport system (ITS), visible light positioning (VLP), vehicle to vehicle and underwater communication, the demand of data rate has also increased up to gigabit range (Lifi Application, 2020).

The development of wireless communication networks began in early 1970, and within the last 30 years,' technologies have changed the total communication strategy in every aspect of human life. The progression of wireless technology started from first-generation (1G) systems based on analog frequency modulation and mostly operated in the 450 MHz frequency band. The second-generation (2G) systems were based on digital modulation and mainly used for voice transfer over cellular phones. In 2005, the third-generation (3G) system based on wideband CDMA facilitated transferring more text, high-quality images, and videos, and operated in 900 MHz and 1800 MHz frequency bands (Hanzo et al., 2012). The maximum data rate of that system was 2 Megabits per second (Mbps). For better speed, fourth-generation (4G) wireless technology was introduced after 2010, transmitting data from 100 Mb/s up to 1 Gb/s (S. Chen et al., 2014). The latest version of 4G technology is called 4G Long Term Evolution (LTE) approved by the International Telecommunications Union (ITU). Finally, 5G experimentally implemented in 2020, and the data rate from 1 Gb/s up to 10 Gb/s with its high-frequency signal (Jastrow et al., 2008). Although there has been progress in the Gigahertz frequency range (between RF and microwave spectrum) for outdoor application, with new 5G infrastructure, visible light come to the stage with 10,000 times larger unregulated spectrum (~ 400 THz) mostly for indoor application as represented in Figure 1.1 and without additional cost (O'Brien et al., 2008).

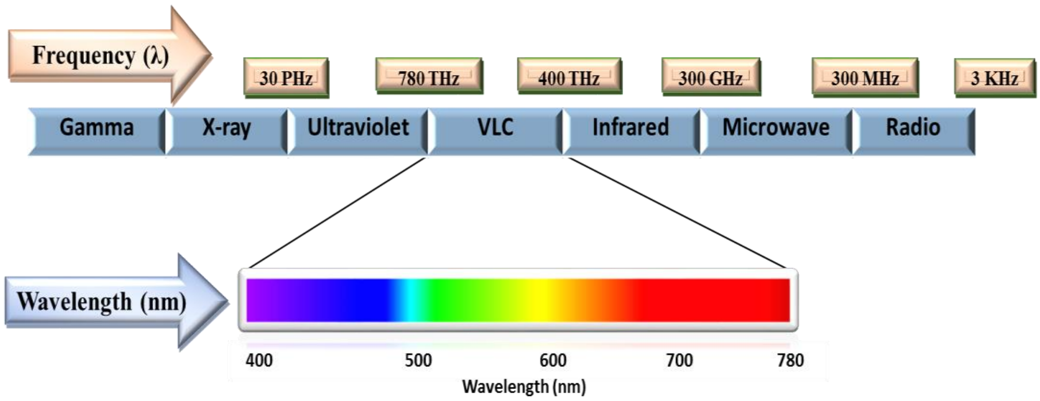

Figure 1.1: Full electromagnetic spectrum

The early research efforts on the LED-based VLC system actuated from Keio University, Japan. They proposed white LED as a transmitter for home access network at Visible Light Communications Consortium (VLCC) in 2003 (O'Brien et al., 2008). In 2009, the home Gigabit Access project (OMEGA) was started by the EU (Rahman et al., 2020). They established visible light communication, which was more secured and enhanced compared to RF communication network. Over 20 European countries also started a research project regarding optical wireless communication named 'OPTICWISE' in 2015 (O. research Group, 2019). A research group of King Abdullah University and Technology (KAUST) Saudi Arabia is working to improve transmitter capacity, such as high-speed super luminescent diode with a high bandwidth (807 MHz (Alatawi et al., 2018) for gigabit-class VLC. They demonstrated an optical receiver device, such as 15 pairs of InGaN/GaN MQW based micro photodetector (PD), to achieve a 3.2 Gb/s VLC link (Ho et al., 2018).

Professor Nan Chi (and her group) from Fudan University is working to transmit multi-Gigabit data per LED light and to overcome the technical difficulties of VLC optical receivers (Tanaka et al., 2000). Sant'Anna School and TCI LED professionals demonstrated object detection system at the "LIGHT & Building 2018" event in Germany. Istituto TeCIP (in Italy) established 3.4 Gb/s VLC link with the RGB LED. They developed a communication system for an outdoor environment using an optical wireless link for integrated VLC applications (Tanaka et al., 2000). Oxford University has comprehensive research background on multi-Gb/s VLC systems, including hybrid equalization method for modulated optical sources, LD-based VLC link, VLC receiver for IoT applications, and GaN-based micro-LED fabrication (Chun et al., 2016). Prof. Harald Haas (PureLiFi's CSO) established a LiFi center at the University of Edinburgh and is working on high-speed bidirectional VLC link (C. Chen et al., 2019), LiFi mobility (Xiping Wu & Haas, 2019), Spatial Modulation (Yesilkaya et al., 2019), micro-LED and improvement for optical wireless networks. Furthermore, North Umbria University is working on applying polymer LEDs (PLEDs) for 5G networks. Monash University is working on higher data transmission in VLC, LED modeling, and modulation techniques. Special lighting quality effects and dimming effect have been taken as an interesting research area by Keio University. University of Boston and Yeungnam university are working for RF/VLC hybrid methods, Nano photonics, and LED fabrication (Islim et al., 2017). On the other hand, some industries are involved with academic research to produce commercial VLC product for future green communication and intelligent transportation system. The data rate of the VLC system can be increased by adopting multi-channel LEDs/μLEDs as a transmitter, high bandwidth photodiode (PD) array at the receiver side, high order modulation scheme, wavelength division multiplexing (WDM), and Multiple-input multiple-output (MIMO) techniques to compete with 5G technology.

1.3 Focus of the Thesis

In optical fibers, three different types WDM have been employed – (i) normal WDM, which uses two predominant wavelengths (1310nm and 1550nm), (ii) Dense WDM

(DWDM), which uses C band (1530nm-1565nm), and (iii) Coarse WDM (CWDM), which uses bands from O to U (1265nm-1665nm) (Al-Rubaye et al., 2009). Channel spacing between individual wavelengths in DWDM and CWDM are different. DWDM system generally has 20 channels at 200GHz (1.6nm) spacing, 40 channels at 100GHz (0.8nm) spacing, and 80 channels at 50GHz (0.4nm) spacing as standardized by ITU (ITU, 2020). According to ITU CWDM grid, channel spacing of 20nm (2.5THz) can be implemented within a multiband frequency range from 1270 nm to 1675nm (i.e., 400nm range) (Nebeling, 2002), and same concept of CWDM has implemented in VLC system with its 400nm visible range from 380nm to780nm. A baseline of WDM-VLC system was developed and explore the implementation of CWDM in VLC for the first time.

The use of high bandwidth LED arrays can help to increase the data rate of VLC systems. The possibility of using narrow-band LED arrays in the CWDM-VLC system has been explored. The number of quantum wells (QWs) in InGa/InGaN LEDs has been varied and changed each layer's thickness to produce a narrow band LED for achieving the wavelengths required for the CWDM-VLC system.

Considering data transmission capacity, energy, and spectral efficiency, 5G has more advantages than the existing 4G network. 5G wireless technology is probably utilizing an RoF network for data transmission between the central office (CO) to the customer unit (CU). With the advancement of wireless communication, the demand for more data capacity drives the technology to the millimeter-wave (mmWave) spectrum of the microwave region. The mmWave band refers typically to the frequency range from 3 GHz to 300 GHz with wavelengths ranging from 1mm to 100mm (C.-X. Wang et al., 2014). Compared to mmWave, VLC has similar advantages such as high bandwidth and the ability to support gigabit-per-second data rates due to its high security, low co-channel interference, interference-free communications between indoor and outdoor users. A.M. Khalid et.al., reported for the first time a hybrid integrated system using of Radio over Fiber (RoF) and VLC. In that hybrid system, optical fibers are used as a backbone to connect with radio communication and VLC was used at the user end for indoor communication (Khalid et al., 2011). A new RoF (5GmmWave)-VLC hybrid model has been proposed, where mmWave is generated by optical multi-tone sending through the fiber connect to indoor VLC. Typically, VLC links are good for downlink communication, but there is a performance problem in the uplink. The desired mmWave signal at 60 GHz and 37.5 GHz with a baseband are produced. At CO, an electrical BPF selects the tones at 37.5 GHz and 60 GHz to transfer through a low pass filter (LPF) filter for adjustment with LED driver for indoor VLC customer unit (CU). Other output goes to an optical band pass filter (OBPF) for VLC uplink as frequency reuse and mmWave based uplink shows better transmission quality.

1.4 Objectives of the Research

The aim of this project is to investigate and develop methods for Gigabit-Class visible light communication systems. The objectives to achieve this aim are:

1. Simulate and experimentally validate a multi-channel WDM-VLC system using state-of-the-art RGBA LEDs with various modulation schemes such as OOK and m-Quadrature Amplitude Modulation (QAM).

2. Investigate the CWDM-based multi-channel VLC system in order to increase the VLC channels and compare the performance with WDM based VLC system.

3. Develop high bandwidth narrowband InGaN/GaN MQWs LEDs with specific requirements for CDWM implementation.

4. Develop a hybrid Radio over fiber VLC (RoF-VLC) communication model combined with a CWDM-VLC downlink system and 5G-mmWave based uplink for reducing uplink complexity and high-speed full-duplex transmission.

1.5 Organization of Thesis

The thesis is organized based on the following chapters.

Chapter One: Introduction

This chapter is the introductory part of the thesis, which provides an overview of the problem statements, objectives, research contributions, and chapter outline.

Chapter Two: Literature Review

This chapter provides an intensive summary of the VLC system and relevant literature associated with all technologies which were used to achieve Gigabit link by LED-based VLC system. High bandwidth LED modeling work, and fabrication process are discussed in this chapter. Moreover, the multicarrier modulation scheme, WDM systems for VLC application, equalization techniques and multiple input multiple output (MIMO) are highlighted as mechanisms to increase data rate of VLC systems in this chapter. Finally, hybrid Networks with VLC based downlink and uplink systems, heterogeneous networks with VLC, and recent commercial advancements are also explained elaborately. This chapter categorizes techniques used in the existing literature to achieve high-speed VLC communication and identifies the gaps to justify the objectives of this research.

Chapter Three: Wavelength Division Multiplexing (WDM-VLC) System

This chapter starts with existing WDM-VLC related work from the literature and derives from that the benchmarking work for this thesis. It then provides analytical model of WDM-VLC system and evaluates the effect of using RGBA LEDs with modulation schemes NRZ-OOK and 16 QAM in a WDM-VLC system. It analyzes the performance by considering line-of-side (LOS) and non-line-of-side (NLOS) propagation effects on data rate and compares both simulation and experimental results of indoor VLC. Moreover, the performance has been investigated by total received power at the receiver by changing the field of view (FOV) concentrator angle. Combination of multiplexing system with different modulation schemes can provide data transmission rate at gigabit range with acceptable BER.

Chapter Four: Multi-Channel Gigabit Class CWDM-VLC System

In this chapter, the concepts of CWDM and VLC are explained using the literature and based on that the possibility of using CWDM in VLC is explored. Then, for the first time the concept of CWDM-VLC is introduced to increase the number of channels in VLC and the performance of this system is evaluated using different optical filters. Finally, the conventional WDM system performances with 10 channels and 20 channels of CWDM-VLC system was compared in this chapter.

Chapter Five: FDTD Analysis of GaN/InGaN Based High Speed LED

In this chapter, the techniques to enhance the efficiency of GaN-LEDs are explored based on the works in the literature. Using this as basis, novel high bandwidth InGaN/GaN-based multiple quantum well (MQW) LEDs are designed coupled with and without nano-lens on the top layer of the LED structure. Using the finite-difference time-domain (FDTD) technique, three different peak wavelength LEDs was designed and compared the performance using recombination lifetime, light extraction efficiency (LEE), and beam divergence. The thickness of QWs is changed within a fixed active area and the number of QWs are also changed to attain the desired peak wavelengths in this chapter. Silicon dioxide (SiO_2) parabolic lens array is used on the top layer to reduce field divergence. With these designs, a proof-of-principle of CWDM-VLC grid modeling was presented in this chapter.

Chapter Six: Hybrid Radio-over-Fiber mmWave VLC System

In this chapter, different types hybrid RoF-VLC systems from the literature are highlighted. Then, a hybrid RoF-VLC system is proposed, producing 5G mmWave signal with baseband in the RoF system as a backhaul and distribution to the VLC access point for indoor communication link. With the help of different optical multitoned signals, three different 5G signals are produced and one of them is re-used as a carrier frequency for VLC uplink for the first time. The structure of the VLC transmitter uses CWDM to increase the number of data channels for high-speed indoor communication. How this system can incorporate with mmWave signal and CWDM-VLC for gigabit-class downlink and uplink transmission is also explained in this chapter.

Chapter Seven: Conclusion

This chapter summarizes the major outcomes from this thesis and outlines the future work that can be followed in this area.

1.6 Contribution of Thesis

The contribution of each chapter in this thesis are summarized and explained below:

Chapter 2: A comprehensive literature survey is compiled looking into the relevant areas associated with off the shelf LED-based VLC systems. This chapter provides the foundation based on what the key contributions were identified for the subsequent chapters. This chapter provides an intensive summary of the

a) Prospects of VLC system and relevant literature associated with all technologies which were used to achieve Gigabit link by LED-based VLC system.

b) Limitations of pc-LEDs and RGB LEDs compared to high bandwidth LEDs in the gigabit class VLC systems and their modeling work and fabrication approaches for better light extraction efficiency and bandwidth.

c) Impacts of multicarrier modulation scheme for data rate enhancement of VLC systems.

d) Pros and cons of optical wireless receivers in WDM-VLC systems for increasing the number of VLC channels.

e) Comparison of pre (at the transmitter) and post (at the receiver) equalization techniques for achieving gigabit class data rate, which can be based on software or hardware.

f) Investigation of the non-imaging and imaging MIMO systems and their performance to deliver high data rate.

g) Evaluation of hybrid networks with VLC based downlink and WiFi/IR based uplink systems, and heterogeneous networks with VLC.

h) Recent commercial advancements.

i) Different applications of VLC such as Intelligent Transportation System (ITS), underwater communication, indoor positioning, smart lighting and implementation challenges such as mobility, modulation bandwidth, nonlinearity and illumination constraints.

Chapter 3: This chapter provides an analytical model of WDM-VLC system and evaluates its performance for indoor VLC application. Specifically,

a) Simulate the RGB/RGBA conventional four channel VLC system using available LED bandwidth configuration.

b) Demonstrate the VLC system and compared both simulation and experimental results of indoor VLC

c) Evaluate the WDM-VLC system performance with different modulation schemes in both simulation and experimental setup.

d) Model and analyze the performance of the conventional WDM-VLC model under LOS and NLOS conditions with different numbers of LEDs.

e) Achieved 290 Mb/s using OOK and 1.16 Gb/s using 16 QAM using simulation, and 260 Mb/s using OOK and 1.04 Gb/s using 16 QAM through experimental work using RGBA LEDs, when the distance between transmitter and receiver is 3 m.

Chapter 4: This chapter proposes for the first time a novel CWDM based VLC system with:

1. Accurate characterization of CWDM grid with narrow LEDs spectrum for high speed communication.

2. Development of 10 channel and 20 channel CWDM-VLC model.

3. Formulation of simulation framework for optical tunable filters at each channel receiver to maximize signal performance while minimizing crosstalk.

4. Enhancement of the communication capacity with the CWDM-VLC system data rate compared to the traditional WDM-VLC system.

5. Achievement of 7.19 Gb/s data rate using 20 channel CWDM grid with acceptable BER.

Chapter 5: This chapter proposes a high bandwidth GaN/InGaN MQW- LED structure by finite-difference time-domain (FDTD) analysis. Specially,

a) Propose a model of InGaN/GaN-based multiple quantum well (MQW) LED coupled with and without nano-lens on the top layer of the LED structure.

b) Optimize linewidth of LED to be used for CWDM using parabolic nano lenses.

c) Investigate the optical properties of highly polarized LED using FDTD technique and compare the performance with different QWs and changing thickness of the QW layer.

d) Produced three different LEDs with peak wavelength 510nm, 530nm and 550nm with SiO2 lenses on the top layer to reduce field divergence to 20 nm, and achieved maximum modulation bandwidths of 6.15GHz, 2.27 GHz and 0.18 GHz.

Chapter 6: This chapter proposes a hybrid Radio over fiber-VLC (RoF-VLC) communication model using mmWave based uplink and CWDM-VLC for downlink. Specifically,

a) RoF-VLC heterogeneous network with millimeter-wave signal generated using optical triple tone (heterodyning method) and extended through a 20 km fiber optic link from the central office (CO) to customer unit (CU).

b) Self homodyning method to down-convert the signal at the VLC access point and send it to a multi-color CWDM-VLC system for indoor downlink.

c) Compare the downlink VLC performance using different optical filters.

d) Analyze the signal quality for both downlink and uplink based on BER of signals, power levels for different indoor link range and beam divergence.

1.7 Publications

During this PhD research work, the following journals and conference papers were published. A few more manuscripts have been submitted for publication, which are currently under review.

Journal Publications

1. **M. T. Rahman**, R. Parthiban, M. Bakaul (2020), Modeling and analysis of multi-channel gigabit class CWDM-VLC system, **IET Optoelectronics**, 460, 125141.

2. **M. T. Rahman**, ASM Baki Billah, R. Parthiban, M. Bakaul (2020), A Review of Advanced Techniques for Multi-Gigabit Visible Light Communication, **IET Optoelectronics**, 460, 125141.

3. **M. T. Rahman**, R. Parthiban, M. Bakaul (2020), FDTD Analysis of GaN/InGaN Based High Speed LED with Different MQWs, **Optics Letters**. [Under review]

4. **M. T. Rahman**, R. Parthiban, M. Bakaul (2020), 5G mmWave Communication with Hybrid ROF-VLC System, **IEEE Access**. [Under review]

Conference Proceedings

5. **M. T. Rahman**, M.Bakaul, & R. Parthiban, (June 2020), Integration and Evaluation of Hybrid RoF-VLC Network. **Proc. International Conference on Photonics (ICP2020)**, Kelantan, Malaysia.

6. **M. T. Rahman** (August 2019), Analysis of Multi-Channel Gigabit Class CWDM-VLC System, **Advanced Engineering Colloquium (AEC) 2019**, Monash University, Malaysia

7. **M. T. Rahman**, R. Parthiban, M. Bakaul, & P. Kumar, (March 2019, Published in 2020), Approaches of Gigabit-Class Transmission for VLC with µLED-Based WDM System, **Proc. Optical and Wireless Technologies (OWT'2019)**, India.

8. **M. T. Rahman**, M.Bakaul, & R. Parthiban, (November 2018), Analysis of the effects of multiple reflection paths on high speed VLC system performance, **Proc. 28th International Telecommunication Networks and Applications Conference (ITNAC),** Sydney, Australia.

TECHNIQUES TO ACHIEVE HIGH-DATA RATE FOR VLC

2.1 Introduction

Visible light communication (VLC) is a promising candidate for future indoor wireless communication. Light emitting diodes (LEDs) are popular choices as transmitters for VLC, since they are energy efficient and have the ability to provide illumination and data transmission simultaneously. Incandescent lamps started the artificial lighting era in the late 19th Century, and the technology marginally transmuted over a century. With the advancements of lighting technology, light emitting diodes (LEDs) have become the most energy-efficient light source due to high luminescence and long lifespan. Moreover, due to the rapid development of optical fibers, which are capable of transmitting gigabit range data under low attenuation condition, uses of high-speed semiconductor lasers and LEDs increased after 1970. A breakthrough came in 1994 when Nakamura et al. developed the first high energy-efficient gallium nitride (GaN) blue LED (Nakamura, 1997). In the following years, integrated phosphor coating was used on a blue LED to convert a part of the blue spectrum to longer wavelengths of light and produce white light. The most prevalent 'white' LEDs turned from blue emission are attained from a solid state device (SSD) by utilizing luminescent phosphor. White light also can also be produced with the combination of red, green, and blue (RGB) LEDs. Additional benefits of LED include tunable illumination, high data transmission, and prolonged lifespan compared to conventional lighting. VLC is attractive for reasons such as security, the ability to use a license free spectrum, and broad bandwidth. VLC network algorithms, implementation challenges, system design, applications, VLC systems for high-speed data communication in the gigabit range and the techniques to achieve such high data rates, such as LED modelling and fabrication process, recent commercial advancements of VLC products, and hybrid/heterogeneous networks to achieve high data rate are highlighted in this chapter. These literatures also cover recent advancements in commercialization of VLC technology, and recent progress made by various research groups.

2.2 Economic Benefits of LEDs

Total lighting sector consumes 19% of the total world energy, and it is considered as the principal source of greenhouse gas emissions. The economic demand for lighting has grown by 87% from 1987 to 2007 and is expected to grow 80% more by 2030 (Penning et al., 2016). Recently, Navigant Consulting, Inc. (NYSE: NCI) has published a research report on commercial lighting sector, which points to a dramatic increase in global commercial LED sales until 2021. There will be a slight decrease in LED revenue from 2019 to 2024 and a significant decrease in lamp revenue by lamp sales, such as fluorescent lamps (T5, T8, and T12), compact fluorescent lamps, and high-intensity discharge lamps as shown in Figure 2.1. From the McKinsey Global Lighting Market Model, the total market share of LEDs will accelerate over the next few years with high revenue (Guidehouseinsights, 2017). Figure 2.1 shows that global revenues from the LED sales reached 52–88 billion EUR from 2010 to 2020, which represents ~80% of the total lighting market.

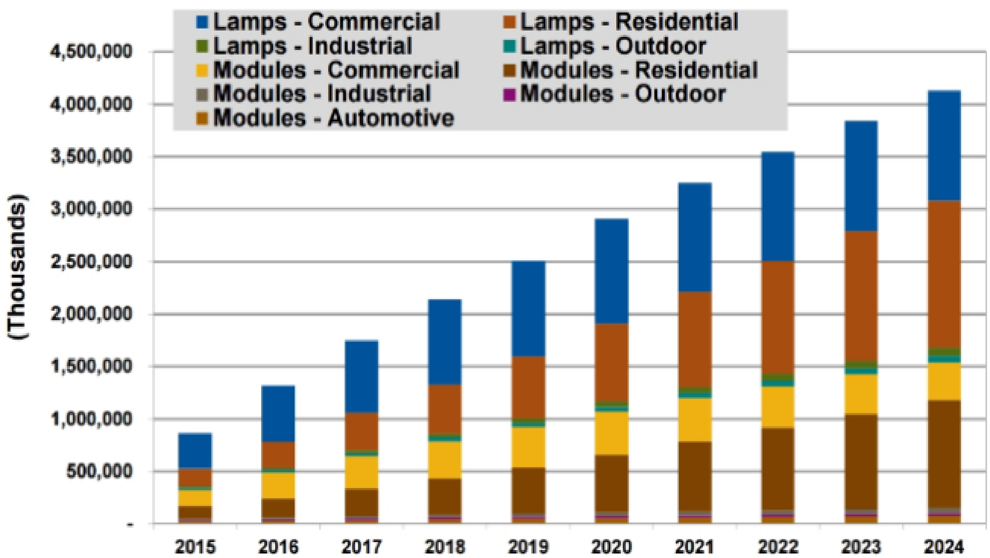

Figure 2.1: LED Lighting: Global Markets: 2015-2024 (Guidehouseinsights, 2017)

At present, visible light communication (VLC) has become one of the most important communication medium in the optical wireless communication field due to its high bandwidth capacity. Moreover, as a common transmitter of VLC, LEDs are used for data communication as well as illumination. With the increasing demand of VLC applications, such as light fidelity (LiFi), robotics, intelligent lighting system, intelligent transport system (ITS), visible light positioning, vehicle-to-vehicle and underwater communication, the demand for data rate has also increased up to gigabit range (Kadam & Dhage, 2016).

2.3 Research Trends of LED Based VLC

The early research efforts on LED-based VLC system actuated from Keio University, Japan and they proposed white LED as a transmitter for home access network at Visible Light Communications Consortium in 2003(O'Brien et al., 2008). In 2009, the home Gigabit Access project (OMEGA) was started by EU (Javaudin et al., 2008), and they established VLC, which was more secured and enhanced compared to radio frequency (RF) communication network. Also, over 20 European countries started a research project regarding optical wireless communication named 'OPTICWISE' in 2015 (OPTICWISE, 2010). A research group of King Abdullah University and Technology (KAUST) Saudi Arabia is working to improve transmitter capacity, such as high-speed super luminescent diode with high bandwidth (807 MHz (Shen et al., 2016) (>400 MHz (Alatawi et al., 2018) for gigabit-class VLC. They demonstrated an optical receiver device, such as 15 pairs of indium gallium nitride (InGaN)/GaN multiple quantum well (MQW) based micro-photodetector to achieve 3.2 Gb/s VLC link (Ho et al., 2018). Professor Nan Chi (and her group) from Fudan University is working to transmit multi-Gigabit data per LED light and to overcome the technical difficulties of VLC optical receivers (Tanaka et al., 2000). Sant'Anna School and TCI LED professionals demonstrated object detection system at the 'LIGHT & Building 2018' event in Germany. Istituto TeCIP (in Italy) established 3.4 Gb/s VLC link with the RGB LED. They developed a communication system for an outdoor environment using an optical wireless link for integrated VLC applications (Cossu et al., 2011).

Oxford University has comprehensive research background on multi-Gb/s VLC system including hybrid equalization method for modulated optical sources, LD based white-light communications link, VLC receiver design for Internet of Things (IoT) applications, and GaN-based micro-LED (µLED) fabrication (Chun et al., 2016)(Rahaim et al., 2011). Prof. Harald Haas (PureLiFi's CSO) established a LiFi center at the University of Edinburgh and is working on high-speed bi-directional VLC link (C. Chen et al., 2019), LiFi mobility (Xiping Wu & Haas, 2019), spatial modulation (SM) (Yesilkaya et al., 2019), µLEDs (Islim et al., 2017), and improvement for optical wireless networks. Furthermore, North Umbria University is working on the application of polymer LEDs for 5G networks. Monash University is working on higher data transmission in VLC, LED modelling, and modulation techniques. Special lighting quality effect and dimming effect have been taken as an interesting research area by Keio University. The University of Boston and Yeungnam University are working on RF/VLC hybrid methods, nano-photonics, and LED fabrication (Cossu et al., 2011)(Borogovac et al., 2011). On the other hand, some industries are involved with academic research to produce commercial VLC product for future green communication and intelligent transportation system. To compete with 5G technology, the communication data rate of the VLC can be increased by adopting multi-channel LED/µLED at the transmitter and high bandwidth photodiode (PD) array at the receiver side along with high-order modulation schemes, wavelength division multiplexing (WDM), and multiple input multiple output (MIMO) techniques.

2.4 Description of VLC System

A VLC system is enabled by a modulated light signal from an emitting device such as an LED or a laser diode (LD). The modulated light propagates over the free space, and the transmitted data is consequently recovered at the receiver using different photodetectors, such as imaging sensors and non-imaging sensors. The transmitter part based on semiconductor devices such as LEDs are connected to driver circuits to drive the current and this intensity modulated signal is directly detected at the receiver by PIN photodiode or avalanche photodiode (APD). Figure 2.2 shows the basic diagram of a VLC system, which is used to transmit data signals through LED. It emits white light by combining emissions from multiple solid state device (SSDs) and single-color emission with color converting material, where each emitter emits a wavelength. The first approach to produce white light is to combine blue-emitting LEDs with yellow coated phosphor (Ce: YAG) known as phosphor-coated (PC) LED. Another approach to create white light is to combine three monochromatic color light sources (red, green, and blue). The multi-color approach is quite costly, but offers more flexibility of color tuning facility, which also gives the opportunity to implement WDM in VLC.

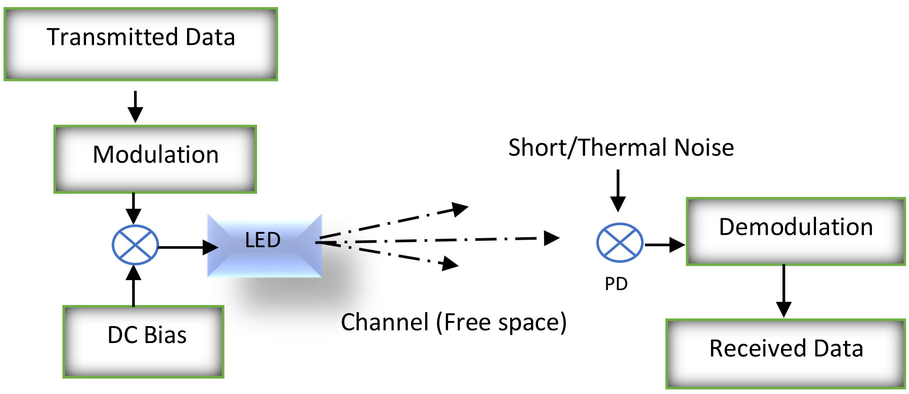

Figure 2.2: Basic Diagram of LED-based VLC System

The yellow phosphor-based illumination is cost-effective, has a long lifetime, and is available in the market. However, it has bandwidth limitations of few MHz for VLC applications (Steigerwald et al., 2002)(Le Minh et al., 2008). On the other hand, the bandwidth of RGB LED is limited to 15–35 MHz only. Apart from PC-LEDs (Steigerwald et al., 2002) and RGB LEDs (Pessa et al., 2002), there are other types of LEDs such as, resonant cavity (RC) LEDs (Schubert et al., 1992), organic light emitting diodes (OLEDs) (Oh et al., 2008)(Chun et al., 2012), and µLED (Islim et al., 2017). Recently, some researchers have achieved data rate up to 11.28 Gb/s using µ-LEDs arrays (Pessa et al., 2002). Different types of LEDs with applications and related bandwidth is given in Table 2.1.

Table 2.1: Different LEDs and their Bandwidth and Applications

Type	**Bandwidth**	**Application**	**cost**
OLED	1-5 MHz	illumination	Average
Pc LED	3-5 MHz	Illumination+ communication	Low
RGB LED	15-35 MHz	Illumination+ communication	High
Multichip	25-30 MHz	Color channel	Average
RC LED	~ 100 MHz	Communication	High
Micro	350~900 MHz	Sensing + communication	High
GaN nano wire based	~1 GHz	High-speed communication	High

In a point-to-point link, a narrow beam transmitter is connected to the receiver using a narrow field of view (FOV). This link supports a high-speed data transmission because of low geometrical loss and offload inter-symbol interference (ISI) (Noshad & Brandt-Pearce, 2013). Alternatively, diffused non-line-of-sight (NLOS) links use wide angle transmitters and large FOV of receivers. Diffused paths are created by the reflection of light from multi-type surfaces together with walls, ceiling, and floor. Sometimes these multi-reflected paths can help to increase the signal strength at the receiver. The total light measures received optical power from diffused paths, which depends on room dimensions, the divergence angle, the length between transmitter and receiver, and orientation of sources. Due to path variances in the diffused channels, the received signal is affected by ISI (Ravinder Singh et al., 2013). The optical receiver converts the received light into an electrical signal. Existing VLC receivers consist of PDs, APDs or image sensors. Modern electronic devices like smartphone, camera, and laptop are using complementary metal-oxide semiconductor (CMOS) based image sensors as VLC receiver. Furthermore, the typical VLC receiver consists of an amplifier, an optical filter, a concentrator, and different types of silicon photodiodes (S. H. Lee et al., 2015). Silicon (Si) photodiodes are more appropriate for high-speed VLC applications because of its high external quantum efficiencies (EQEs) within the visible light range. Among the families of silicon photodiodes, PIN PDs and APDs are commonly used for VLC applications. Figure 2.3 shows different

VLC links such as direct line of side, non-line of side, diffuse link and quasi diffuse links between the transmitter and the receiver.

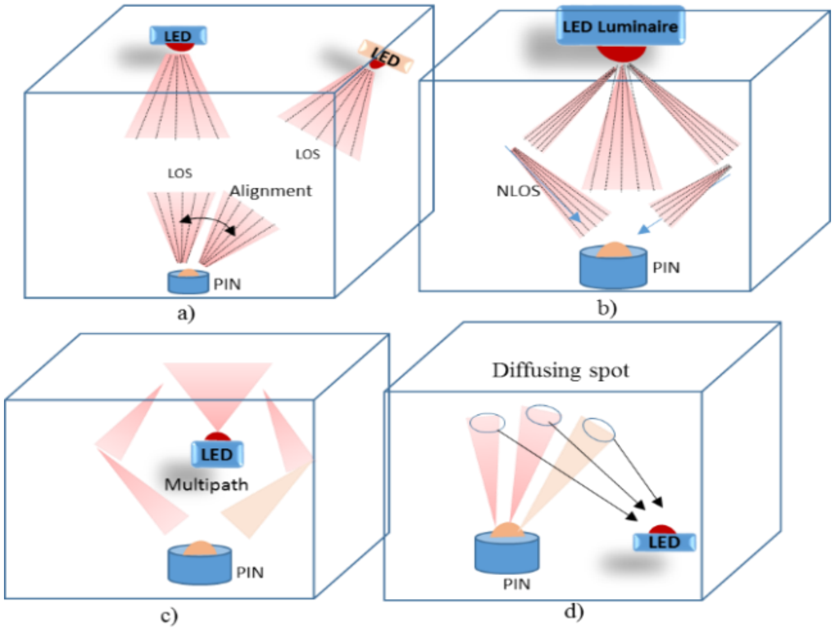

Figure 2.3. a) Direct Line-of-Side (LOS) Link, b) NLOS Link c) Diffuse Link and d) Quasi-diffuse Link

Ambient light noise is one of the primary sources of noise in the visible light communication. It is caused by sunlight or solar radiation from windows, or open part of the room. Some shot noise and thermal noise arise in the photodetector when it detects the light signal. When the ambient noise is filtered out, the SNR at PD can be calculated using the combination of shot noise and thermal noise at the receiver as

$$SNR = \frac{P_{R_E^2}}{(\sigma_{shot})^2 + (\sigma_{thermal})^2} \tag{2.1}$$

where σ_{shot} and $\sigma_{thermal}$ are standard deviations of shot noise and thermal noise, respectively. The shot noise is due to the number of photons collected by the photodetector. The variance of shot noise is calculated as follows (Ghassemlooy et al., 2019)

$$(\sigma_{shot})^2 = 2qP_{R_E B + 2qI_b\, I_2 B} \tag{2.2}$$

$$(\sigma_{shot})^2 = \frac{8\pi k T_k}{G_{ol}} C_{pd} A l_2 B^2 + \frac{16\pi^2 k T_k \eta}{g_m} C_{pd}^2 A^2 I_3 B^3 \quad (2.3)$$

where B is the bandwidth of the photodetector, κ is the Boltzmann's constant, I is the photocurrent due to background radiation, G_{ol} is the open-loop voltage gain, T_k is the absolute temperature, C_{pd} is the capacitance of the photodetector per unit area, η is the channel noise factor, g_m is the channel trans conductance, and I_2 and I_3 are the noise-bandwidth factors, respectively. Shot noise and thermal noise are dependent on some external effects, such as room temperature, ambient light, etc (Komine & Nakagawa, 2004).

2.5 Techniques for High-Speed VLC Network

To compete with the next generation 5G communication technology, the data rate of VLC system has to be increased. In this paper, the key methods for high-speed VLC link have been classified and analyzed. There are several prospects to do further research on system performance and transmission link of VLC to make it more robust and error-free optical wireless network.

2.5.1 High Bandwidth LED

High bandwidth LED offers an opportunity to achieve gigabit VLC system due its high modulation bandwidth, but the fabrication of µLED is still in the development stage. Many methods have been reported to improve the modulation bandwidth of LEDs such as multilayer restructuring within quantum wells (QWs), changing the thickness of LED active layer, injecting surface plasmon (SP) at interfaces or changing the RC structure (Zhu et al., 2017). Increasing current density within the active area can affect the carrier lifetime of an LED. In (Alatawi et al., 2018), a modulation bandwidth of 440 MHz was achieved within 24 µm diameter active area of a µLED, where current density was 17.7 kA/cm2.

Another approach was used to decrease electron lifetime and modulation bandwidth of LED by applying an external strain within MQW (Du et al., 2016). The conventional vapor deposition techniques for hetero-structure can improve the performance of nanowire LEDs, which help to make them as core–shell device structures (Shunfeng Li & Waag, 2012). In 2010, 225 MHz blue-emitting μLED with gallium-doped zinc oxide was reported by Liao et al. in (Liao et al., 2013), and 245 MHz bandwidth was measured with GaN μLED arrays in (Chun et al., 2016). Subsequently, a green-emitting μLED with a bandwidth of ~463 MHz has been reported by Maaskant et al. (Maaskant et al., 2013), and 400 MHz bandwidth was demonstrated using cyan μLED by Wun et al. (Wun et al., 2012). Koester et al. showed GHz bandwidth in their experiment using μLEDs (Koester et al., 2015). Table 2.2 shows some LED technologies and their related bandwidth and life time.

Table 2.2: GaN-based LEDs and their Lifespans and Bandwidth

LED Technology	Lifespan	Bandwidth (MHz)
High power broad area LEDs	Commercial mass production	20
GaN RCLEDs	Academic prototypes	200
GaN micro-LEDs	Last stage of R&D	> 400
Non-polar GaN LEDs	Academic and industrial research	~ 1000
GaN Nano-wire LEDs	Purely academic research	1100

2.5.1.1 Modeling Approaches

Group III-nitride materials, e.g. InGaN LEDs have different applications in solid-state lighting, such as color displays, backlighting, and high-speed VLC links. Conventional InGaN QW LEDs are developed on the surface of polar c-plane orientation.

However, it suffers from quantum confined stark effect (QCSE) due to its significant internal polarization field effects, which degrades radiative recombination rate and efficiency. With the high polarized QW structure, the carrier lifetime of c-plane LEDs can be increased, which significantly limits their performance for achieving high modulation. Most of the LED modelling works have been proposed with different techniques, such as flip-chip LEDs, metallic grating coated LEDs, and surface roughening by chemical etching (Zhao & Zhao, 2012). Moreover, placing a photonic crystal on the top layer (Liu et al., 2015), micro or nanostructure improvement, sub-wavelength structure changing on the top layer of GaN (Son et al., 2015), reducing Fresnel reflection, patterning sapphire substrates (Pan et al., 2013), and reducing far-field divergence by implementing nano-lens (Demory et al., 2018) are also considered. High bandwidth LED structure design literature are tabulated in Table 2.3. LED modelling by FDTD method was done to find the enhancement of external and internal quantum efficiency (Ahsan et al., 2016), the angular distribution of light, transmitted power distribution, recombination time, Purcell factor, and the modulation frequency of the LED (H. Chen et al., 2016).

2.5.1.2 Fabrication Process

The development of GaN LEDs over the last 20 years has significantly improved solid-state optoelectronic emitters. In the recent times, a different dimension of LED research is being explored in industrial laboratories and academic research labs to enhance light extraction efficiency and communication capacity. InGaN-based QWs LED emits blue-violet spectrum coated by color conversion materials, and this color mixing technique makes it more efficient over the incandescent and fluorescent light sources (Castro et al., 2017). Currently, most of the GaN LEDs are fabricated by metal-organic chemical vapor deposition machines, where the LED structure is fabricated on a single crystalline substrate (D. Y. Kim et al., 2017). The shortage of free carriers in an LED's P–N junction is known as depletion region, and some carriers diffuse into the natural regions where recombination happens.

Extra thin functional layers have to be placed above and below the active region to maintain the electron carrier injection. LED carrier lifetime in a typical bandgap semiconductor is 1– 100 ns depending on the active region doping concentration and

Table 2.3: Summary of LED Design based on Higher Modulation Bandwidth

Ref	Methods	Analyse	Materials	Structure	Modulation Bandwidth
(Fattal et al., 2008)	Optical pumping (Modelling work)	Intensity power, recombination time	$GaAs_{0.885}P_{0.115}$ QW, Ag, $AL_{0.35}Ga_{0.65}As$	surface plasmons (SPs) produced by metallic grating	10 GHz
(H. Chen et al., 2016)	light polarization	LEE, IQE, EQE, Purcell factor, Modulation frequency of LEDs	GaN/InGaN	Metallic grating on top surface	5.4 GHz
(Rashidi et.al., 2018)	Changing current densities in the active layer	power dissipation and efficiency	InGaN/GaN micro LED	Metal ring on top layer (ITO)	1.5 GHz
(Ferreira et al., 2016)	Increasing current	Carrier lifetime, junction temperature	GaN-Based Micro-LEDs, palladium (*Pd*)		833 MHz
(Lan et al., 2018)	Increasing current densities	Effects of QW numbers on modulation bandwidth, Optical power	GaN blue micro LED	Single and triple QWs based epitaxial structure	752 MHz
(Rajabi et al., 2018)	Reducing quantum-confined Stark effectin the active layers	Recombination rate, thickness of QWs, EQE	Ultra-thick InGaN /GaN	semi-polar substrates	536 MHz
(He et al., 2019)	Higher current densities	Electrical, Optical, and Modulation Bandwidth Characteristics	AlGaN/ GaN	Deep- UV-C µLEDs	438 MHz
(Zhu et al., 2017)	Increasing current density	Heat dissipation, light extraction, the modulation bandwidth and optical power	GaN, Cr/Al/Ti/Au	Flip-chip parallel µLED	227 MHz
(Zhu et al., 2015)	Surface plasmon (SP) coupling with QW	IQE, emission rate	18 pairs InGaN/ GaN, Ag Nps	Nano rod array by HfO2, Ag, SOG	15.1MHz (Nano rod) 29.8 MHz (Ag Nps)

the quality of materials. There are two alternative substrate materials, namely silicon (Si) and bulk GaN/InGaN, to compete with the future commercial LEDs. Silicon offers some advantages in terms of the lower price, convenience to find larger (200 mm diameter or more) substrates, and compatibility with current injection. The basic structure of III-Nitride LED is shown in Figure 2.4, where the P-type layer and MQW regions have been fixed, allowing a lower electrical contact to the n-type layer (Nakamura et al., 1994). The lower part of the LED structure contains sapphire substrate that allows light extraction exclusively through the substrate.

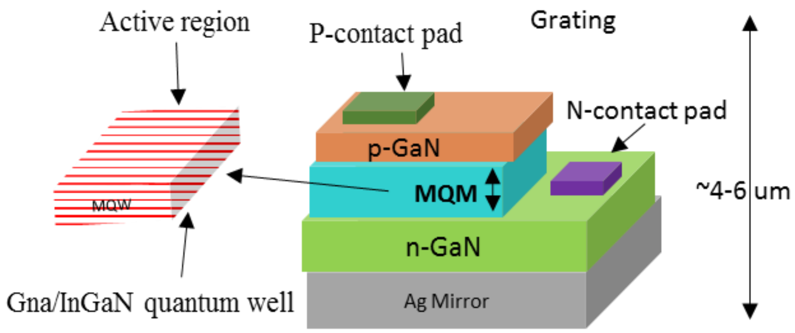

Figure 2.4 A Simplified Cross-section View of a Typical III-Nitride LED.

2.5.1.3 LEDs and Its Types

In 1907, Henry J.Round invented LED using silicon carbide to overcome its previous lighting limitations such as structure, speed, size, life time, and efficiency. The LED emits light when an excited electron (n-type) from conduction band falls back into the valence band transition by recombining with the hole (p-type).

$$v = \frac{W_g}{h}$$

$$\lambda = \frac{c}{v} = c.h/W_g \tag{2.4}$$

Here c is speed of light, h is Plank constant, and W_g is energy bandgap (W_c-W_v). This energy bandgap of semiconductor materials effects on LEDs bandwidth, frequency and wavelength. In addition, different semiconductor materials are showing different energy bandgap like Ga, Si, GaAs, GaAsP, GaInN are 0.7eV, 1.1 eV, 1.4 eV, 2.0eV, 2.9eV respectively (Milnes, 2012). In case of direct bandgap, the number of electron and holes in the energy state of semiconductor are same, and for indirect bandgap condition, electron and holes are not equal because of their momenta or piezoelectric characteristics. So that recombination can't perform without containing phonon in their vibrational stage and for that results heat are generated. Therefore, carrier recombination life time or electron life time of semiconductor materials such as Gallium nitride (GaN)) have the most significant influences on the LED modulation bandwidth. So, controlling the atomic ratio of GaN can change the operational wavelength, piezoelectric efficiency and the carrier life time of the LED. Therefore, Blue LED bandgap is 2.51eV and green LED is 2.30eV because of different quantum efficiency. For the recombination process Blue LED shows faster electron life time than green and red. VLC chip design and optimization of semiconductor material's strain at the fabrication time has a great effect on LED modulation bandwidth, so the compensation of strain is one the method of improvement the bandwidth up to GHz. Some of the key features of available LEDs are organized here with its VLC application and performances.

a) pc-LEDs:

pc LED is Phosphor layer coated blue LED which produces white light. Most popular wavelength-converter materials are phosphor which is doped by an inorganic and optically active element - cerium named Yttrium aluminum garnet (YAG: Ce^{3+}) phosphor. The YAG phosphor can be made as a powder and put off in epoxy resin to deposit on the LED die which emits the blue light. Because blue light is absorbed by the YAG phosphor and emits white light. Shapes and thickness of the phosphor layer causes for changing wavelength and Correlated Color Temperature as (CCT). These LEDs are low cost but bandwidth is limited (only few MHz) because of the yellow phosphor (Rao et al., 2012). Recently Cree has invented high brightness LED 231 lm/W in their lab, and available efficacy of the commercial white LEDs > 150 lm/W are also available in the market.

b) RGB LEDs

These LEDs are made up of multi LED chips with different colors. Most popular is Red, Green and Blue (RGB) LED chip to produce white light. The main advantage of RGB LED is the color and light intensity level can control by its driver circuit. Therefore, three or more color LED chip can use as a different communication channels, and each LED can provide approximately 45-60 MHz bandwidth.

c) Resonant Cavity LEDs

Resonant Cavity Light Emitting Diodes (RC LED) has some sort of improvement over conventional LEDs because of its higher intensity, better emission pattern and better quantum efficiencies. RC LED cavity is fabricated by multi-layer flat substrate within the active region. Moreover, for the big difference in refractive index GaAs or other semiconductor materials perform better than other commercial LEDs. The cavity also has few dielectric mirror for high brightness to make it better applicant in VLC for lighting aspects with very narrow line width. Moreover, for communication it can modulate the data ~ 100MHz. The first time resonant cavity improved by Schubert et al. in 1992 (Schubert et al., 1992) .

d) Organic Light Emitting Diodes (OLED)

An organic light-emitting diode (OLED) which is consists of the emissive electroluminescent layer of organic compound between positive and negative carriers that emits light from the active area. Ching W. Tang et.al built the first OLED in 1987 (Oh et al., 2008) using two-layer structure combined with hole and electron was used in transporting layers. So the recombination and light emission can have occurred in the middle of the organic layer. The frequency of the OLEDs is 100's of kHz and mostly used for television or computer screen and, mobile screen etc. OLED's are also used in multiple-input/multiple-output (MIMO) wireless optical channels. Red and green OLED have longer lifetimes than blue OLED which is about 230,000 hours (Chun et al., 2012).

2.5.2 Modulation Schemes for VLC

Modulation schemes are used in VLC to control the intensity of light for communication and have an impact on illumination. Demodulation depends on direct detection of the light signal at the receiver. The light intensity can be controlled using different LED driver circuits also (Rea, 2000). On–off keying (OOK), pulse position modulation (PPM), and m-pulse amplitude modulation (PAM) are very useful single-carrier modulation schemes for VLC. However, they suffer from unwanted effects such as non-linear signal distortion from LED and ISI caused by frequency shifting in dispersive optical wireless channels (Yiguang Wang, Wang, et al., 2014). To overcome these effects and to facilitate for high-speed VLC network, multi-carrier modulation (MCM) schemes are widely used.

2.5.2.1 On-Off Keying (OOK)

OOK is one of the well-known and simple modulation schemes, and it provides a good trade-off between system performance and implementation complexity. The implementation of OOK is comparatively easy, i.e. when LED is on, the data bit is one, and when LED is off, the data bit is zero. LED is not completely turned-off for zero bit, because of its tuning ability. OOK is the most popular modulation technique for LED, which was proposed in (S. B. Park et al., 2007) and was used to demonstrate a 10 Mbps VLC link. Similarly, the data rate can be increased to 125 Mbps (Vucic et al., 2009) using OOK with an analogue equaliser at the receiver end. A combined data rate of 477 Mbps was achieved using RGB LEDs with OOK, while maintaining proper illumination levels by Singh et al. (Ravinder Singh et al., 2013).

2.5.2.2 Pulse Width Modulation

Pulse Width Modulation (PWM) is the best technique to control the intensity and illumination of LEDs. Correlated Color Temperature (CCT), Color Rendering Index (CRI), and light intensity are the key parameters to analyze the lighting aspects of LED (D'Andrade & Forrest, 2004). The data rate of the transmitted signal could be adjusted by changing the dimming level of LED. PWM, also is known as a digital dimming pulse trains to drive the LED to maintain the constant current level. The average duty cycle represents the equal analog signal level, and it varies proportionally to the dimming percentage (O'Brien et al., 2008). The duty cycle can be expressed as

$$D = t_{ON}/T \tag{2.5}$$

where t_{ON} is the amount of time the pulse is on and T is the PWM symbol duration. The main two parts of the PWM signal are duty cycle and frequency. The duty cycle defines the amount of time for signal high (on) and low (off) state and the total time to complete the full cycle. The frequency describes how faster or within 1 second how many cycle can achieve by the PWM. For example, 1000 Hz means 1000 cycles per second and changes its high and low states. By increasing switching capability (off and on state) at a high rate with a specific duty cycle, the output seems like a constant analog signal connected to devices (J. Huang et al., 2011). PWM is easy to implement with digital circuits; a steady drive over a wide range of intensities can be ensured. The display image has to be blinking anyway to avoid flickering when the motion picture is rendered on screen, so the periodicity of PWM is in synergy with this requirement (Galkin et al., 2011).

2.5.2.3 Color Shift Keying (CSK)

Color Shift Keying (CSK) is a modulation scheme for visible light intensity introduced works with multi-colored LED sources drawn by IEEE 802.15.7 standard (Rajagopal et al., 2012). It can transmit data invisibly through the variation of the color emitted by RGBY LEDs. Transmitted signal power is fixed in CSK, and the main advantage is it controls the fluctuations in light intensity for the safety of the human eye. CSK constellation points are placed on the CIE1931 chromaticity diagram, where each channel can produce the constellation point. Under the IEEE standard 802.15.7 maximum data rate of 96 Mb/s achieved and provided 4, 8, and 16 point CSK constellations for communications with 24 MHz clock pulse by (Rajagopal et al., 2012). Therefore, some researchers have been done to enhance the performance of CSK modulation. In (Drost & Sadler, 2010), a billiard algorithm is used to optimize the CSK constellations at various target and the main weakness of this scheme is limited distance capability among the symbols (D.-F. Zhang et al., 2020). CSK is a more controlled version of CIM because of lower intensity fluctuations observed by the human eye. Human health difficulties, such as biliousness or epilepsy, can cause by CSK flickering effects. D.F. Zhang et.al., proposed multi-user joint constellation (JC) to make an efficient multi-user communication by CSK (D.-F. Zhang et al., 2020). By the divergence luminous fluxes of QLEDs, special CSK designed named 3-CSK was proposed at (Liang et al., 2017). To get better error performance associated with other conventional CSK, a new 4-CSK scheme proposed adjusting various constellation points (Tzikas et al., 2019). Quadri-chromatic LED (QLED) cluster is consists of a four-color LED that is suitable for concurrent illumination and communications. Its extra color quality provides not only one new WDM data channel but also better color quality for lighting. This paper examined the constellation diagram of CSK to maximize the pairwise Euclidean distance (MED) and optimized data communication capability considering quality CRI and CCT (Liang et al., 2017). CSK constellations are optimized by minimizing the symbol error rate (SER) via non-uniform m signaling. The authors (Gao et al., 2015) presented a unique design with adaptive DC-bias on WDM-VLC systems by getting advantage of color and frequency domains. This way, the CSK constellation space can be increased the system's SNR gain, reduced power and reliability.

2.5.2.4 Multi-carrier Modulation Scheme

MCM is introduced to make better use of LED's limited bandwidth with its orthogonal subcarriers that can carry the modulated signal. This type of modulation can decrease ISI. To address the bandwidth limitation of white LEDs and achieve high data rate in VLC systems, a number of techniques, including higher order modulation techniques are investigated in several research works. Orthogonal frequency division multiplexing (OFDM) was proposed for the first time in (Armstrong & Schmidt, 2008) for indoor VLC applications. OFDM modulation divides the entire frequency into many narrow-band flat-fading subcarriers suitable for high data rate communication. The data is transmitted in parallel sub-carriers with low symbol rates and efficient multipath propagation adaptability without complex equalization, and this results in negligent ISI. For high-speed VLC, OFDM is the preferred modulation scheme due to its high spectral efficiency, robustness against multipath reflections, and simple equalizers. The major challenge to implement OFDM in a VLC system is the non-linearity of LED (Kashani & Kavehrad, 2014), which is related to current and voltage characteristics in a semiconductor. OFDM allows adaptive bit and power loading techniques on each subcarrier to enhance the system performance. Asymmetrically clipped optical OFDM (ACO-OFDM) (Burchardt et al., n.d.) is another type of optical OFDM scheme, where Hermitian symmetry is applied. Asymmetrically clipped direct current biased optical OFDM (ADO-OFDM) (T. Q. Wang et al., 2016) is a combination of DC biased optical OFDM (DCO-OFDM) and ACO-OFDM, where DCO-OFDM is used on even subcarriers, and ACO-OFDM is used on odd subcarriers (Islim & Haas, 2019). A novel optical asymmetric modulation scheme was proposed to outperform alternative modulation schemes without any hardware complexity, when it was compared with OOK-based SMP and generalized space shift keying (GSSK) modulation schemes in (Marshoud et al., 2018). A scaling QAM modulation was considered to reduce signal noise in a real-time VLC system in (D. Zheng et al., 2019) and geometrically shaped 8-QAM modulation was proposed for underwater VLC application in (Xingbang Wu et al., 2018). Binary optical orthogonal codes based on CDMA scheme using OOK modulation were demonstrated to achieve high spectral efficiency for multiple user VLC model by Li et al. (Xingbang

Wu et al., 2018). This orthogonal code frame structure outperformed conventional Walsh–Hadamard code in increasing reliability in checking data redundancy in the data interface between Ethernet and multi-user VLC system. Different modulation schemes are used for VLC for different applications, and their performances can vary. They are tabulated in Table 2.4.

When establishing high data rates in VLC networks, single carrier modulation schemes such as OOK, PPM and PAM suffer from non-linear signal distortion and ISI. On the other hand, GSSK scheme has a higher spectral efficiency than conventional OOK and PPM techniques, but the main limitations of this scheme is that its error performance depends on channel gain, which limits data rate and link distance. CAP, OFDM and Hamdamard modulation schemes perform much better to establish long distance VLC communication compared to single carrier schemes in terms of data rate, long distance and spectral performance.

Table 2.4: Different Modulation Methods in VLC

Modulation	**Spectral Performance**	**Data rate**	**Distance**
OOK	High	Low	Short
PPM	Low	Moderate	Medium
PAM	Moderate	Moderate	Medium
CAP	High	High	Long
OFDM	High	High	Long
CSK	Moderate	Low	Short
GSSK	High	Low	Short
Hadamard	High	High	Long

2.5.2.5 Hadamard Coded Modulation

Hadamard coded modulation is an alternative to OFDM modulation for indoor VLC to provide high-speed downlink communication that also requires high average optical powers to satisfy illumination needs. Peak-to average power ratio (PAPR) can cause high amplitude signals in higher-order modulation schemes to be clipped by the peak power constraint of LEDs, which leads to high signal distortion (Noshad & Brandt-Pearce, 2016). Hadamard coded modulation was introduced to achieve low error probabilities in LED-based VLC systems requiring high average optical powers. This technique uses fast Walsh–Hadamard transform to modulate the data as an alternative modulation technique to OFDM (Noshad & Brandt-Pearce, 2016). However, OFDM is not normally ideal for VLC because of transmitted power for eye safety issues (Dimitrov et al., 2012). It has also high PAPR which makes OFDM signals penetrate to non-linear devices (Sheu et al., 2017). Compared to RF outdoor channels, the indoor environment is generally more stable for channel fading.

2.5.3 Wavelength Division Multiplexing (WDM)

WDM permits higher data rates for indoor VLC combined with multiple modulated colored light sources. Most of the experiments done with WDM use RGB LEDs. A typical WDM system with RGB-LEDs is shown in Figure 2.5. However, further channels by using amber (Cossu et al., 2015) or yellow (Yiguang Wang, Tao, et al., 2015) can be used to increase the system data rates. Optical receivers and filters corresponding to each WDM channel or color are used to isolate individual channels with minimum interference. The WDM system's data rate depends on channel SNR, signal power, channel crosstalk, and PD noise. By using 12 WDM channels with different color LEDs, a combined data rate of 5.1 Gb/s was achieved by (Cui et al., 2016). This is more than ten times of the data rate of a single LED channel system. The maximum data rates achieved using WDM were 3.375 Gb/s (Yiguang Wang, Huang, et al., 2015), 4.05 Gb/s (Yiguang Wang, Huang, et al., 2015), and 8 Gb/s (Oubei et al., 2015) over 1 m indoor free space.

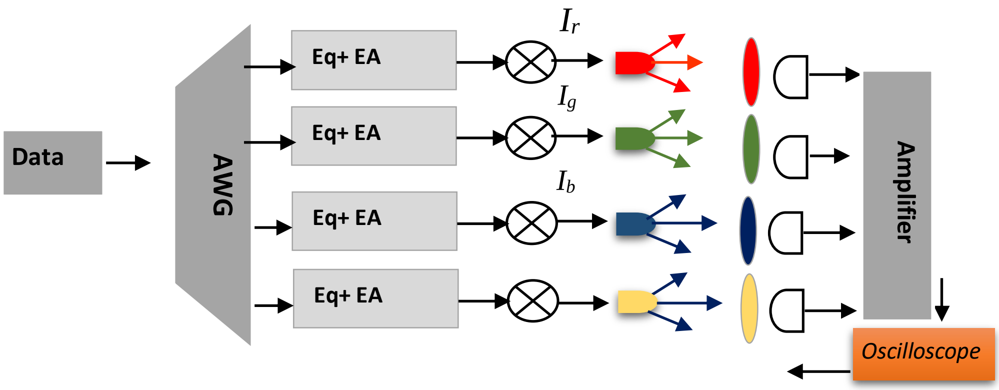

Figure 2.5: Simplified WDM-VLC System using RGBY LEDs (LED Bias Currents are I_r, I_b, I_g, I_y)

The highest data rates in VLC systems have been demonstrated using WDM techniques. Spectrally narrow FWHM LED are also being looked at for enhancing both channel bandwidth and the number of VLC channels.

2.5.4 Equalization Techniques

Equalization can be applied in VLC systems either at the transmitter (pre-equalization), receiver (post-equalization) or both ends at the same time. Pre-equalization targets to extend LED modulation bandwidth or correct the fast deterioration of LED frequency response (Zhou, Liang, et al., 2016). Post-equalization can focus on correcting either frequency-domain or time-domain characteristics of the VLC system. Time-domain corrections reduce ISI, which is required for high-speed data transmission. Some of the time-domain equalization methods include constant modulus algorithm, cascade multi-mode algorithm (CMMA), modified-CMMA, decision directed least mean square (DD-LMS) algorithm and recursive least square (RLS) based algorithm (X. Huang, Shi, et al., 2015). Moreover, pre- and post-equalization techniques can be based on software or hardware. Le Minh et al.(Le Minh et al., 2009) enhanced the LED's modulation bandwidth from 14 to 50 MHz and attained 100 Mbps link by an RC-network integrated first-order analogue post equaliser. Burton et al. (Burton, Bentley, et al., 2014) increased 3 dB bandwidth of the blue LED from 12 to 77 MHz using analogue pre-emphasis circuit. For PAPR reduction, single-carrier frequency-domain equalization (SCFDE) was applied and this resulted in 3.25 Gb/s data rate with pre and post-equalization. Liao et al. (Liao et al., 2014) extended the modulation bandwidth of LED 50 times more and demonstrated 340 Mbps VLC link using two passive and one active equaliser. Zhou et al. (Zhou, Liang, et al., 2016) investigated the difference between software-based equaliser and hardware equaliser and showed software equaliser could provide more accurate equalization. Hybrid modulation approach combined with artificial neural network (ANN) equaliser has been proposed in (Guan et al., 2018). A combination of PAM and PWM was proposed using joint spatial and temporal equalization with an ANN for MIMO-VLC system in (Rajbhandari et al., 2019) for increasing the transmission rate by four times compared to the traditional equaliser based system. In a VLC network employing carrier less amplitude and phase (CAP) based 64 QAM modulation, deep neural network and least mean square (LMS) linear equaliser were used to achieve a data rate of 2.4 Gb/s (G. Li et al., 2019). Moreover, CAP32, CAP64, and CAP128 modulation schemes have been demonstrated with three-stage hybrid post-equaliser to increase the transmission rate of a high-speed LED-based VLC system (Chi et al., 2018). Different equalization techniques for gigabit class VLC system are tabulated in Table 2.5. (Zhou, Liang, et al., 2016)

Table 2.5: Comparison of equalization techniques for achieving Gb/s data rate

Ref.	Data Rate	Equalization	Objectives	Modulation	Comments
(Yiguang Wang, Tao, et al., 2015).	8Gb/s	Post equalization	Eliminate both linear and nonlinear distortions	CAP Modulation	A Volterra series based nonlinear equalizer, and a DD-LMS equalizer.
(X. Huang, Shi, et al., 2015)	4.22-Gb/s	Post-equalization	Improve data rate	m-QAM OFDM	Combination of FDE and decision directed least mean square (DD-LMS).
(M. Zhang et al., 2017)	4.05 Gb/s	Post-equalization	Improve data rate	PS-Manchester coded Nyquist PAM-8	Nyquist filter and hybrid time-frequency equalizer.
(Yuanquan Wang et al., 2014)	3.25 Gb/s	Pre and post equalization	Improve spectral efficiency	m-QAM SC-FDE .	Hybrid equalizer.
(Zhou, Zhao, et al., 2016)	2.32 Gb/s	Pre and post equalization	Decrease low power frequency components and increase high power frequency components.	BPSK/QAM-OFDM	Two-staged linear software equalizer.
(Zhou, Liang, et al., 2016)	2.08Gb/s	Pre equalization	Improve the LED bandwidth from 14 to 50 MHz	OFDM	Compared with hardware and software equalizer.
(X. Huang, Wang, et al., 2015)	1.6 Gb/s	Pre-equalization	To improve data rate	m-QAM OFDM	Constant-resistance symmetrical bridged-T amplitude equalizer circuit.

A novel phase-shifted (PS) Manchester coded Nyquist PAM-8 modulation with hybrid time– frequency domain equalization scheme was proposed, and this was experimentally demonstrated to achieve a data rate of 4.05 Gb/s (M. Zhang et al., 2017). A hybrid post equaliser with CAP modulation was introduced in a VLC system by Wang et al. (Yiguang Wang, Tao, et al., 2015). A hybrid time–frequency adaptive algorithm was implemented with DD-LMS equaliser to attain 4.22 Gb/s in (X. Huang, Shi, et al., 2015). Using four channels of RGBY LEDs, where Y refers to yellow color, 8 Gb/s data rate was achieved using a hybrid equaliser in (Yiguang Wang, Tao, et al., 2015). Table 2.6 shows recent research that used equalization to achieve Gigabit class

Table 2.6: Research in Gigabit-class Performance in Indoor VLC System

Year	Tx	Rx	Modulation	Equalization	Multiplexing	Data rate (Gb/s)	Distance	Ref
2019	RGBY	PIN PD	DCO-OFDM	Dichroic mirrors	WDM	15.73	1.6 m	(Bian et al., 2019)
2019	RGBYC	PIN	64QAM-DMT	UVLC system	WDM	15.17	1.2 m	(Zhou et al., 2019)
2018	RGB	PD	m-QAM OFDM	Adaptive bit & power	WDM	10.2	50 cm	(Bian et al., 2018)
2015	RGBY	PIN PD	CAP	hybrid post-equalizer	WDM-VLC	8	1 m	(Yiguang Wang, Tao, et al., 2015).
2014	RGBY	APD	DMT		WDM	5.6	1.5 - 4 m	(Cossu, Wajahat, et al., 2014)
2019	RGBY	APD	64QAM-DMT	2x2 MIMO with FPGA	WDM	5.0	2 m	(Shi et al., 2019)
2016	µLED	PD	DCOFDM	N/A	-	5	1 m	(Ferreira et al., 2016)
2019	µLED	PD	64QAM-OFDM	3x3 MIMO	-	4.81	1 m	(Koester et al., 2015)
2015	RGB	PIN PD	CAP	RLS based adaptive equalization	WDM	4.8	1.5 m	(Oubei et al., 2015)
2014	RGB	PD	512QAM + OFDM	Decision-directed least mean square (DD-LMS) post-equalizer.	WDM	4.22	1 m	(X. Huang, Shi, et al., 2015)
2017	RGB	PIN PD	PAM-8	PS-Manchester coded Nyquist and Hybrid Time-frequency domain Equalization	WDM	4.05	1 m	(M. Zhang et al., 2017)
2015	LD and RGB LED	PIN PD	32QAM + OFDM	N/A	FDM+TDM	4	65cm	(C. Lee et al., 2015)
2016	RGB	PD	PAM-8	PS-Manchester coding and S-MCMMA equalization.	WDM	3.375	1 m	(Chi et al., 2016)
2014	RGB	APD	512QAM + OFDM	single carrier frequency domain equalization (SC-FDE)	WDM	3.25	65 cm	(Yuanquan Wang et al., 2014)
2013	RGB LED	APD	CAP modulation	Pre-compensation and decision feedback equalization (DFE)	EDM	3.22	25 cm	(F.-M. Wu et al., 2013)
2019	Blue LED	PIN	64QAM-DMT	UVLC system	WDM	3.08	1.2 m	(F. Wang et al., 2019)
2014	µLED	APD	OFDM	Pre-equalization and adaptive bit and energy loading.		3	5 cm	(Tsonev et al., 2014)
2016	LED	PD	OOK	High-sensitivity integrated circuit (IC) receiver	CMOS Technology	2.5	12 m	(Fahs et al., 2016)
2016	Pc LED	PIN PD	BPSK-OFDM	Two-staged quasi-linear software equalizer		2.32	1 m	(Zhou, Zhao, et al., 2016)
2015	Micro RGB LED	APD	DMT	by adjusting input power and bias current of the LEDs	WDM	2.3	1.5m - 4 m	(Manousiadis et al., 2015)
2016	Pc LED	PIN PD	BPSK, PSK, 8/16QAM-OFDM	software pre-equalization		2.08	1 m	(Zhou, Liang, et al., 2016)
2016	Pc LED	PIN PD	16QAM-OFDM	a cascaded bridged-T amplitude pre-equalizer		1.6	1 m	(X. Huang, Wang, et al., 2015)

performance in indoor VLC systems.

2.5.5 Multiple Input Multiple Output

MIMO systems are generally used in RF, such as 4G and LTE, to achieve higher data rates. Multiple LEDs are used as multiple transmitters to get higher illumination, and higher spectral efficiency in VLC systems and PDs, APDs or image sensors are used in the receiver side to detect the light signal (Zeng et al., 2009). Individual PDs or APDs fall under non-imaging receivers, which are a set of independent photodiodes, which have individual light sensing points. These receivers have a very high gain because of their narrow FOV, but very accurate alignment is needed between transmitters and receivers for high capacity transmission. These receivers have to rely on the MIMO decoding algorithm for detection of signals. The designs of imaging and non-imaging optical MIMO systems are shown in Figure 2.6.

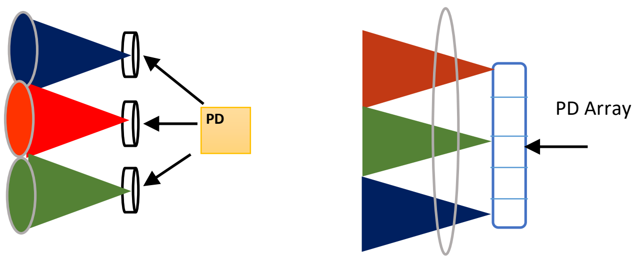

Figure 2.6: a) Non-imaging Optics b) Imaging MIMO System

Since an image sensor contains a projection lens and a large matrix of photodiodes, it has a higher potentiality to create a MIMO link. Slight miss-alignment is not considered as a barrier for the received signal throughput due to its large FOV. In the non-imaging MIMO, a separate focusing lens is required in front of each PD. A hybrid VLC MIMO receiver combining imaging and non-imaging sensor has been shown to achieve high data rate with broader FOV and lower path loss (O'Brien, 2009). Three different popular VLC MIMO systems have been reported in the literature. The first one is repetition coding MIMO, where equal signal is transmitted from each LED in an array to increase overall gain (Fath & Haas, 2012). The second one is SMP, where each LED transmits different data (in this MIMO system multiple parallel single input single output channels are created) (Takase & Ohtsuki, 2004). The third one is spatial modulation (Chau & Yu, 2001), where a single LED transmits data to every PD at the same time (Chau & Yu, 2001). The receiver estimates which LED is activated based on the received signal because each LED is allocated a specific symbol and data. Butala et al. (Butala et al., 2014) proposed a new framework to characterize the performance using SM and SMP normalization under both imaging and non-imaging receivers. Without Hermitian symmetry and using polar coordinate, an optical MIMO special modulation scheme has been proposed to convert the complex signal to real positive signal by Kim et al. (J. Kim et al., 2019). Generalized SM (denoted by MGSM) transmission technique for multi-user VLC system is analyzed by Jha et al. (Jha et al., 2019). They compare its performance with conventional MIMO and SMP MIMO. In their work, generalized MIMO outperforms over conventional SM MIMO and SMP MIMO. Moreover, dimming conditions are used to completely eliminate the flicker effect on human eye using MGSM (Bui et al., 2018). To improve the spectral efficiency of the O-OFDM signal for time/frequency domain, a fully generalized index-spatial LED modulation scheme has been proposed in (H. S. Hussein & Hagag, 2019) and for 16×16 MIMO-OFDM in (Yesilkaya et al., 2019). In addition, improvement of spectral efficiency by SM combined with space shift keying and spatial pulse position modulation was investigated by Olanrewaju et al.(Olanrewaju et al., 2018). PAM-based low low-complexity SM receiver algorithm was designed for multi-channel VLC according to the polarity of LEDs (L. Wu et al., 2019) and to reduce mode dependent loss of multi-mode optical fiber in (Damen & Othman, 2019). Link capacity of the MIMO system is measured by Shannon's channel capacity formula as follows

$$C = Blog_2(1 + SNR) \tag{2.6}$$

where C is the channel capacity in bits/Hz, B is the bandwidth. The MIMO scheme can increase the transmission speed with the minimum number of Tx and Rx. The received signal at any discrete-time instance k for a MIMO system is given by

$$y(k) = H_x(k) + n(k) \tag{2.7}$$

where x(k) is an (n ×1) vector of the transmitted signal, **y**(k) is an *(n ×1)* vector of a received signal, *n(k)* is an *(n×1)* noise vector, and H is a *(n x m)* channel matrix. The channel H-matrix is given by

$$H = \begin{bmatrix} h_{11} & h_{12} & h_{1m} \\ h_{21} & h_{22} & h_{2m} \\ h_{n1} & h_{n2} & h_{nm} \end{bmatrix} \tag{2.5}$$

where *hij* is a channel gain between Tx and Rx. The channel H-matrix must be full-ranked for an optimum MIMO system.

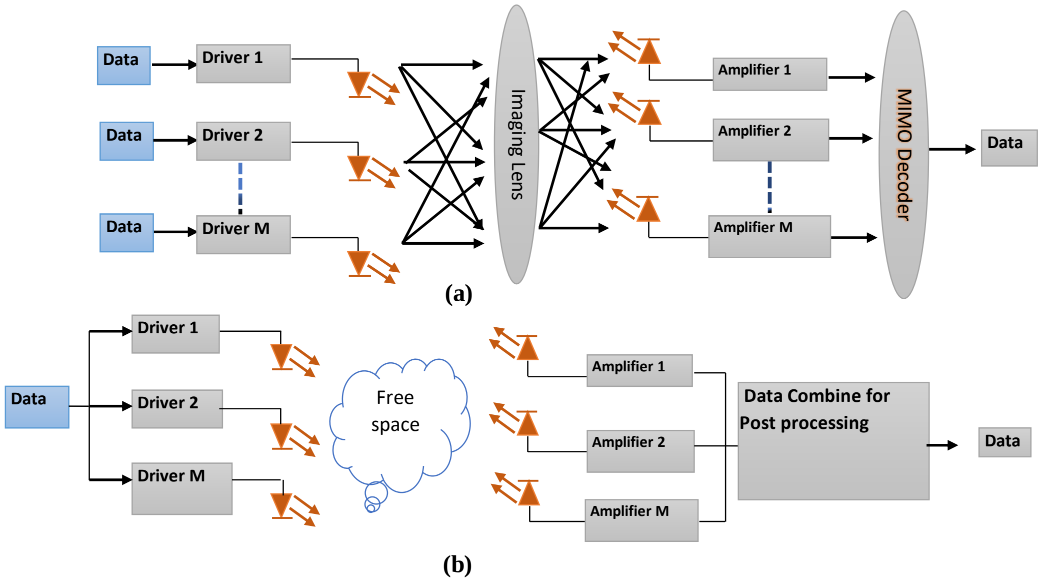

Figure 2.7: Individual Driver to Drive Multiple LEDs using (a) Ganging Method and (b) MIMO System.

Figure 2.7 shows that this multiplexing capacity is proportional to the minimum of transmitters M and receivers N. MIMO Visible Light Communication (MIMO-VLC) is a promising broadband communication method because of its low power consumption and high capacity.

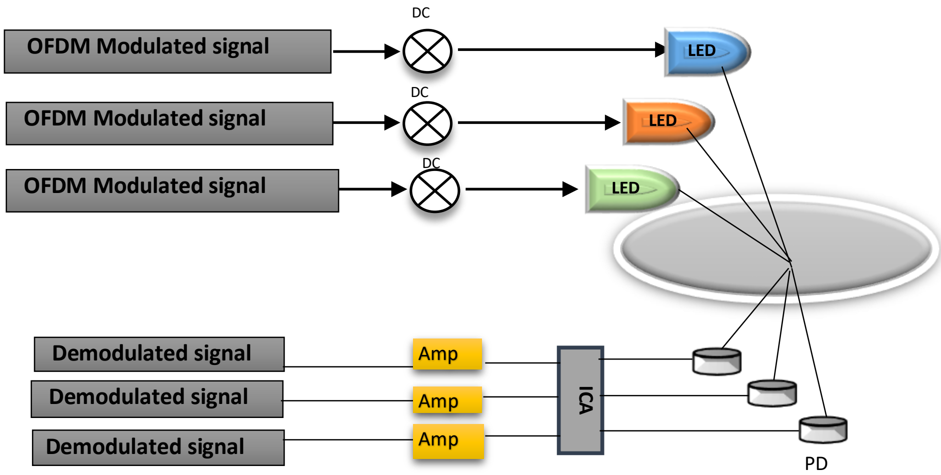

Figure 2.8: ICA based MIMO-OFDM System

The MIMO technique has been proposed to increase the data rates in (Collins et al., 2015). Using special μLEDs, 4 × 4 imaging MIMO system has been demonstrated to achieve a data rate of 920 Mb/s (Burton, Le Minh, et al., 2014). Multiband CAP (m-CAP) modulation schemes are used to improve the MIMO transmission quality. A numerical study has shown that SMP has a higher spectral efficiency than SSK (Butala et al., 2014) using a system with four transmitters and one receiver. To reduce the channel equalization complexity, independent component analysis (ICA) based efficient blind source techniques were proposed in (Jiang et al., 2015) to separate the mixed VLC MIMO signals. This system is shown in Figure 2.8. Least square (LS) and minimum mean square error (MMSE) algorithms were used for channel estimation, which reduce the computational complexity of the MIMO scheme. FPGA-based universal software radio peripheral devices were used to allow adaptive communication MIMO signals (P. Deng & Kavehrad, 2016). The authors used three different MIMO systems spatial diversity, SMP, and SM (Di Renzo et al., 2013) to maximize the spectral efficiency of a 2 × 2 MIMO system. Popoola et al. (Popoola et al., 2013) studied GSSK scheme to increase spectral efficiency in MIMO. SSK is also applied in a 3 × 3 imaging MIMO-OFDM system with commercial PC white LEDs (Ijaz et al., 2015). This application increased the modulation bandwidth of white LEDs from 10 to 100 MHz (Hsu et al., 2016). Moreover, 3 × 3 non-imaging MIMO system with a pre-equaliser circuit was used to extend the bandwidth of an LED from 14 to

103 MHz in (Popoola et al., 2013). Andrew Burton et al. experimented 4×4 non-imaging MIMO channel to get 50 Mbps data using NRZ-OOK (Burton, Le Minh, et al., 2014). Zero forcing with pseudo-inversion, MMSE, and vertical Bell labs layered space-time algorithms are popular to reduce the complexity of MIMO de-multiplexers.

2.5 Hybrid VLC Network Architectures

In a VLC network, downlink typically consists of LED transmitters for illumination purposes. The uplink can be constructed using other transmitters and receivers. This leads to hybrid systems. Two different versions of these hybrid systems are explained in the sections below. After that, the integration of VLC systems with other types of networks is discussed.

2.5.1 Hybrid Networks with VLC Based Downlink

LED based VLC system are using LEDs for downlink data and as a transmitter technology. For up-link transmission, data quality degradation is the main concern for the VLC system and most of the current studies are based on IR or RF system based uplink (Basnayaka & Haas, 2015). Hybrid network based on IR LEDs and RF system uplink are discussed here.

2.5.1.1 IR Based Uplink

IR light covers wavelength from 780 nm to 1 mm adjacent to the visible light range between 380 and 780 nm. IR band is not licensed and can offer high-speed connectivity. IR cannot penetrate objects, because of its high frequency range and hence it is mostly used in indoor environments. The data rate of IR can reach up to 1 Gb/s and the signal can be carried over a distance of several meters (Boucouvalas et al., 2015). IR communication can occur in defused mode, also known as scatter mode.

The transmitter and receiver do not need to be in the line of sight (LOS) in this sort of communication. However, the communication devices must be close to one another. Otherwise, it would be difficult to establish an indoor wireless network. IR LEDs are mainly used for uplink transmission in VLC networks. In (Alresheedi et al., 2017), a fast adaptive beam steering IR (FABS-IR) system is proposed to reduce the channel delay and enhance the received optical power signal in a high data rate communication. A typical system that uses IR for uplink transmission and VLC for downlink transmission is shown in Figure 2.9. The performance of the system is enhanced by coupling FABS-IR with imaging receivers. It is found that data rate up to 2.5 Gb/s is possible for the indoor environments using IR-VLC network.

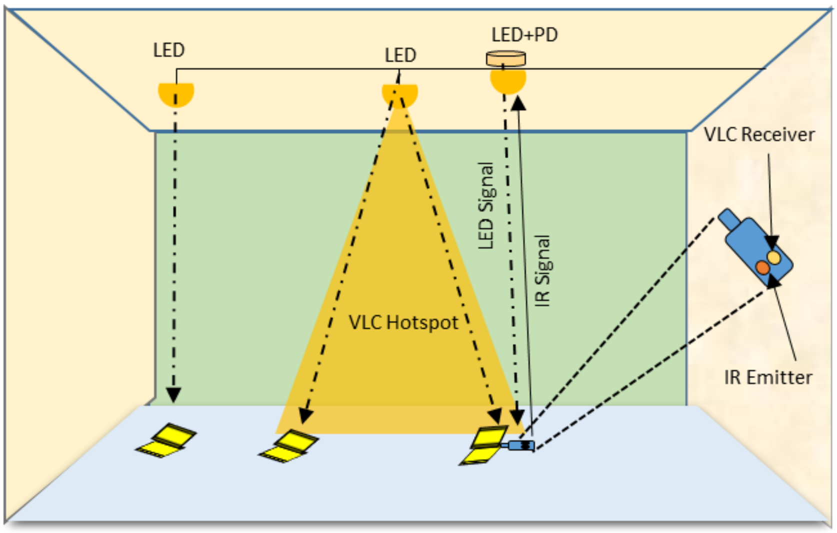

Figure 2.9: IR-VLC Communication Model using USB

Another research developed a VLC-IR system for passengers to access the internet in airplanes. The VLC-IR system does not interfere with airline radio systems; thus, it can provide personalized entertainment utilizing wireless media. Even in the presence of other illumination sources, it can ensure good functional capability, good downlink signal strength for receivers, and minimum error rate for a short distance (2 m) communication. Moreover, the system is evaluated for live video streaming and collaborative games.

2.5.1.2 WiFi Based Uplink

Hybrid networks have high throughput with dense positioning of optical access points (APs). It enhances the system performance, quality of service (QoS), and mobility among users. This heterogeneous (VLC and RF) network can reduce interference between these two systems and increase the combined throughput in the same area network. Radio devices can operate under the main three center frequencies 2.4, 5, and 60 GHz based on IEEE 802.11ad standard and commercially known as Wireless Gigabit Alliance (WiGig).

LED and RF combined hybrid bi-directional network has been demonstrated to communicate with the central unit (CU) with a data rate of 7 Gb/s (C. Lee et al., 2015). The universal AP mechanism and the handover protocol are essential for this heterogeneous integrated network to perform multitask in the mobile environment. As a result, future wireless terminals are proposed as multi-standard supporting wireless devices. In this regard, VLC can be a complementary technology with the existing radio-based technology to provide service in indoor environments. Rahaim et al. (Rahaim et al., 2011) proposed two different types of vertical handover (VHO) schemes between radio and optical communications, such as immediate VHO, dwell VHO, and fuzzy-logic-based VHO integrated algorithm for WiFi-IR LED system. Horizontal handover and VHO protocols are presented to support VLC HetNet (heterogeneous) model, especially for solving the multiuser mobility problems.

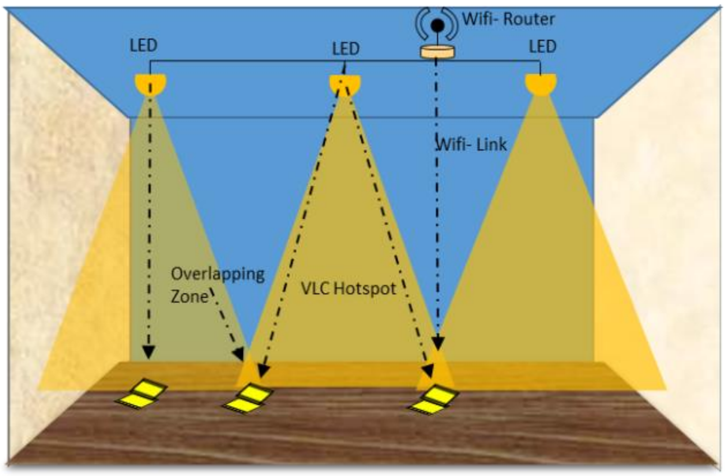

Figure 2.10: Heterogeneous (VLC and RF) Network

Subsequently, each user is assigned to a CU through an AP. Figure 2.10 shows a typical heterogeneous (VLC and RF) network hybrid model within a room condition where WiFi and VLC networks are working together, and users can move from one AP to another AP.

In between, if there is any low light signal or interruption, the user will automatically connect to the Wi-Fi network. Shao et al. (Shao et al., 2015) designed and analyzed an integrated system, which is Light Radio (LiRa) WLAN without any mobile devices to emit light or infrared. The bi-directional Wi-Fi and VLC links are fully utilized in this LiRa system to improve the achievable throughput and uplink channel network controller. VLC uplinks will need narrow beam widths lighting sources for better communication throughput, but need multiple LEDs to provide proper illumination avoiding shadows connected to a single light source. To minimize VLC controller latency and broadcasting Wi-Fi traffic for VLC downlink AP-Spoofed Multi-client ARQ (ASMA) hybrid system was designed by Naribole et al. (Naribole et al., 2017). Hybrid FSO and WiFi hybrid system based on optical femtocell architecture was used to maximize mobility and to achieve a data rate of 50 Mbps over 3 m distance for each femtocell by Liverman et al. (Liverman et al., 2018). This Wi-Fi system could perform seamless handover from one AP to another, and a microcontroller was used to handover from an FSO transmitter to a Wi-Fi supported optical receiver. Abdallah Khreishah (Khreishah et al., 2018) demonstrated a hybrid RF-VLC system to reduce the power consumption using VLC front-ends designed by Fraunhofer-HHI and Wi-Fi with a dual Band Gigabit Wireless Router WNDR4500, while maintaining acceptable level of illumination. Furthermore, Kashef et al. (Kashef et al., 2016) investigated the energy efficiency of an indoor heterogeneous network constrained by the required data rates consisting of RF and indoor VLC AP. Marwan Hammouda et al. presented a cross-layer study of a hybrid RF/VLC system for sustainable QoS constraints considering limitations of data overflow, delay probabilities, random user location, and effective capacity in the main link.

2.5.2 VLC Based Downlink and Uplink

VLC system used LEDs and LD for downlink data as a transmitter technology. These two transmitter technologies sometimes use for up-link data transmission. So visible light based downlink and uplink system are given below.

2.5.2.1 LED-PD Based Downlink and LD-PD Based Uplink

LD and LED-based hybrid VLC system is shown in Figure 2.11. The receiver consists of both photo-sensors and LD. LD is used for uploading data to the hybrid AP. VLC systems with LDs can achieve Gb/s data rates and they can be used for long-distance communication.

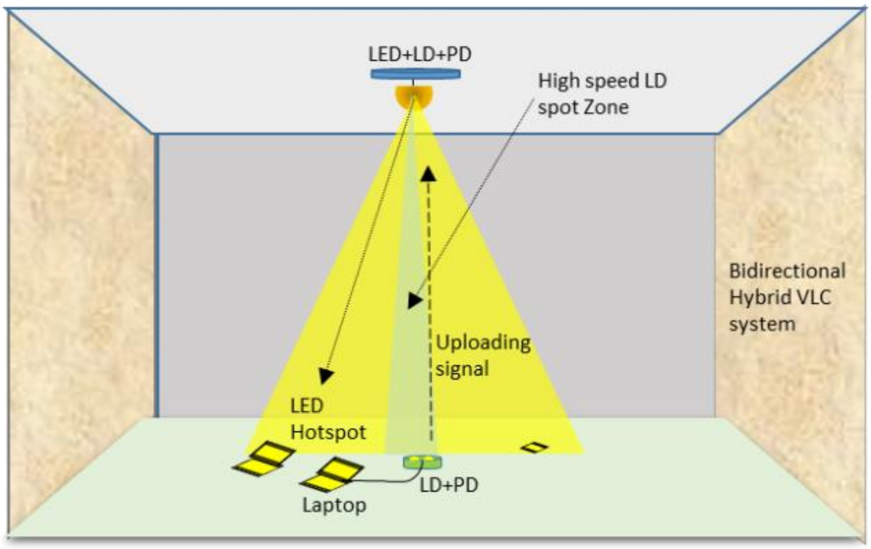

Figure 2.11: LD and LED-based Hybrid VLC Network

Janjua et al. (Janjua et al., 2015) demonstrated 4 Gb/s VLC link with RGB LD, where red LD was used for communication, and blue and green LDs were used for illumination. Hussein et al. verified 5 Gb/s data rate link by OOK based LD-VLC systems with the modelling work (A. T. Hussein & Elmirghani, 2015).

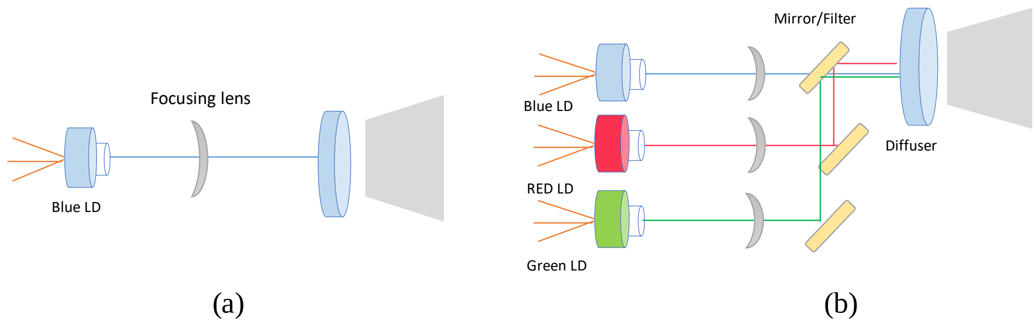

Figure 2.12: White Light Generation by Utilizing (a)Single Source Approach and (b) Multi Source Approach

Figure 2.12 shows the techniques to generate white light by LD. The white light can either be generated by using a blue LD with phosphor coating with a focusing lens or by mixing three color (RGB) LD sources. However, LEDs have superior performance for illumination and hence they are preferred for downlink communication (Bian et al., 2019). However, the uplink communication can be designed without much consideration for illumination. For this reason, this can be achieved through LD, because of its superior modulation bandwidth. This hybrid solution has gained attention for gigabit-class communication (see the “LD-LED VLC” column of Table 2.7).

2.5.2.2 LED-to-LED Based Downlink and Uplink

In a typical VLC system, the photodetector is used as a receiver, and LED is used as a transmitter. Most of the experiment has been performed with a one-directional (downlink) VLC scheme. In order to get full advantage of the large bandwidth of the VLC system, it is preferable to use a bi-directional VLC system for uplink and downlink communication. To implement a bi-directional VLC system, LED and photodetector have to be used at both downlink and uplink (Schmid et al., 2013)(Schmid, Ziegler, Corbellini, et al., 2014). However, an LED to-LED VLC model has been demonstrated based on the theory presented in (Dietz et al., 2003). The capacitance of the LED changes with receiving light intensity. In Zurich, Disney Research center demonstrated a VLC link relayed to a toy car using a smartphone

(Schmid, Ziegler, Gross, et al., 2014). The apparent disadvantage is that LED is less sensitive to the light; thus, a high-intensity light is required. Multiple LEDs can be used for transmitting and receiving of data for this purpose. This implies the necessity of multiplexing techniques. Fine tuning is needed to maintain the LED illuminated without any important data being transmitted, but it will reduce the maximum data rate that could be achieved. In (Yiguang Wang, Chi, et al., 2014), a full fiber integrated LED-to LED VLC system is proposed, where fiber-optic link is utilized to connect each VLC AP (VAP). The authors designed a hybrid system protocol using frequency division multiplexing (FDM) and time division multiplexing (TDM) for the uplink and downlink in the fiber and bi-directional VLC transmission. Total data rate achieved was 8 Gb/s using eight VAPs, each having a data rate of 500 Mb/s. It is possible to extend the same network architecture to achieve up to 100 Gb/s for a wireless access network. Li et al. (Shuai Li et al., 2016) suggested a scheme that utilizes LED-enabled devices to interact on a di-directional VLC channel without using a PD, while offering quality illumination at the same time. The authors employed Manchester coding with OOK modulation to achieve the best trade-off between lighting and data rates. In (Yeh et al., 2017), a 682 nm visible vertical-cavity surface-emitting laser is used to attain 10.5 Gb/s downstream traffic and 2 Mb/s upstream traffic using QAM-OFDM modulation scheme.

2.5.3 Heterogeneous Networks with VLC

mmWave for short haul communication and VLC for indoor communication can be the most promising technologies in the 5G communications era to establish gigabit-class data transmission link. These kind of heterogeneous VLC network discussions are presented here.

2.5.3.1 PLC-VLC Hybrid Model

Typically, power line communication (PLC) is used to link all VAPs internally and externally to the remainder of the network. VLC needs connectivity between VAPs and internal networks to provide a completely functional indoor system. Connecting VAP using separate cables is the easiest solution. This simple VAP connection through distinct cables is quite costly because of its cabling design, labor, and installation process. PLC uses the electrical power lines which already exist for broadband connection (I. 1901 W. Group, 2010). PLC has been effectively used for over a decade to broadcast radio programs, home networking, home automation (remote lighting and equipment control), web access, and automated meter reading (Galli et al., 2011). PLC has the benefit of its reliable infrastructure like VLC, which is easily accessible. A hybrid WiFi–VLC system called PLiFi is proposed that provides low-cost internet connectivity, VAP inter-connectivity, and seamless WiFi integration for uplink transmission (Hu et al., 2016) for better user mobility and frequently changing device orientation. In order to resolve co-channel interference owing to neighboring LEDs in a hybrid PLC–VLC system, a narrower and distributed VAP together with a MAC protocol was proposed in (Ndjiongue et al., 2017), where the authors analyzed the impact of PLC channel and VLC transmitters on signal propagation. To determine the transfer function for channels characterizing over time, the accessible channel frequency response was used. PLC–VLC's cascaded channel route may have many impairment sources, but not restricted to attenuation and unwanted noise. Their hybrid model pretends to analyze the attenuations of the cascaded channel correctly. However, noise is ignored, which in the PLC–VLC setting can be a cause of deficiency. Yan et al. conducted experiments with three-LED lights to create a single frequency network to investigate the possibility of VLC-PLC hybrid system for indoor communication (Yan et al., 2015). Their scheme ensures high-speed communication and higher coverage of the signal with less alteration of the current infrastructure. Similar research is proposed in (J. Song et al., 2016), where a full-duplex hybrid PLC–VLC system uses marginal protocols to obtain a data rate of 5 Mb/s, which can be extended up to 30 Mb/s.

2.5.3.2 5G mmWave-VLC Hybrid Model

Hybrid radio-over-fiber (RoF)–VLC system was demonstrated by Khalid et al. (Khalid et al., 2011). For the first time, they reported hybrid RoF–VLC system where optical fiber was used as a backbone network to link user and main central office. 5G systems have much higher capacity, data rate, spectral efficiency, and energy efficiency compared to the existing 4G systems. mmWave spectrum has also become a promising technology for 5G networks to enable gigabit-class transmission. The mmWave band refers typically to the frequency range from 3 to 300 GHz with wavelengths ranging from 1 to 100 mm (Rangan et al., 2014). Compared to mmWave, VLC has similar advantages, such as broad spectrum, the ability to support gigabit-class data rates, high security, license free, low co-channel interference, interference-free communications, and so on (Feng et al., 2016). A probable bi-directional RoF-VLC hybrid system, where mmWave 5G will be used for uplink and LED will be used for downlink is shown in Figure 2.13. A large amount of traffic can be off loaded from mmWave-based systems to VLC-based systems.

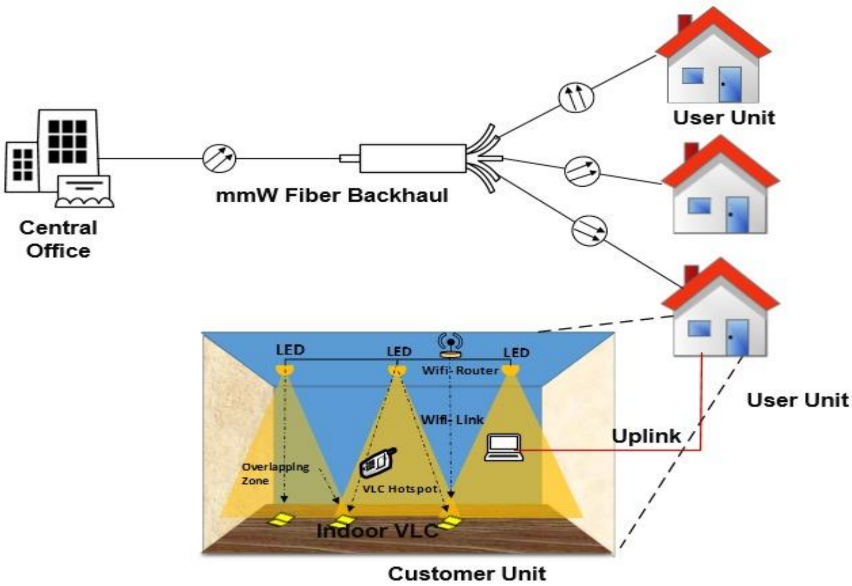

Figure 2.13: 5G mmWave based RoF-VLC Communication Model

Table 2.7: Different Hybrid-VLC Network Architectures

	IR-VLC	WiFi-VLC	LD-LED VLC	LED-LED VLC	PLC-VLC	mmWave-VLC
Link connectivity		Bidirectional WiFi & VLC				
Uplink	Infrared link	WiFi	Laser diode	LED	WiFi AP+ Ethernet PLC modem	5G antenna
Downlink	LED	LED	LED	LED	PLC+LED via PLC VLC modem	mmWave signal+LED
Handover scheme	Coordinated multipoint transmission (CoMP) handover / Homogenous Poisson point process (HPPP)	Immediate vertical handover (I-VHO) scheme/ Fuzzy logic (FL)-based dynamic handover	N/A	N/A	N/A	Markov Decision Process (MDP)
Energy efficiency	Highest	Less		High	Low	Medium
backhaul	Fiber	Auto cell	Wireless/ Fiber	Wireless/Fiber	Power line	Supercell
Signal attenuation	Low	high	Low	Low	high	Medium
Frequency range	300 GHz and 430 THz	2.4 GHz	> 300 GHz	400–790 THz	~30 MHz	~40 GHz
Frequency brand	Terahertz waves	RF waves	Terahertz waves	Terahertz waves		millimeter-waves

2.6 Recent Commercial Advancements

One of the LED-based VLC application is LiFi that holds different challenges to 5G technology. LiFi system provides reliable and secure communication with high data rate. Some commercial companies are trying to develop VLC solutions for end users in the last few years, such as pureLiFi, Philips Lighting, Huawei, Velmenni, OledComm, Firefly LiFi, Allnet GmBh, and Nextlifi. Their target is to provide smart lighting and maximum data transmission under Global Light Communications Standards 802.11bb. PureLiFi first demonstrated a Gigabit LiFi kit in a tiny chip, where the data rate was 1 Gb/s. Moreover, they produced an integrated laptop, LiFi enabled luminaire, photosensitive mobile casing, and silicon chip (data rate of 86.4 Mbps for maximum 16 users) (PureLifi, 2019). Oledcomm is a French company that started in 2011 and works on LiFi technology. It provides complete LiFi solutions using their microcontroller based modem, LiFi photo-receivers (dongles or bridges), and dedicated LiFi Cloud for online and offline. Recently, they demonstrated a product called LiFiMax that offers 100 Mb/s speed for 16 users within the range of 92 feet and an LED desk lamp with 23 Mb/s data rate. They are also working on medical services like centralised intravenous additive services (Lifi Application, 2020). US-based VLC research company VLNComm developed a bi-directional Li-Fi enabled USB adapter 'LumiStick 2' with a downlink speed > 108 Mb/s, an uplink speed of 53 Mb/s and a FOV of 120°. In 2018, they offered a Li-Fi LED lighting panel for industry applications that can be used for more than 500 users (VLNComm, n.d.). Some other emerging companies, such as Signify, Velmenni (India), Nextlifi (currently known as Diodar, Australia), Firefly LiFi (Germany) are trying to bring new products for energy efficient lighting, IoT services, and smart city technologies and infrastructure (Signifi, 2019).

2.7 Challenges in VLC

The usage of LEDs has been increasing in lighting and data communication, but there are still some challenges that have to be noted for future research in VLC applications. These are listed below:

a. Mobility and coverage: High-speed VLC applications consider a narrow line-of-side link that can be utilized for a solid state device of LEDs. There are some fundamental challenges to achieve high-speed VLC, such as high spatial density because of higher inter-carrier interference (ICI), small coverage area, and frequent handover for mobility. ICI can be minimized using different wavelengths at adjacent cells, but, for illumination, changing wavelengths is not permitted in VLC. Therefore, a MIMO concept can be introduced where the receiver can solve the ICI problem. For frequent hand-over, transmitter divergence angle and diffuse link coverage area have to be minimized.

b. Modulation bandwidth of LEDs: The lighting industries are still using PC blue LED to produce white light. However, it has a bandwidth limitation, because of the slow responsivity of phosphor that causes a substantial barrier for gigabit-class communication. If the industries realize the additional revenue that could be generated by using different types of LEDs with better modulation bandwidth, this can influence the market penetration of VLC.

c. Commercialization: Though VLC has prospective applications for high-speed transmission and illumination, the business market expansion will take time. A survey forecasts that the annual growth of VLC will be increased from 2014 to 2020 might be over 87% (Ravi Singh, 2020). Few companies, such as Pure LiFi (UK), Disney (Switzerland), Phillips (Netherlands), Huawei Communications (UK), OLED Communication (France), AXRTEK (US), and HHI (Germany) are involved in the development of VLC system, and they are also offering commercial solutions. VLC business market depends on the progress of optical wireless eco-friendly green communication in the future. One of the crucial challenges to implement VLC setup is to offer a cheaper price product for mass users (Jovicic et al., 2013).

d. Non-linearity: The characteristic of voltage-current relationship of LEDs is non-linear, and this non-linearity has a significant impact on the amplitude and phase distortion. For higher order modulation schemes such as OFDM, the non-linearity effect can result in high PAPR (Oubei et al., 2015). Nonlinearity can be minimized by setting an optimized biasing point for LEDs using adaptive equalizers.

e. Merging with existing systems: VLC has to compete with the current RF network for high-speed secure data transmission. However, some innovative research is going on to integrate the VLC with the existing wired and wireless infrastructure. Significant work needs to be done in developing hybrid networks to help VLC penetrate in the market.

f. Levels of illumination: In a high-speed VLC network, it is necessary to keep satisfactory illumination levels with required CCT and CRI values. Different illumination levels are needed for various conditions, e.g. street lighting, indoor lighting in a big conference room, underwater, and so on. For a standard indoor environment, the required illumination is around 300–1000 lux to get proper white light. Maintaining this illumination level with high-speed VLC link is quite challenging. At night time, the light also should be dimmed to minimum power to minimize illumination. With this power, continuing communication simultaneously can be even more challenging.

g. Receiver design: A PD or an imaging sensor is used as a VLC receiver. The use of PD is more suitable than other receivers, because of its larger FOV, which can be aligned with an LED to receive high optical power. Current imaging sensors show slow performance in data communication, and they consume more energy. Thus, it is challenging to design a receiver for better device movements and FOV alignment.

2.8 Applications of VLC

Flawless high-speed internet service is required for IoT applications, human interaction, and automated industrial machinery. Different applications have different requirements, such as big storage for big-data, high-speed connectivity, security, an uninterrupted connection between machines and a server. Considering all those requirements, VLC could provide a better solution for all kinds of future applications than RF communication. Some of the prospective applications of VLC are given below:

a. ITS: The lightning infrastructure is beginning to adopt LEDs for building lights, street lamps, and automotive lights. VLC is now considered for communication between vehicle-to-vehicle (Rihawi et al., 2016) and vehicle-to-central office (Arnon, 2010). To make VLC viable for ITS applications (Căilean & Dimian, 2017) in outdoor environments, some other factors such as ambient light, fog, rain, and smoke have to be considered.

b. Underwater communications: VLC has a strong capability for underwater communication, specifically for high-speed aquatic transportations, underwater communication, vehicle to vehicle, and vehicle to driver communication (Oubei et al., 2015). RF signal is currently used for long distance underwater communication. However, it suffers from low transmission rate and high latency due to the ocean's salty water and high attenuation. Hence, LD based VLC is considered as a suitable candidate for underwater transmission, which can effectively overcome the limitations of microwave or sound waves also (Popoola et al., 2013).

c. Indoor positioning: Global positioning system (GPS) technology does not work properly in indoor environments, but an indoor positioning system is crucial for tunnels, coalmines, supermarkets, exhibition halls, and hospitals. VLC can be used for indoor localization and navigation systems (Luo et al., 2017). VLC-based positioning systems are less responsive to multipath transmission, and location accuracy is much better than RF-based indoor positioning systems.

d. Intelligent lighting: Automated lighting systems can control the lighting based on users' needs. LED-based VLC systems can be used for intelligent lighting, because of LEDs' switching capability, low energy consumption, and color control ability. Recently, Philips made an intelligent lighting control system that can control the color and dimming using a smartphone (Philips Hue, 2017). An integrated sensor board was used to control the smart home lighting infrastructure by Tang et al. (Tang et al., 2017). Across the globe, most of the lighting industries are involved in producing smart lighting services. There is an expectation that transportation networks and IoT will be connected using VLC.

e. Other applications: VLC system can be used in applications related to hospitals, mines, and petrochemical plants (Cossu et al., 2011). Most of the medical equipment requires isolation from radio frequency interference (RFI), and VLC is suitable for providing communication between medical equipment and staff. An inbuilt communication network can provide industrial lighting and safe communication within the areas with igneous materials (Tang et al., 2017).

2.9 Summary

The limitations of the bandwidth in RF communication encourage the use of visible light as a medium of communication in VLC. LEDs are commonly used as VLC transmitters because of its energy efficient quality and duel capabilities for communication and illumination simultaneously. All these literatures examined VLC link structures for high-speed communication with transmitter, modulation and receiver technologies. Some key advantages of LED technologies, types of LEDs, their bandwidth capacity, fabrication process, and economic expectations in the near future. In this chapter, the existing literature associated with the basic fundamental of VLC network in terms of communication and the techniques used to achieve high data rate VLC (i.e. in the range of Gb/s) are presented. The growing trend towards replacement of traditional lighting infrastructures with energy efficient LEDs opened up the scopes for concurrent data transmission and illumination industry. Advanced research and innovative techniques that can push the data rate from Mb/s to Gb/s range for VLC were also highlighted in this study.

Considering the high demands and growing number of wireless communication devices, optical wireless communication is required at gigabit class range, which can be effectively delivered utilizing WDM techniques in VLC. However, how the total visible light frequency spectrum can be utilized for this purpose has not been explored in the literature. Although, the of RGBY/RGBA LED-based VLC systems are already implemented for WDM system, how the number of channels can be increased beyond this systematically has been explained in the literature.

InGaN/GaN based MQWs LED has the promising future in terms of communication aspects, so proper modelling and fabrication process of this is necessary to increase the number of channels for VLC. This can help to increase the data rate of VLC.

VLC can be used for downlink indoor communication with high data rates. For uplink, different alternatives are being explored. This leads to hybrid or heterogeneous networks. RoF-VLC system is one possible heterogeneous network. How this network can be designed in such a way to accommodate high number of channels for VLC downlink and high data rate for uplink is still an open question in the literature.

Recent commercial advancements in VLC and the challenges to overcome were also highlighted in this review. Some of the prospective applications of VLC such as intelligent transportation system, LD based underwater communication, indoor positioning and intelligent lighting were also briefly explained in this review.

CHAPTER THREE

GIGABIT WDM - VLC SYSTEM

3.1 Introduction

In the previous chapter, different types of techniques to improve the data rate in VLC system such as WDM, high order modulation techniques, MIMO-OFDM, special pre and post equalization methods and usage of high bandwidth LEDs were highlighted. With the increasing demand for VLC in the applications of Lifi, vehicle to vehicle communication (V2V), robotics, IoT, and underwater communication, the data rate demand has increased further. In a WDM system, where LEDs transmit independent data streams with different colors or channels, commercially available off the shelf pc-LEDs are mostly used in VLC applications due to their cost and availability. However, μLEDs or UV LEDs and LDs can also be used in VLC. It was also discussed how a WDM system is implemented in LED based VLC system and their ability to provide a high data rate. Based on this, the following research questions can be asked:

- How do RGBA LEDs influence the aggregate data rate as individual WDM channels under different modulation schemes?
- How do the multipath reflection constraints and FOV affect the data rate?

In this chapter, the effect of using RGBA LEDs with modulation schemes NRZ-OOK and 16 QAM in a WDM-VLC system has been investigated. The results were obtained using simulation and experiment. Mathematical model for a single VLC channel, WDM –VLC system, and multipath reflection with LOS and NLOS propagation in VLC system in Section 3.3. In Section 3.4, the simulation approach for WDM-VLC and multipath system are described. After that, the experimental setup used for WDM-VLC system is illustrated. Finally, the results from the simulation and experiments are described and compared in Section 3.6. These WDM-VLC systems form as a baseline work for the subsequent chapters.

3.2 Wavelength Division Multiplexing (WDM) System

WDM system can transmit higher data rates due to multi-channel concept as each colored LED use as an individual channel, which can be modulated separately. On the receiver side, optical filters are used to recognize individual channel wavelength. WDM helps to increase the aggregate data rate due to multiple parallel data streams. Though multiple VLC channels can be considered by applying RGB LEDs or LDs, the output should be a proper white light (Tanaka et al., 2003). The fundamental operation of WDM systems using red, green, blue, and yellow channels is described in Figure 3.1.

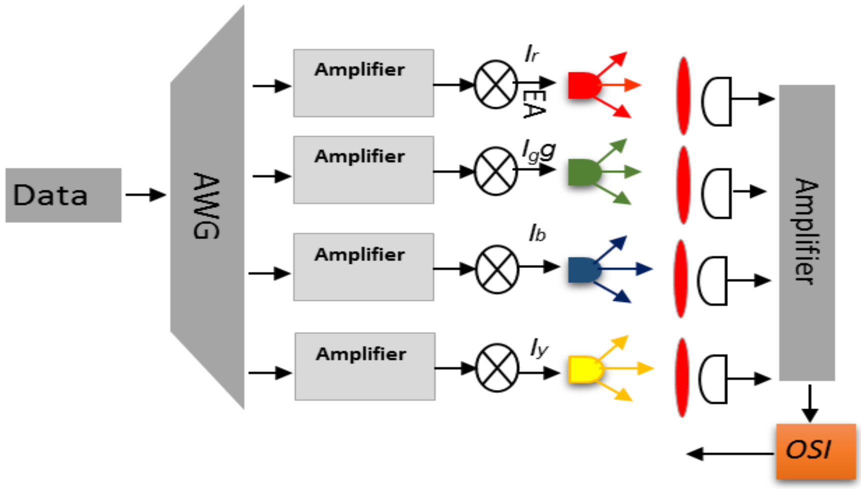

Figure 3.1: WDM-VLC system using RGBY LEDs with biasing current I_r, I_b, I_g, I_y

The performance of each WDM channel will be different and depends on output power, range of optical filters and photodetectors' responsivities. Typical WDM-VLC system demonstrations have used RGB LEDs (Vučić et al., 2011). However, additional channels using amber or yellow can be used to increase data rates further and each LED can be controlled independently. The highest data rate in VLC system has been demonstrated up to 15.73 Gb/s using off the shelf RGBY LEDs (Bian et al., 2019).

Table 3.1 shows the comparison difference between WDM-VLC system performances using off-the-shelf LEDs. There are usually two types of photodetectors used in VLC systems: PIN PD and avalanche PD (APD), which has comparatively higher gain. Spectrum slicing or WDM technology is generally used in fiber-optic communication, and it also implemented into the high-speed VLC system. RGB LEDs

Table 3.1: WDM-VLC system related research

Tx	Rx	Modulation	Equalization	LED type	Data rate	Distance	Reference
RGBY	PIN PD	DCO-OFDM	Dichroic mirrors	Off-the-shelf	15.73Gb/s	1.6 m	(Bian et al., 2019)
RGBYC	PIN	64QAM-DMT	UVLC system		15.17 Gb/s	1.2 m	(Zhou et al., 2019)
RGBY	PIN PD	OOK	hybrid post-equalizer	Off-the-shelf	477 Mb/s	0.4 m	(Ravinder Singh et al., 2013)
RGB	APD	OFDM	Pre-equalizer	Off-the-shelf	410 Mb/s	0.9 m	(Cossu et al., 2011)
RGBY	PIN	OOK	N/A	Off-the-shelf	614 Gb/s	0.4 m	(Fujimoto & Yamamoto, 2014)
RGB	PIN	16QAM	Bidirectional link		575 Mb/s	0.66 m	(Yuanquan Wang et al., 2013)
This Research (RGBY)	PD	OOK 16 QAM	N/A	Off-the-shelf	240 Mb/s 1.10 Gb/s	3 m	Thesis

are used as the optical source of the VLC system and the three or more colors are considered as different channels of the visible light spot zone. The maximum data rate of 15.73Gb/s, 15.17 Gb/s and 477 Mb/s have successfully achieved by the RGB and RGBY-LED with different equalization, OFDM/DMT modulation scheme (Bian et al., 2019), (Zhou et al., 2019) and (Ravinder Singh et al., 2013) simultaneously but their distance was below 2m. In the research work, (Fujimoto & Yamamoto, 2014) received 614 Mb/s data rate with RGBY LED, but the distance was only 0.4 m. In other work, (Cossu et al., 2011) and (Yuanquan Wang et al., 2013) received data rate about 410 Mb/s and 575 Mb/s with OFDM and 16 QAM modulation, but the distance also were 0.9m and 0.66m only. In this work, the length has been extended to 3m and, without any offline processing or high order modulation scheme, received 240 Mb/s data by OOK and 1.10 Gb/s data using 16 QAM signal.

3.3 Mathematical Model for Single LED WDM and Multipath System

In a WDM-VLC system, multichannel LEDs work as a separate channel, and optical filters are mandatory to recognize them. However, channel crosstalk can be increased because of the LEDs' overlap when additional channels are added. In this model. Optical peak power is a function of an input current and the responsivity of the LED which is calculated by

$$\rho = \sigma.h.f.\frac{i(t)}{q} \tag{3.1}$$

where σ is quantum efficiency, f is the emission frequency, h is the Planck's constant, and q is the electron charge, and $i(t)$ is modulating current. Modulated current depends on electron lifetime and the device of the diode as a transfer function, which is

$$H(f) = \frac{1}{1+j.2.\pi.f.(\tau_n+\tau_{rc})} \tag{3.2}$$

Where τ_n is electron lifetime and τ_{rc} is RC constant. LEDs have Lambertian radiant intensity emission, which can be explained using equation (3).

$$R_i(\emptyset) = (m_l + 1)cos^m(\emptyset)/2\pi \tag{3.3}$$

$$m_l = -ln2/ln(\cos(\emptyset_{\frac{1}{2}})) \tag{3.4}$$

where $\emptyset$ is irradiance angle, ml is the order of Lambertian emission, which relates to the LED's semi-angle at half power $\emptyset_{\frac{1}{2}}$ as shown in Equation (3.4). Luminance expresses the brightness of an illuminated surface. Field of view (FOV) is one of the important factors of LED-based transmission link. Color optical filters can change the light propagation range, which affects the active region of the receiver or FOV. The gain of the receiver photodetector is given by (Al-kinani et al., 2016).

$$P_r = H_d(0)P_t \tag{3.5}$$

where P_r is the received power, P_t is the transmitted power by LED, and $H_d(0)$ is DC channel gain of the VLC link. If the direct line of sight (LOS) is considered, then the equation of the DC gain in the (Sivabalan & John, 2003)

$$H_{d(0)} = \begin{Bmatrix} \frac{(m+1)A}{2\pi d^2} \cos^m(\theta) T_s(\psi) \ell(\psi) \cos(\psi) \\ 0 \le \psi \le \psi_c, \psi > \psi_c \end{Bmatrix} \tag{3.6}$$

where $\ell(\psi)$ is the gain of FOV concentrator, Ψc is the field of view at receiver, d is the distance between LED and photodiode receiver and m is the Lambertian emission, which is related to LED's half-power semi angle

If the reflected path is considered, the DC gain is (Sivabalan & John, 2003)

$$H_{ref(0)} = \frac{A(m+1)}{2\pi(d_1 d_2)^2} A_{wall} \cos^m(\theta_r) \cos(\beta_r) T_S(\psi) \ell(\psi) \cos(\psi) \tag{3.7}$$

where d_1 is the distance between transmitter and reflected point, d_2 is the distance between a reflected point and receiver PD. A_{wall} is the reflective area of the wall, θ_r is the irradiance angle from the reflected point, α_r is the incident angle at the reflected point, and β_r is the angle of irradiance to the receiver, ψ_c is the angle of incidence from the transmitter. In a VLC system, the received power at a point for both the direct and the first-order reflected paths is given by (Miramirkhani & Uysal, 2015)

$$P_r = \sum \left\{ P_t H_d(0) + \int P_t \, dH_{ref}(0) \right\} \tag{3.8}$$

The total path delay can be calculated from multipath receive power levels. Total delay spread is given by

$$D = \sqrt{\delta^2 - (\delta)^2} \tag{3.9}$$

where the mean value of delay is

$$\delta = \frac{\sum_{i=1}^{M} P_{d,i} + \sum_{j=1}^{N} P_{ref,j}}{P_r T} \tag{3.10}$$

$$\text{and} \quad (\delta)^2 = \frac{\sum_{i=1}^{M} P^2{}_{d,i} + \sum_{j=1}^{N} P^2{}_{ref,j}}{P_r T} \tag{3.11}$$

The total data rate of the VLC link in the multi-channel reflection environment depends on the delay of the propagation path. Furthermore, total power gain can be increased by narrowing the angle of the FOV of the LED. The most significant noise source in VLC systems is shot noise arising due to striking to the detector. Shot noise Gaussian distribution of the detector is modeled as (Al-kinani et al., 2016)

$$\sigma_{shot}^2 = 2.q.\left(i_{sig} + i_{noise}\right).ENB \tag{3.12}$$

where Gaussian distribution is a randomly generated value between 0 and 1. Another significant noise source is thermal noise within the receiver front end of the PD, which is calculated as follows (Sivabalan & John, 2003).

$$\sigma_{thermal}^2 = \frac{4.k_B.T}{R_L}.ENB \tag{3.13}$$

T is the device's absolute temperature, R_L is the receiver load resistance, and k_B is the Boltzmann Constant, and ENB is receiver equivalent electrical noise bandwidth (ENB). The total noise at the output up to pre-amplifier is then

$$\sigma(f) = \sigma_{shot}(f) + \sigma_{thermal}(f) \tag{3.14}$$

Moreover, noise calculation such as thermal noise, shot noise, signal-ASE noise has important effects on signal bandwidth and total bit rate of the system

3.4 Simulation Approach for WDM-VLC

To make the high-speed gigabit class VLC research baseline, a WDM-VLC system with NRZ-OOK and 16 QAM modulation schemes was designed by optical simulator Optisystem. The distance between transmitter and receiver was considered 3m. The simulation model was fit according to the preliminary experimental results, and data rates was achieved 290 Mb/s for OOK and 1.16 Gb/s for 16QAM using simulation.

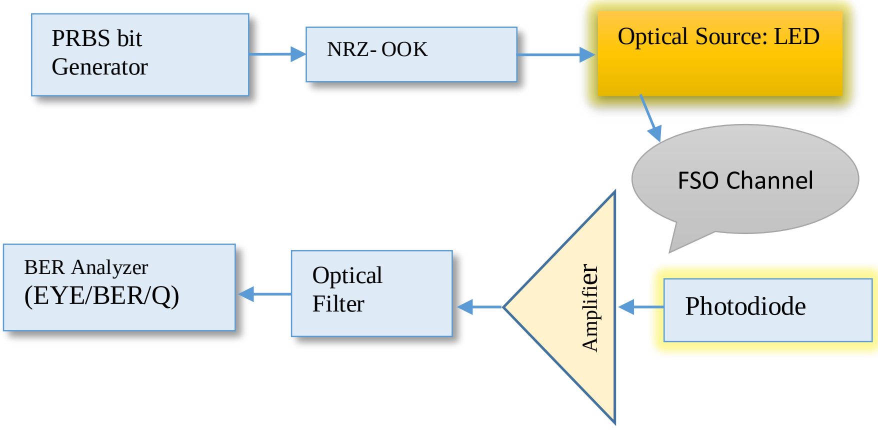

Figure 3.2. Model of NRZ-OOK based VLC system.

Figure 3.2 shows the simulation model for OOK-VLC model. Most of the VLC research has been done using Red, Green, Blue, Yellow, or Amber (RGBYA). QAM-VLC model was modeled in Optisystem, and the expected results were over 1 Gb/s. A 16-QAM based VLC system was designed as an input signal and generated the electrical constellation plot. Figure 3.3 shows the simulation model for the QAM-VLC model.

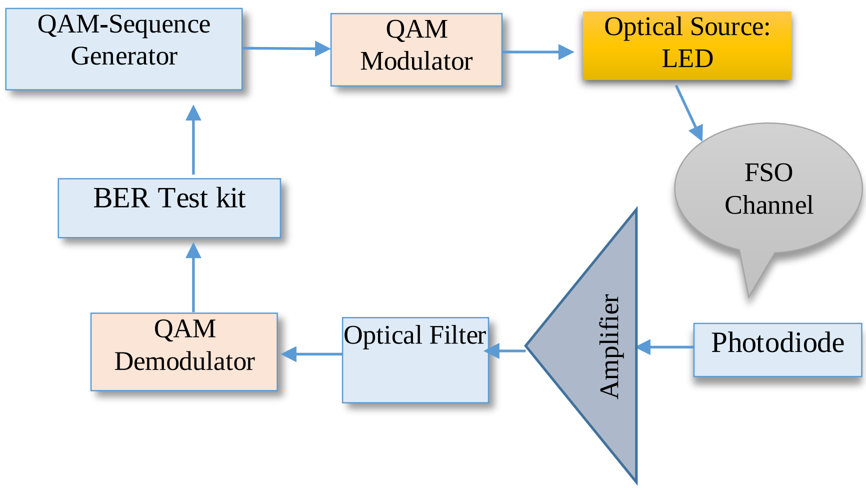

Figure 3.3: Simulation model of 16QAM-VLC

3.4.1 Multipath Reflection Analysis

To design the conventional multipath indoor communication, Barry et.al (Barry et al., 1993) have proposed a multipath diffusing link. Recently, LED-based VLC has attracted the attention of lighting industries, and academic researchers, because of its maximum transmission and illumination capability (Beshr et al., 2012). VLC channel can have two different paths: line of site (LOS) and non-line-of-side (NLOS).

The main advantage of LOS is a high-speed communication capability. Still, it also has some limitations such as shadowing effect and small coverage area (M. Beshr, C. Michie, and I. Andonovic, 2015), which are not suitable for mobile users. The mathematical derivation of the LOS and NLOS channel links with reflected path and total receive power calculation is explained in section 3.4.1.2. VLC systems can be investigated in a multi reflection environment using Optisystem simulation tools (Din & Kim, 2014). When the distance between the transmitter and the receiver increases, the data loss decreases. The transmitter and receiver of VLC system should be in line of sight (LOS) condition for optimal signal quality, but the ambient light or reflected light from surrounding walls for NLOS degrades the actual link performance. This section analyzes visible light communication performance by considering LOS and N-LOS propagations for data rate and the output power of the LEDs. In LOS propagation, only the direct path with a single LED as a transmitter was considered. For the NLOS case, both single LED and multiple LEDs are considered as transmitters. Some key global parameters for multipath reflection analysis are given in Table 3.2.

Table 3.2: Global and Major Parameters for the Simulation

	Parameters	**Value**
Transmitter	Wavelength(nm)	550
	Electron life time, T_n(ns)	4.5 ns
	RC constant, T_{RC} (ns)	4.5 ns
	Slope efficiency (W/A)	
Channel	Distance	3m
	FOV concentrator	45 deg
	Tx half angle	60 deg
	Irradiance angle	20 deg
	Incident angle	20 deg
Receiver	Modulation bandwidth	45 nm
	Responsivity (A/W)	0.65
	Thermal power density (W/Hz)	100 e^{-24}
	Noise distribution	Gaussian

3.4.1.1 Case 1: LOS/NLOS Propagation Model with Single LED

In this propagation model, both the direct and reflected paths of light was considered. For LOS, direct path and for NLOS condition, two side (2D) multi reflection are considered for the single LED. For multiple, propagation model considered is shown in Figure 3.4. Three propagation scenarios was considered (i) Direct LOS using a

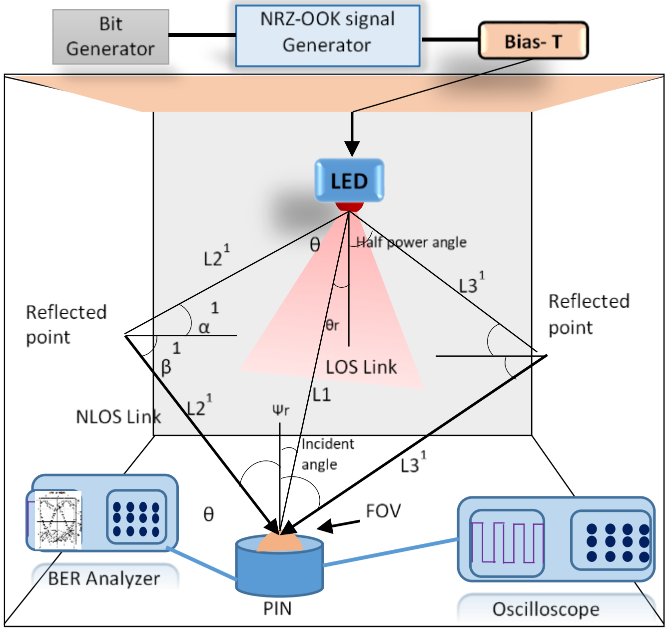

Figure 3.4: Simulation model for multipath indoor VLC

single LED, (ii) Direct plus two reflected paths NLOS for a single LED (for 2D environment) and (iii) Multi reflected propagating paths using multiple LEDs. After 3m in free space, desired light signal is received by photo detector (PD) and filtered out unwanted ambient light using a low pass filter. For the reflected path calculation, 2~5 dB attenuation was added to account for the drop in signal quality in reflections. The standard indoor condition was considered in this simulation, where the distance between transmitter and receiver was 3m and consider that all light is coming from LED.

Moreover, no interference was considered for point-to-point links, and incident and irradiance angles were set based on practical experience. The LED radiates red light with 550 nm wavelength, which carries the optical information and is passed through a diffuser lens. PIN photodiode is used to receive the light signal at the receiver end and filtered through a low pass Bessel filter to remove the optical frequency interference. This component converts an optical signal into electrical signal based on device's responsivity. Here silicon photodiode was used among Ga, InGaAs and other user defines materials. The central frequency was followed the same as LED's visible range peak wavelength.

3.4.1.2 Case 2: Multi Reflection Propagation Model with Single LED

In the multi reflection propagation model, LOS path and other 4 reflected light signal from 4 walls (3D environment) was considered as shown in Figure 3.5. Multi reflection propagation model with a single LED which reflects from surrounding four walls. All direct and reflected light signal received at PD and received signal degraded by the reflected light.

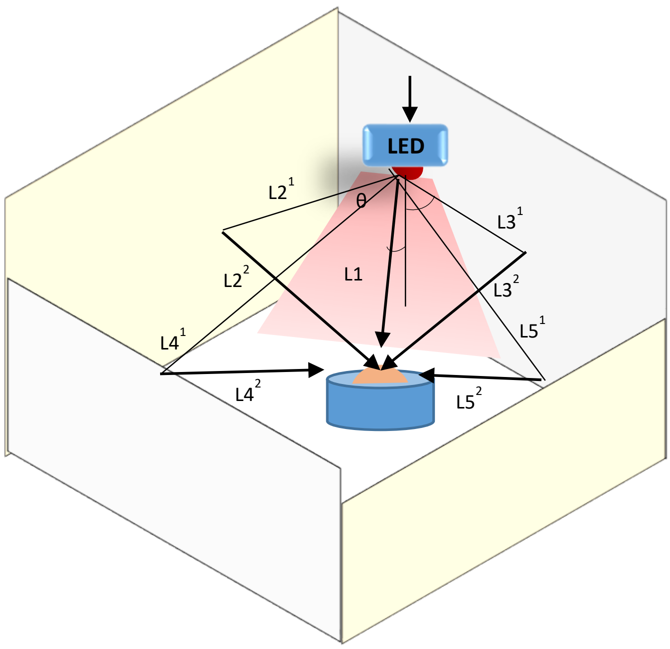

Figure 3.5: Multi reflection NLOS propagation model using single LEDs.

3.4.1.3 Case 3: Multipath Propagation Model with Multiple LEDs

In Case 3, multiple LEDs were considered for both LOS and NLOS links, where L1 and L4 are direct paths, and L2, L3, L4, and L6 are reflected paths, as shown in Figure 3.6. Incident angles, irradiance angles, received optical power, and BER is tabulated in Table 3.7. BER for the signal from LED1 was 2.27×10^{-7} and, for LED2, was $1.83 \times 10^{-10.}$ Average BER for both LEDs was around $2.17 \times 10^{-5,}$ and the related eye diagram is shown in Figure 3.12.

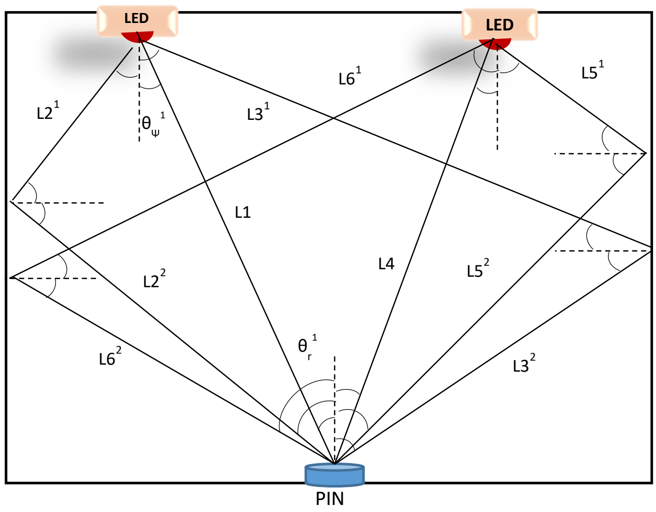

Figure 3.6: Multipath VLC propagation model using multi LEDs.

3.5 Experimental Setup of WDM-LED-VLC

A list of devices used for the experimental analysis is provided in Table 3.3 and the experimental setup is in Figure 3.7 using the numbering specified in Table 3.3. The complete VLC system used in this work is depicted in Figure 3.2. This experimental setup investigates only Case I mentioned in Section 3.4.1.1. The line of sight (LOS) VLC link uses an off the shelf RGBA LED (OSRAM LCW CP7P). The LED was attached to a heat sink to ensure the effect of the junction temperature variation is minimized during the experiments. Using blue filtering, the bandwidth of the RGBA LED can be extended to ~ 60 MHz (Grubor et al., 2008).

A low pass optical filter (Thorlabs FES500) was used to remove the slow component and increase the system bandwidth. The modulated waveforms were generated using ARB Rider Arbitrary Waveform Generator AWG-4022. It has two channels, each of which can sample up to 2.5 GS/s, 2.5 GHz analog bandwidth, and 14-bit vertical resolution. MATLAB ® was used to create the required waveforms with different modulation schemes which were uploaded to the AWG. A power amplifier was used to amplify the signal connected after photodiode. A wideband coaxial bias tee (Mini Circuits ZFBT-4R2GW-FT) was used for biasing the LED at the operating region and combine to the DC power supply with the high frequency modulated waveforms, and it operates at 350 mA. A circular lens (15° beam angle) was fixed in front of the LED to focus the light on the receiver.

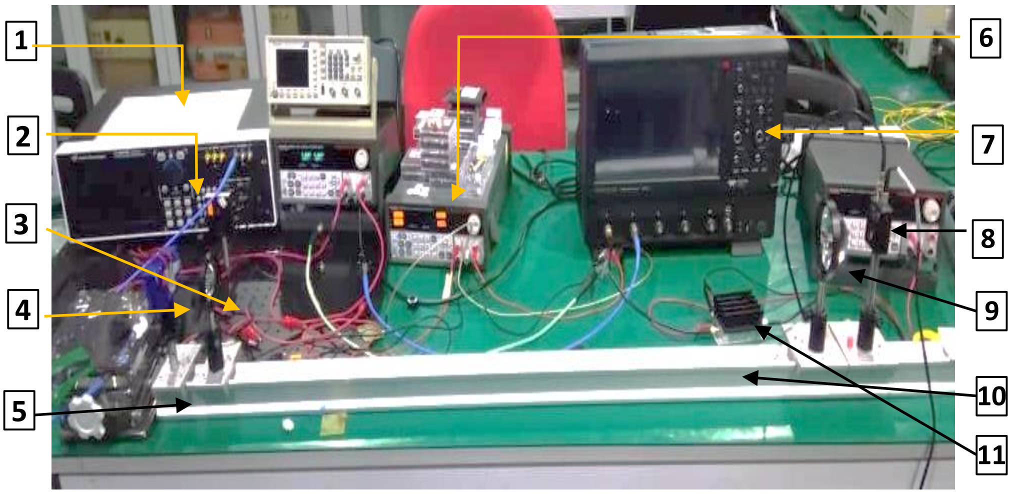

Figure 3.7: VLC Experimental Link Setup

A Silicon PD (Thorlabs PDA-10A) was used as the receiver in this experiment which has an active detection area of 0.8 mm2; wavelength sensitivity ranges 200-1100 nm, with a peak responsivity of 0.45 A/W. Initially, NRZ-OOK signal was used for the experiments. The sampling rate of the AWG was set as 10 MS/s, and the frequency of the signal was defined up to 60 MHz. Each sample carries one bit for the experiment, and initially it was 60 Mb/s.

For the experiment, single carrier modulation scheme was implemented with available RGBA LEDs. Using OOK, the aggregate data rate was 160 Mb/s, and using 16QAM was around 1.04 Gb/s. This result is better than (H. Li et al., 2014) but also suggested that it might be improved after applying equalization (Fuada et al., 2017).

Table 3.3: Equipment Lists for Experiments

1	ARB Rider AWG-4022 (2.5 GS/s, 14 bit)
2	LED Holder
3	Bias Tee (Mini circuits) ZFBT-4R2GW-FT DC power
4	LED Oslon NUWH CCT ~4000k (LED as a Transmitter)
5	Heatsink
6	DC Power supply
7	Oscilloscope Wave runner 8254 (2.5GHz , 20 GS/s)
8	Photodiode Thorlabs PDA 10A (VLC Receiver)
9	Optical lens (Thorlabs ACL4532U)
10	Optical rail (stage- Thorlabs)
11	Amplifier Mini circuit ZHL-6A+

3.6 Results and Discussion

WDM-VLC system is demonstrated to establish the system's maximum transmission rate using RGBA LED based on the simulation framework presented in Section 3.4, and the findings from sections 3.5. Simulation approaches consist of WDM-VLC model with OOK and 16QAM, Multipath reflection analysis for the VLC, and the effects of FOV on the received power. Finally, a comparison of simulation work and experimental results will be shown.

3.6.1 Simulation Results

The maximum data rate with related BER has been tabulated in Table 3.4. BER analyzer is used to monitor the bit error rate of an electrical signal and eye diagram.

System transmitter LED has been configured as off the shelf LED which has recombination time was set to 4.9 ns Using 16QAM signal, the aggregate data rate can increase 4 times higher than OOK. After transmitting data up to 3m, the constellation diagram for 16 QAM was recorded, and the total data rate was 1.16 Gb/s have shown in Figure 3.8.

Table 3.4: Total data rate from 4 channels of WDM-VLC systems by OOK

Peak Wavelength	BER	Data rate (Mb/s)
420	3.29×10^{-6}	78
525	2.35×10^{-8}	69
610	1.15×10^{-8}	58
645	9.88×10^{-8}	85

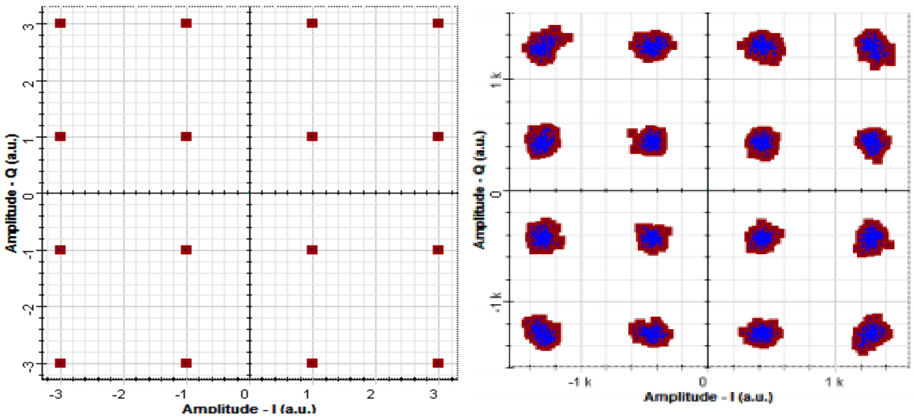

Figure 3.8: Constellation plot of (a) Transmitter and (b) Receiver after demodulated the signal.

3.6.1.1 Results for Case 1

The room dimensions have considered 3m x 3m x 3m. The simulation results for the LOS model is shown in Figure 3.9, and it shows the input and output signals from the oscilloscope and related eye diagram. BER observed was 1.42×10^{-11} and the received optical power level was measured at receiver around -16.39 dBm.

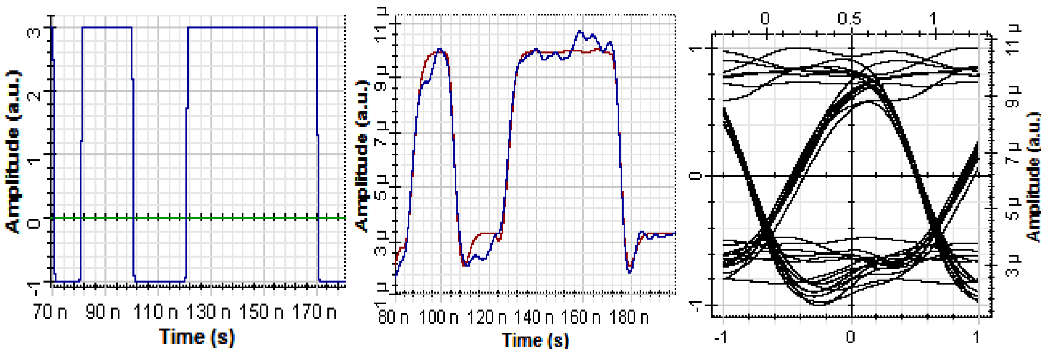

(a) input signal (b) output signal (c) eye diagram

Figure 3.9: (a) input signal (b) output signal and (c) related eye diagram.

In the duel NLOS model with a single LED, one direct and two reflected paths were considered. L1 is the LOS link, and L2, L3 are two NLOS channels as shown in Figure 3.10. The reflections degraded the overall BER from 10^{-11} to 10^{-7}. Table 3.5 shows the received power and BER after reflections.

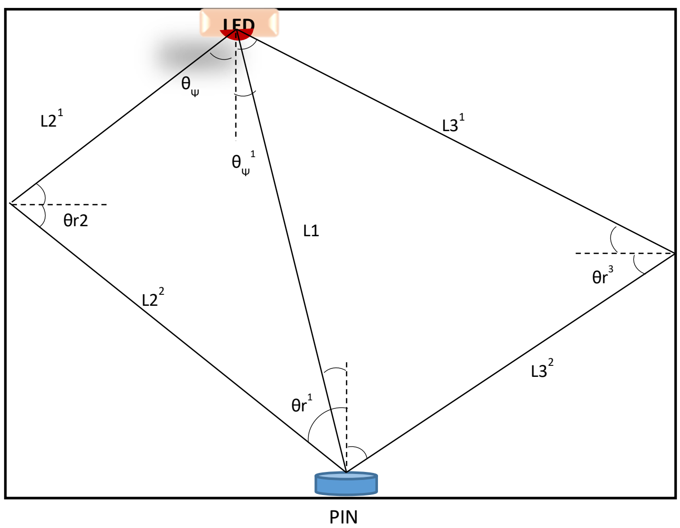

Figure 3.10 Duel NLOS reflection propagation model using single LEDs.

Table 3.5: Results and Parameters of the Single LED Model

LED 1					
Path	**Length (m)**	$\boldsymbol{\theta_\Psi}$	$\boldsymbol{\theta_r}$	**Rx Power**	**BER**
L1	3	22	25	-19.20	
$L2^{1}$	2.5	60	65	-23.38	
$L2^{2}$	1.5	35	60	-71.16	3.36×10^{-7}
$L3^{1}$	1.5	50	45	-21.27	
$L3^{2}$	2.5	38	52	-72.81	

3.6.1.2 Results for Case 2

Figure 3.11 shows the output signal and eye diagram based on the LOS path and LOS path including reflections. More reflections were added in the NLOS model with a single LED, where L1 is the LOS link, and L2-L5 are four NLOS links. The received powers, in this case, are shown in Table 3.6. The overall BER degraded to 10^{-6}.

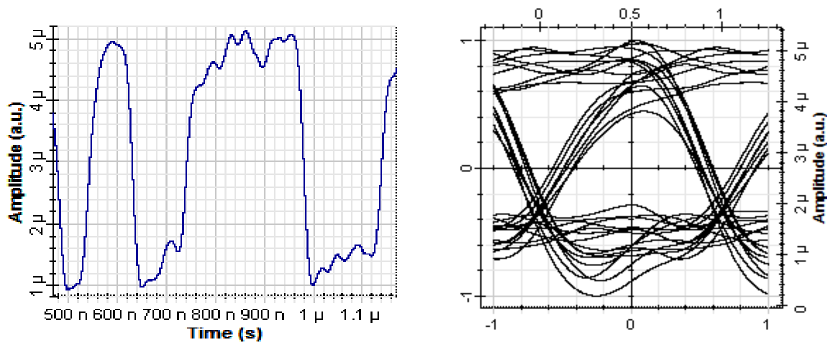

(a)

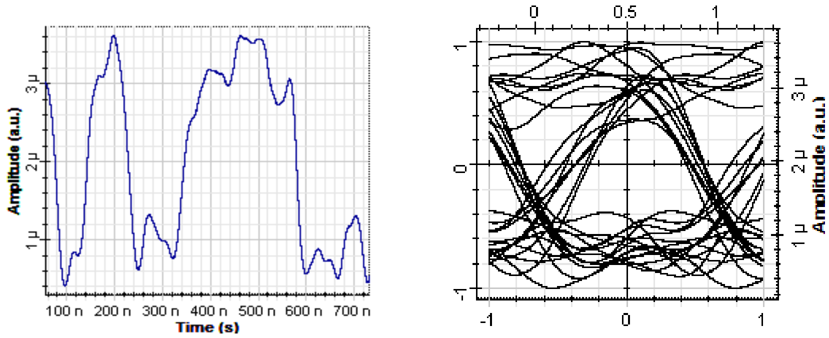

(b)

Figure 3.11: (a) Output signal and related eye considering LOS paths (b) Output signal and related eye for five propagating link paths

Table 3.6: Results of four reflected path using single LED

LED 1					
Path	**Length**	**θ_Ψ**	**θ_r**	**Rx Power**	**BER**
L1	3	22	25	-19.20	3.82×10^{-6}
$L2^1$	2.5	60	65	-23.38	
$L2^2$	1.5	35	60	-71.16	
$L3^1$	1.5	50	45	-21.27	
$L3^2$	2.5	38	52	-72.81	
$L4^1$	2.5	55	35	-25.15	
$L4^2$	2	50	40	-72.92	
$L5^1$	2.5	43	48	-23.03	
$L5^2$	2	40	60	-72.92	

3.6.1.3 Results for Case 3

Most of the available VLC models have been designed based on LOS for its simplicity. However, some reflected light from different surfaces and NLOS needs to be considered at the receiver (Kahn & Barry, 1997). The LOS component has a flat channel bandwidth, while the NLOS diffuse channel shows a much weaker response and the magnitude drops off significantly with frequency. The overall combined wireless channel shows a slight ripple due to the LOS and NLOS paths' frequency components interfering. VLC system performance degrades with the surrounding environment though surrounding reflections have a minor effect.

Table 3.7: Results of multipath two LED's NLOS model

LED 1					LED 2				
Path	Length (m)	θ_Ψ	θ_r	Rx Power	**Path**	Length (m)	θ_Ψ	θ_r	Rx Power
L1	3	15	15	-20.91	**L4**	3	22	22	-19.47
L2^{1}	2.5	60	65	-24.66	**L5**^{1}	2.5	50	38	-23.47
L2^{2}	1.5	35	60	-76.52	**L5**^{2}	1.5	45	45	-73.92
L3^{1}	1.5	50	45	-22.74	**L6**^{1}	1.5	55	35	-22.03
L3^{2}	2.5	38	52	-76.55	**L6**^{2}	2.5	15	75	-81.79

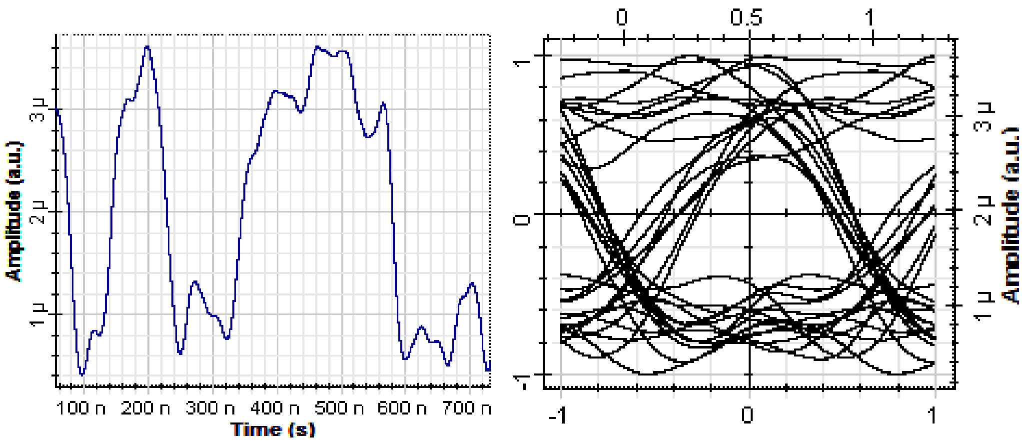

(a) (b)

Figure 3.12 (a) Output signal (b) Output of Final eye diagram using two LEDs' reflected Paths

Thus, a multipath model analysis is more appropriate, and NLOS components must be included for accurate channel estimation in different environments. Considering reflected light and time delay, Lee et.al. sowed the reflected power loss were only about 6% of the total received power by plastic painted walls, whereas it was 39% in the case of normal plaster walls (K. Lee et al., 2011). Due to the much stronger LOS channel gain, the effect of the NLOS does not significantly hamper the optical wireless channel transmission quality.

3.6.2 Field of View (FOV) Effects on Received Power for Case I

The Field of View (FOV) is an important factor for defining the visible light range at the receiver. The total received power performance at the receiver end was analyzed by changing the FOV concentrator angle (Fuada et al., 2017). Narrower FOV can increase the dominance of direct Line of Sight (LOS) path. In Figure 3.13, FOV was varied from 35° to 75° to maintain standerd useable range. In this case, the receive power varied around ~6 dBm. This means proper FOV adjustment is very important for achieving good lighting and a higher data rate in a VLC link. Field of view (FOV) is very closely related to gain, the received optical power of LEDs and the overall data rate of the VLC system.

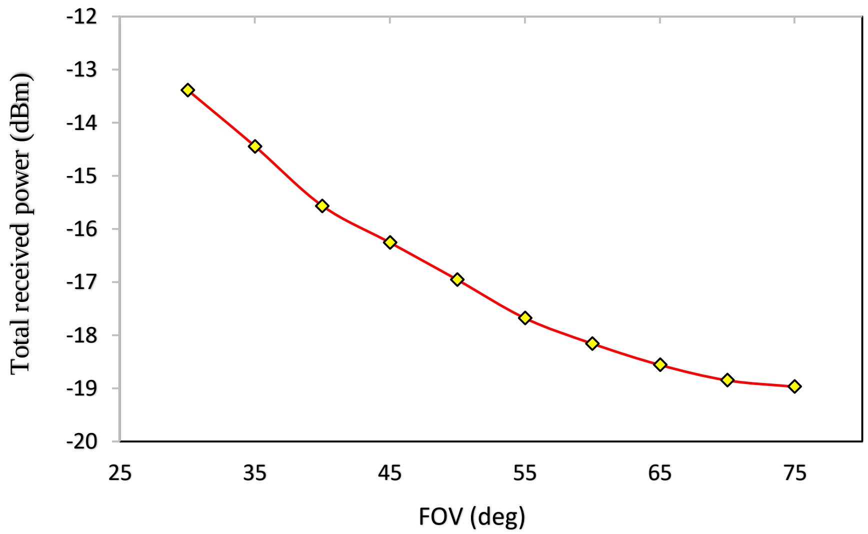

Figure 3.13 Total received power vs. FOV concentrator (deg).

The optical signal receiving device in indoor VLC with concentrator is used to collect surrounding light energy for the receiving surface of photodetector to improve the optical gain (Hao et al., 2019). Wang et al (Hao et al., 2019) reported the performance of the VLC optical receiving antenna. Figure 3.13 shows the average LED received power in dBm vs FOV in degrees. When the FOV was set to 30° under LOS link, the received power was -13.39 dBm. When the FOV was increased to 60° and 75°, the received powers were -16.96 dBm and -18.97 dBm, respectively. When the FOV changes by 45° as shown in Figure 3.13, the received power decreased by 5.58 dBm. Figure 3.14 shows the received power distribution for the two extreme scenarios – FOV 30° and 75° - within the fixed area (length 3m x width 3m) of the room.

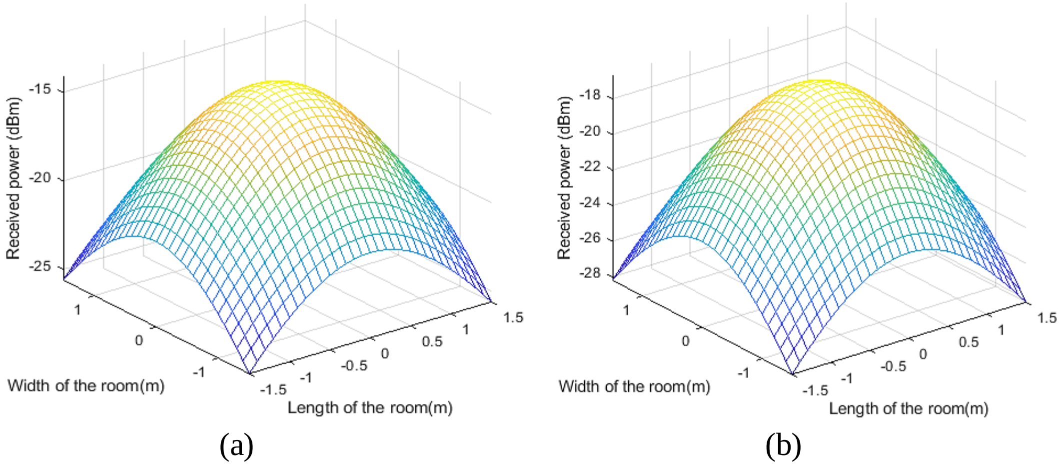

Figure 3.14: Received power distribution for FOVs (a) 30° and (b) 75°

3.6.3 Experimental Results

The overall system performance of the WDM-VLC model was analyzed by changing different data rates using OOK and QAM signals. Therefore, quality factors (Q) and BER were considered the main parameters for checking signal quality. With the increase of sampling rate by AWG, data rate also increased. As a result, the received

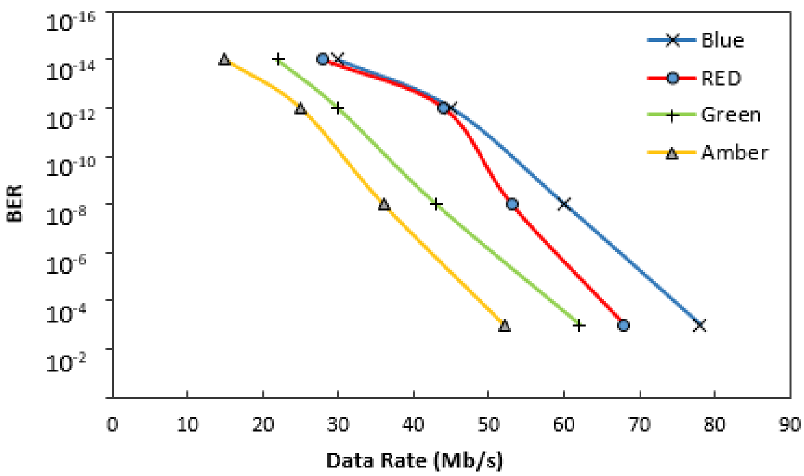

Figure 3.15: BER Vs maximum data rate for available RGBA LED with OOK

signal from PD output was distorted for the high data rate. Figure 3.15 shows the maximum data rate using available off the shelf RGBA LED with OOK signal. Blue LED can transmit a maximum of 78 Mb/s data, and the lowest data rate was using amber LED, about 58 Mb/s. The other two Red and Green were 72 Mb/s and 62 Mb/s data rate.

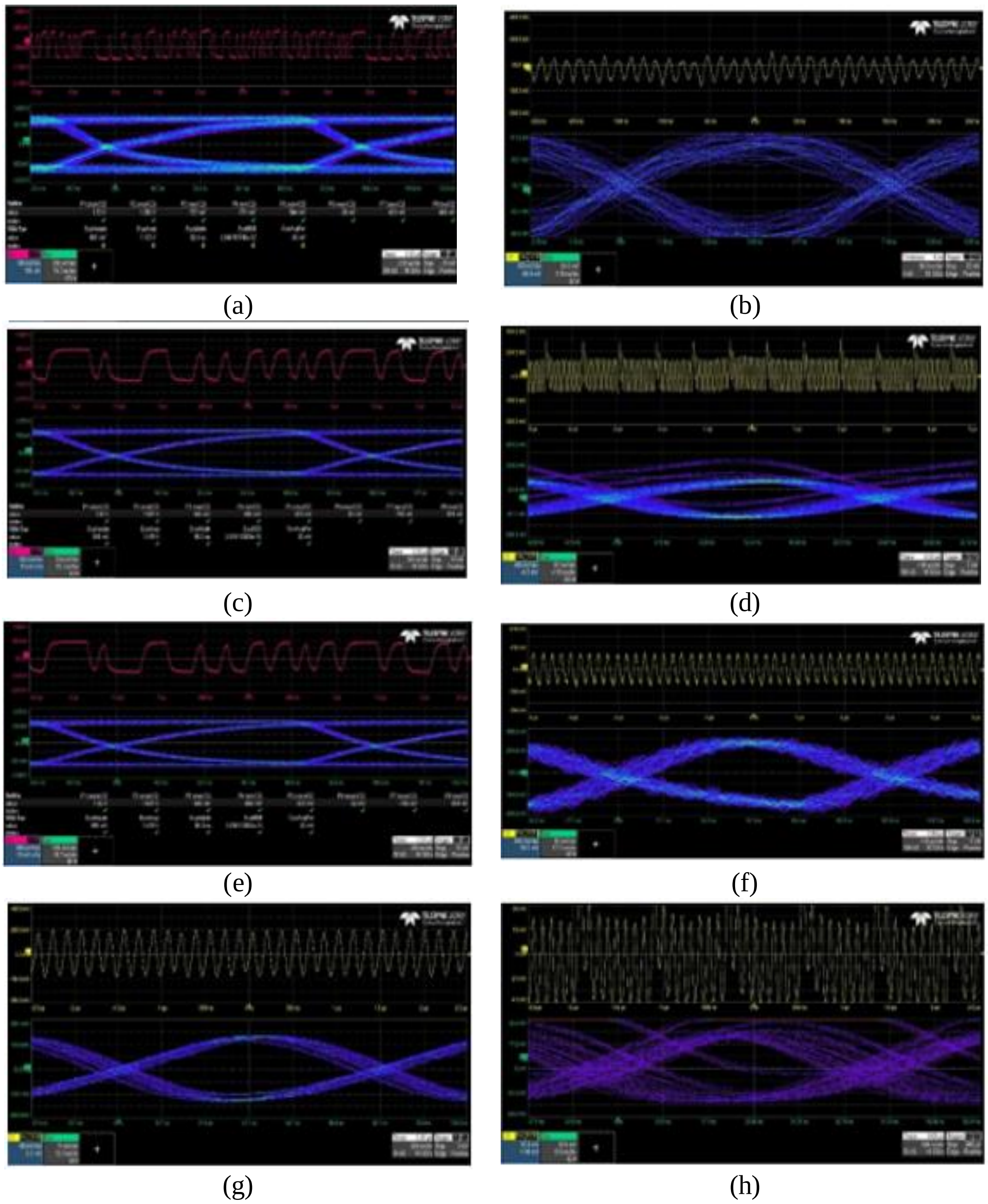

Figure 3.16: Eye diagrams of the transmitted and received waveforms for different data rate using (a) Blue LED input (b) Blue LED output (c)Red LED input (d) Red LED output (e) Green LED input (f) Green LED output (g) Amber LED input (h) Amber LED output

Related eye diagram was recorded for Blue-Red-Green-Amber LEDs with OOK in Figure 3.16 when obtained aggregate data rate was 260 Mb/s. Four peak wavelengths are recorded by photometer CL-500A and related power distribution for RGBA LEDs has shown in Figure 3.17, where peak wavelength was 461 nm, 505 nm, 525 nm and 629 nm. 16 QAM signal transmitter was used in the same model to increase the data rate and constellation diagram of 16 QAM received signal, as shown in Figure 3.18. The maximum data rate achieved 1.04 Gb/s using four all LED channels.

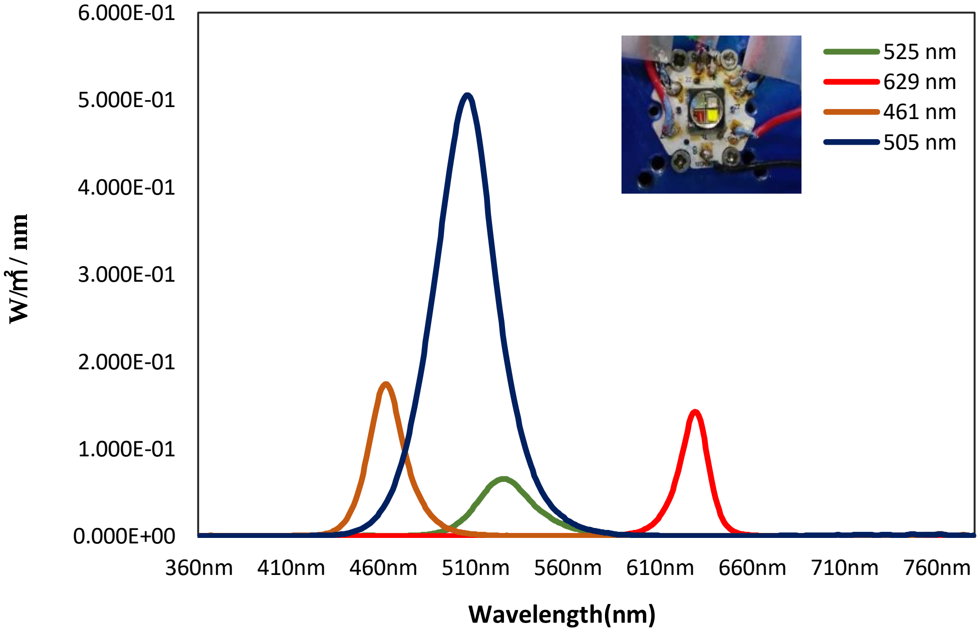

Figure 3.17: RGBA LED (inset) and its spectral power distribution

Figure 3.19 shows the maximum data rate using available off-the-shelf RGBA LED with 16 QAM data mapped signals. Blue LED can transmit maximum 312 Mb/s data, and the lowest data rate was using amber LED, about 208 Mb/s. The other two Red and Green were 272 Mb/s and 248 Mb/s data rate.

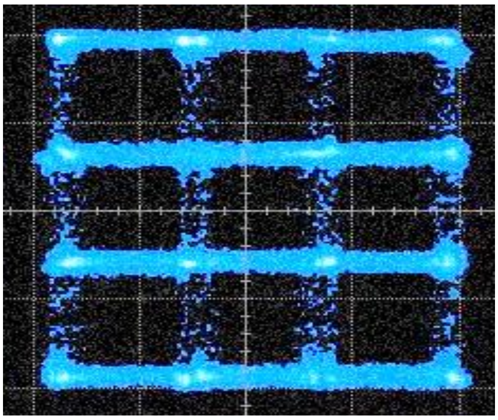

Figure 3.18: Constellation diagram of 16 QAM received signal.

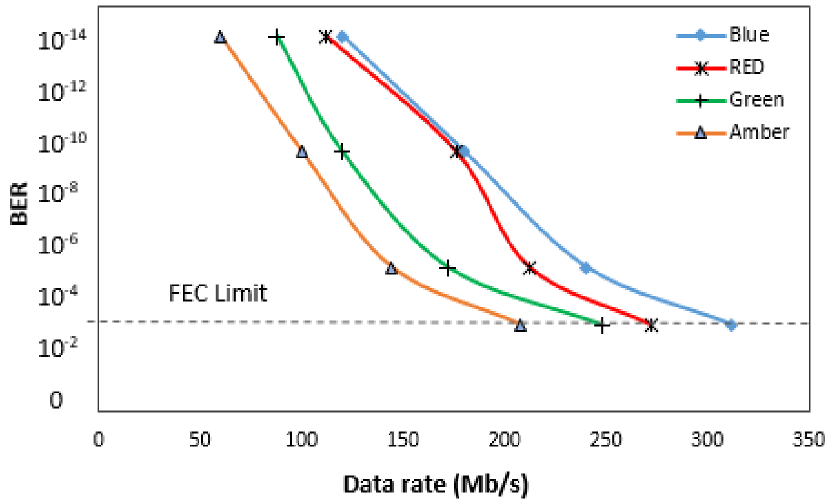

Figure 3.19: BER Vs maximum data rate for available RGBA LED with 16 QAM

3.6.4 Comparison Between Simulation and Experimental Work

To achieve the first objective and make the baseline of the high speed gigabit class VLC research, a VLC experiment has been demonstrated in the university's intelligent lighting lab.

Moreover, to match the experimental work, the VLC system with NRZ-OOK and 16 QAM modulation schemes was simulated in Optisystem. Finally, a comparison table between simulation for Case I and experimental results are shown in Table 3.8, where the data rate achieved were around 290 Mb/s for OOK and 1.16 Gb/s for 16QAM using simulation. Experimentally, data rates were 260 Mb/s using OOK and 1.04 Gb/s using 16QAM with commercially available RGBA LEDs.

Off the self LEDs are used in the experiment and the same configurations were used for the LEDs in Case I simulation model. The results for this case were quite similar to the experimental results as shown in Table 3.8. The comparison between simulation and experimental results indicate the robustness of the WDM-VLC simulation model.

Table 3.8: Comparison between simulation and experimental work

Transmitter	OOK	16 QAM	
RGBA LEDs	290 Mb/s	1.16 Gb/s	Simulation (Case I)
RGBA LEDs	260 Mb/s	1.04 Gb/s	Experiment

3.7 Summary

This chapter builds the foundation for the whole thesis to develop a high data rate VLC system. In this chapter, the VLC system was developed utilizing off the shelf LEDs. The overall objective was to demonstrate simulation and experimental based WDM-VLC system capable of providing gigabit-class range Li-Fi access point for indoor wireless communication. The OOK and 16 QAM modulation schemes were used to encode data due to their flexibility and higher power efficiency.

The simulation was done using Optisystem v.16.1. The data rates achieved using simulation were 290 Mb/s using OOK and 1.16 Gb/s using 16QAM. The aggregate data rates achieved using experimental setup were 260 Mb/s with NRZ-OOK and 1.04 Gb/s using 16QAM.

Moreover, the performance of VLC was analyzed by considering LOS and NLOS propagation effects on the data rate and the output power of the LEDs. Both direct and multi-reflected paths of light was considered. Field of View (FOV) is an important factor for defining the visible light range at the receiver. The total received power performance at the receiver end was analyzed by changing FOV concentrator angle (Fuada et al., 2017). Narrower FOV can increase the dominance of direct Line of Sight (LOS) path. Around ~6 dBm receive power variation was observed, when changing FOV from 35° to 75°.

A combination of multiplexing systems with different modulation schemes can provide data transmission rate at gigabit range with acceptable BER. In the next chapter, extending WDM to CWDM in VLC is discussed.

MODELING AND ANALYSIS OF CWDM – VLC SYSTEM

4.1 Introduction

In the previous Chapter, conventional WDM system has been explained, increasing VLC systems' data-rate. In WDM system, the spacing between the channels can be up to 75 nm and data rates up to 1.97 Gb/s over 3m distance can be achieved using RGBA LEDs. If the spacing between the channels can be decreased, this can increase the number of channels in the WDM system. In this Chapter, the possibility CWDM-VLC system has been explored.

This chapter is organized as follows: Concept of CWDM-VLC is explained in Section 4.2. In Section 4.3, a mathematical model for LED luminaire is described. The simulation approach for CWDM-VLC is defined in Section 4.4. After that, the simulation results to improve the VLC performance using the CWDM grid are explained in Section 4.5.

4.2 Concepts of CWDM-VLC system

CWDM is a special type of WDM technology, maintaining channel spacing 20 nm standardized by ITU-T G.694.2 and G695, for metropolitan area networks (Al-Rubaye et al., 2009). In optical fibers, three different types WDM have been employed – (i) normal WDM, which uses two predominant wavelengths (1310nm and 1550nm), (ii) Dense WDM (DWDM), which uses C band (1530nm-1565nm) and (iii) Coarse WDM (CWDM), which uses bands from O to U (1265nm-1665nm) (Nebeling, 2002). Channel spacing between individual wavelengths in DWDM and CWDM are different. DWDM system generally has 20 channels at 200GHz (1.6nm) spacing, 40 channels at 100GHz (0.8nm) spacing, and 80 channels at 50GHz (0.4nm) spacing as standardized by ITU (ITU, 2020). According to ITU CWDM grid, channel spacing of 20nm (2.5THz) can be implemented within a multiband frequency range from

1270nm to 1675nm (i.e. 400nm range)(ITU, 2020), and the same concept of CWDM has implemented in VLC system with its 400nm visible range from 380nm to780nm. A baseline of conventional WDM-VLC system has been developed in the previous Chapter and explored the implementation of CWDM in VLC.

On the basis of latest knowledge, the conventional WDM VLC system uses a multi-colors version (e.g., RGB, RGBA, RGBY, etc.), the combination of which can give different shades of white or no white color as a result (Cui et al., 2016). A CWDM grid for VLC was introduce and slice the whole visible spectrum (380nm-780nm) into a maximum of 20 different channels. Moreover, performance of this CWDM with a conventional WDM system was compared with a high number LED channels (RGBYA) as reported in the literature (Zafar et al., 2015) using On-Off Keying (OOK) modulation technique for simplicity. Fig 4.1 shows the model of the CWDM-VLC system that was proposed in this chapter. This system model is explained through mathematical equations below.

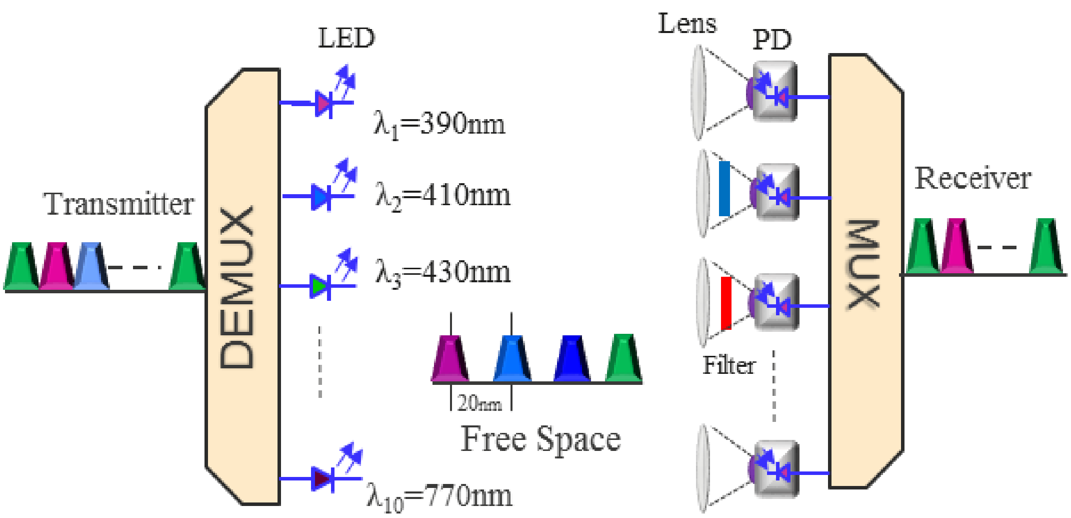

Figure 4.1: CWDM-VLC grid model (20 Channels)

4.3 CWDM Luminaire Design

LEDs have Lambertian radiant intensity, which can be explained using an equation.

$$R_i(\emptyset) = (m_l + 1)cos^m(\emptyset)/2\pi \tag{4.1}$$

$$m_l = -ln2/ln(\cos(\emptyset_{\frac{1}{2}})) \tag{4.2}$$

where $\emptyset$ is irradiance angle, m_l is the order of Lambertian emission, which relates to the LED's semi-angle at half power $\emptyset_{\frac{1}{2}}$ as shown in Equation (2). The luminous intensity at angle φ can be given by:

$$I(\varphi) = I(0)cos^{ml}(\emptyset) \tag{4.3}$$

The horizontal luminance E_{hor} at point *(x, y)* is given by

$$E_{hor} = I(0)cos^{ml}(\emptyset)/r^2 \cos(\varphi) \tag{4.4}$$

where r is the line-of-side (LOS) distance in the free space between the LED and photodiode (PD). Modulated output signal power from LED, $P_0(t)$, can be described as:

$$P_0(t) = P_{LED}[1 + m_i x(t)] \tag{4.5}$$

where P_{LED} is the launched optical power of LEDs, m_i is the modulation index, and *x(t)* is the non-return-to-zero (NRZ) on-off-keying (OOK) signal. The modulated signal depends on the electron lifetime, RC constant, and the materials of the diode. After modulating the signal, the 3-dB modulation bandwidth of the LED can be measured using the following equation (Chun et al., 2016)

$$f_{3dB} = \frac{\sqrt{3}}{2\pi(\tau_n+\tau_{rc})} \tag{4.6}$$

where τ_n is electron lifetime, and τ_{rc} is the RC constant of parasitic capacitance. On the other hand, if the calculated peak wavelength radiated power of the LED is 1W, then the power factor can be described as follows (H. Huang et al., 2015)

$$P_{1W} = \frac{1}{\frac{\sqrt{\pi}}{6}\Delta\lambda_{fwhm} * [1 + erfc\left(\frac{\lambda_0}{\lambda_{fwhm}}\right) + \frac{2}{\sqrt{5}} + \frac{2}{\sqrt{5}}\text{erfc}\left(\frac{\sqrt{5}\lambda_0}{\Delta\lambda_{fwhm}}\right)]} \tag{4.7}$$

where erfc is the error function, λ0 is the peak wavelength, and Δλ is the full width half maximum (fwhm). The optical signal passes through the free space channel, and the DC gain of this channel is measured by (H. Huang et al., 2015)

$$H(0) = \frac{(m_l+1)Acos^{ml}(\theta)\cos(\varphi)T_s(\psi)}{2\pi r^2}\,[\varphi \leq \psi FOV] \tag{4.8}$$

where A is the actual surface area of the photodiode (PD) at the receiver, r is the distance between the LED and PD, $T_s(\psi)$ is the gain of the optical filter at the receiver, ψ is the angle of incidence, and ψ_{FOV} is the field of view (FOV) of PD. On the receiver side, received optical power detected by PD can be given by

$$P_r(t) = RP_0(t)H(0) \tag{4.9}$$

where R is the responsivity of PD, $H(0)$ is the channel gain. The PIN Photodiode device is used to convert an optical signal into an electrical current based on its responsivity. The noise data is calculated from the signal data, whereas the noise and sampled signal data are combined into a single output signal. The incoming light signal and incoming noise bins are filtered by a rectangle filter to decrease the sampling rate.

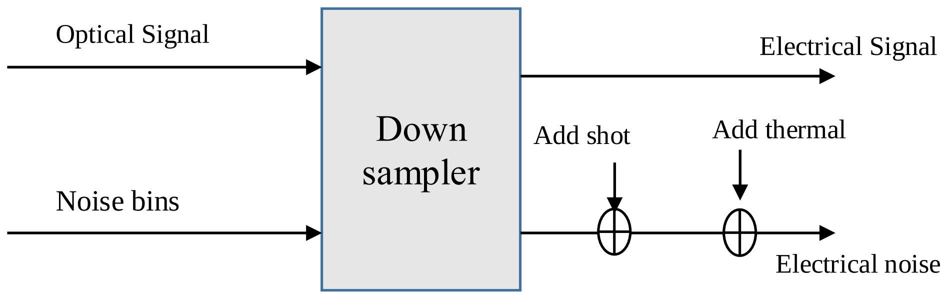

Figure 4.2: Noise calculation type

If optical noise bins are detected at the PIN component's input, the resampled signal bandwidth will be converted to white (Gaussian) noise, as shown in Figure 4.2. The total mean square of receiver noise is calculated by

$$\partial_{total}^2 = \partial_{thermal}^2 + \partial_{Shot-S}^2 + \partial_{Shot-ASE}^2 + \partial_{S-ASE}^2 + \partial_{ASE-ASE}^2 \tag{4.10}$$

Where thermal noise is generally explained by

$$\partial_{thermal}^2 = \frac{4.k_B.T}{R_L}.ENB \tag{4.11}$$

T is the device's absolute temperature, RL is the receiver load resistance, kB is the Boltzmann constant, and ENB is the equivalent noise bandwidth. The shot noise

$$\partial_{Shot}^2 = 2.q.(i_{shot}).ENB \tag{4.12}$$

where q is the electron charge (value is 1.60-19 C), i_{shot} is shot noise current. $\partial^2_{Shot-ASE}$ is shot amplified spontaneous emission (ASE) noise, ∂^2_{S-ASE} is the signal ASE noise and $\partial^2_{ASE-ASE}$ is the ASE-ASE beat noise within the gain medium of PD.

4.4 Optical Filter Effects on WDM-VLC and Optimization

Optical filters are important to produce a narrow LED spectrum for higher bandwidth and reject the ambient light from the selected wavelength. For the Gaussian filter, the frequency transfer function can be given as:

$$H(f) = \alpha e^{-ln(\sqrt{2})(\frac{f-f_C}{\frac{B}{2}})^2} \tag{4.13}$$

where filter transfer function is *H(f)*, *α* is the parameter for insertion loss, *d* is the parameter depth, f_c is the filter center frequency, *B* is the filter bandwidth, and *f* is the frequency. Figure 4.3 shows the output spectral power density (SPD) using Gaussian filter transfer function, where 3dB bandwidth of the LED is 19nm and the power level achieved -14dBm. A guard band is introduced for reducing channel crosstalk. Therefore, the transfer function used for a rectangular optical filter is

$$H(f) = \begin{Bmatrix} \propto, (f_c - \frac{B}{2} < f < f_c + \frac{B}{2}) \\ d \end{Bmatrix} \tag{4.14}$$

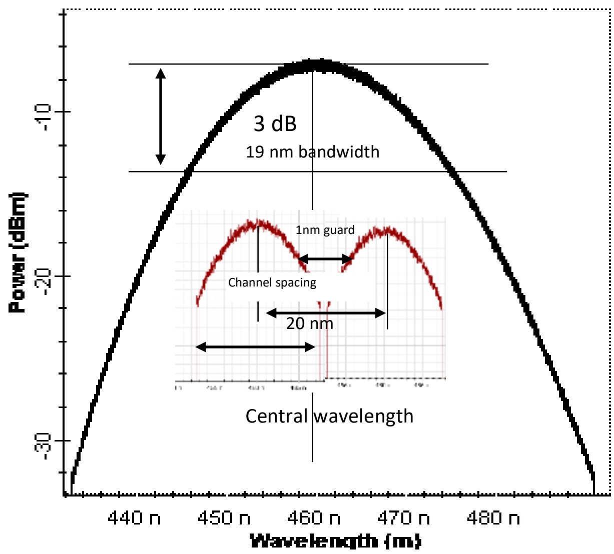

Figure 4.3: Spectral shape using Gaussian function

For the Bessel filter, the transfer function is

$$H(f) = \alpha \frac{d_0}{B_N(s)} \tag{4.15}$$

where N is the parameter order, and d_0 is a normalizing constant and $B_N(s)$ is the filtering order, which can be defined as:

$$B_N(s) = \sum_{k=0}^{N} d_k S^k \tag{4.16}$$

where $$d_k = \frac{(2N-k)!}{2^{N-K}.k!(N-k)!} \tag{4.17}$$

and $$S = j\left(\frac{2(f-f_c).W_b}{B}\right) \tag{4.18}$$

Here, B is the filter bandwidth, and W_b denotes the normalized 3 dB bandwidth (for $N \geq 10$). Band pass filters are used to transmit electromagnetic radiation within a selected spectral region, and filter order defines the amount of light passing through the filters. Narrower emission spectra are more power-efficient than the wider full-width half maximum (FWHM) ranges emission spectra, and these narrow FWHM Filters permit less ambient light and interference from neighboring frequency channel. Gaussian, Bessel, and rectangular filters was used for the receiving light signal, but to observe the effect of filter order at the receiver, Gaussian and Bessel filter were used. The BER of the received signal using NRZ OOK can be measured through

$$BER_{ook} = Q(\sqrt{SNR}) \tag{4.19}$$

4.5 Simulation Process

A typical WDM-VLC system was simulated with 5 channels as a benchmark to compare with the performance of 10 channels and 20 channels CWDM-VLC system. All LED channels were modulated for transmitting data, producing standard white light. At the receiver end, merged white light signal can be detected by a human eye. This light is then separated into color signals and detected by a photodiode according to the original sub-channels. This separation is achieved using specific optical filters, as shown in Figure 4.4. The distance has been considered of 3m between the LEDs and PD. The attenuation was fixed at 0.19 dB/km, which is an acceptable international attenuation for indoor applications (Nebeling, 2002)

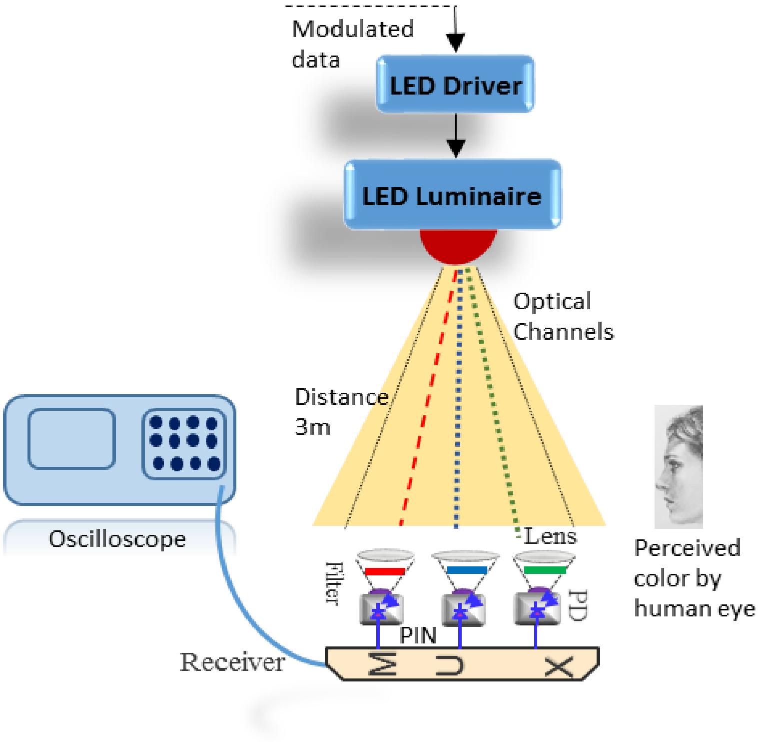

Figure 4.4: Concept of double functionality of LED-based VLC system

The optical attenuator is used at the receiver, which is required for different biasing conditions and correlated color temperatures (CCTs). A pseudo-random bit sequence (PRBS) generator was used to generate 10^6 bits, and then it is encoded by an NRZ pulse generator. The LED, as an optical transmitter, transmits the light signal in free space. The photodiode was designed based on the Thorlabs PD10A datasheet, where the responsivities are different at different wavelengths. Frequency capturing range of PIN PD is 350 to 900 nm, with a maximum responsivity of 0.65 A/W, as shown in Figure 4.5. The channel capacity received optical power from an individual channel, and BER was measured by Optisystem and MATLAB toolbox. System parameters for the simulation of WDM or CWDM- VLC model have been tabulated in Table 1.

Different types of optical filters were placed before PD to make a narrow spectrum and an electrical amplifier is used to amplify the received signal.

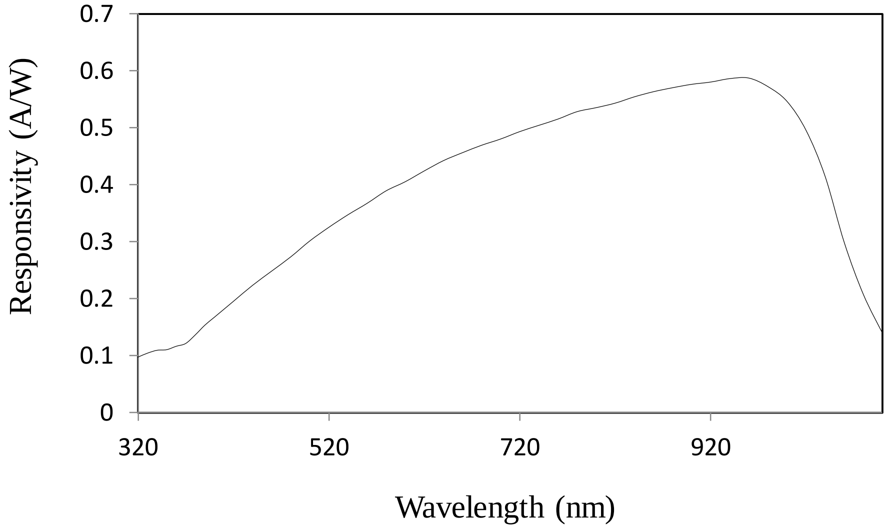

Figure 4.5: Responsivity curve correspondent wavelength

The optical lens is used to collect more light onto the PIN active area, and filters are used in front of each PD to separate each WDM or CWDM channels with the different wavelengths. Multichip LEDs VLC system simulated using a Gaussian function and spectral power distribution (SPD) of CWDM 10 channels and 20 channels were modeled as shown in Figure 4.6 (a) and (b). For 20 channels VLC model, the visible spectrum was considered from 390 nm up to 770 nm with FWHM 20 nm, and channel spacing was considered ~1 nm between 2 consecutive peak wavelengths. The output signals from the PIN diode are stored using a real-time oscilloscope for offline demodulation.

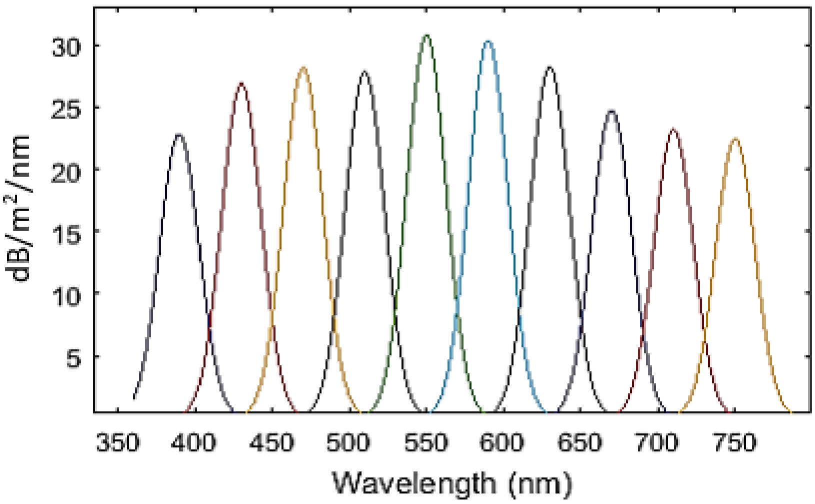

(a)

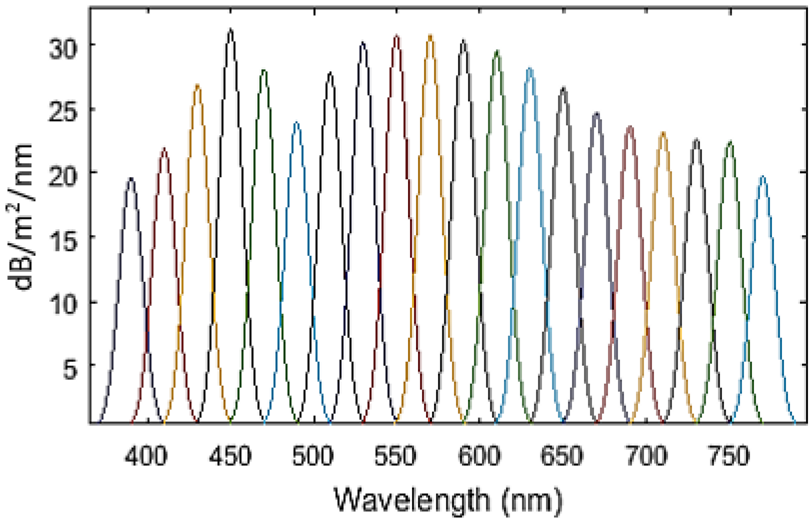

(b)

Figure 4.6: (a): SPD for10 channels LED (b) and 20 channels

Table 4.1: System parameters for VLC model

	Parameters	Value
Transmitter		Wavelength (nm)
	For 5 CH	460,525,560,610,645
	For 10 CH	390, 430, 470, 510,550 590,630,670,710,750
	For 20 CH	390,410, 430,450, 470, 490,510,530,550,570, 590,610,630,650,670, 690,710,730,750,770
	Electron life time,Tn(ns)	1 ns
	RC constant, T_{RC} (ns)	1 ns
	Transmitted power	32 dBm
Channel	Distance	3m
	FOV concentrator	45 deg
	Tx half-angle	60 deg
	Irradiance angle	20 deg
	Incidence angle	20 deg
Receiver	Dark current	10 nA
	Responsivity (A/W)	0.65
	Thermal power density (W/Hz	$100x10^{-24}$ W/Hz
	Load resistance	50 Ohm
	Absolute temperature	298 K

4.6 Results and Discussion

Bit Error Rates (BER) of each channel of the WDM system were investigated using different types of filters, as mentioned before - Bessel, Rectangular, and Gaussian. The result shows that the Low Pass Bessel filter has the lowest BER and adjacent channel crosstalk. 3dB bandwidth of the LED spectrum and received power level are shown in Figure 4.7.

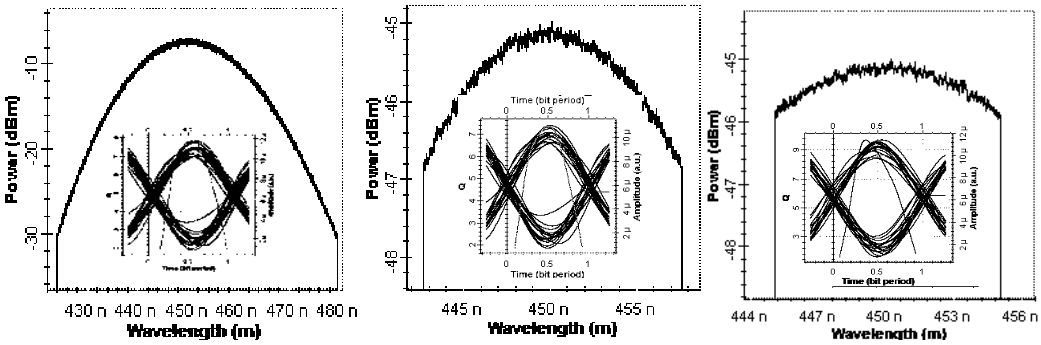

Figure.4.7: LED spectrum using a) Gaussian b) Bessel c) Rectangular filter.

The filter width was adjusted to 19nm, 18nm, 15nm, 10nm, and 5nm with properly optimized filter spacing to improve the signals' received power. As a result, a BER of 10^{-19} was achieved by the corresponding Bessel filter with 19nm spacing. On the other hand, when the wavelength spacing reduced up to 5 nm, the BER of the rectangular filter decreased to 10^{-3} but still under FEC limit, which is explained in Figure 4.8. Bit Error Rates (BER) of the VLC link was investigated using different types of filters such as Bessel, Rectangular, and Gaussian filters for each channel of the WDM system.

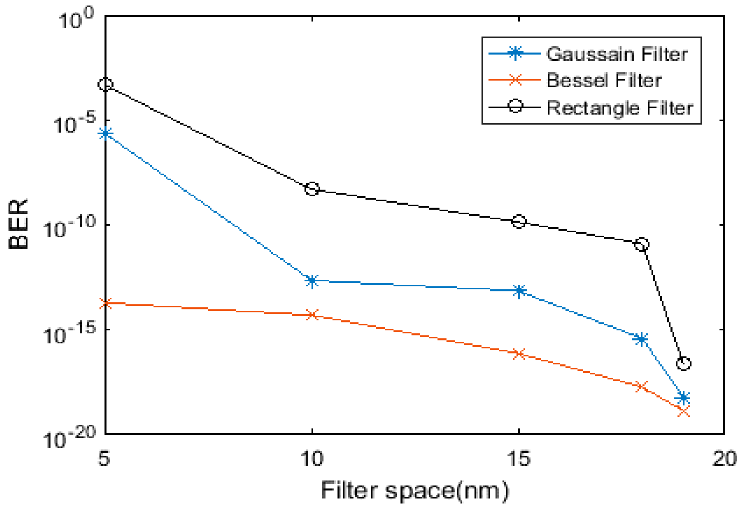

Figure 4.8: Filter wavelength space Vs BER graph.

Bessel filter shows the best performance getting lower BER, which is more than 10^{-15} and rectangular filter shows the best performance when channel spacing 19 nm its around 10^{-16} but it reduced it up to 10^{-3} when channel spacing was 5nm and passed more adjacent channel crosstalk. This system will allow an opportunity to fully utilize the available bandwidth of visible light range and this narrow band filter is required to reduce the crosstalk between the LEDs. The filter factor states the multiplicative amount of light into the filter blocks. It depends on the spectral response curve for maintaining daylight color temperature (CCT). The filter order was considered from 1-10, which indicates the multiplicity of filter factors with current bandwidth. When filter order was increased from 1 to 10 with Gaussian and Bessel optical filters, the portion of light reduced gradually, as shown in Figure 4.9.

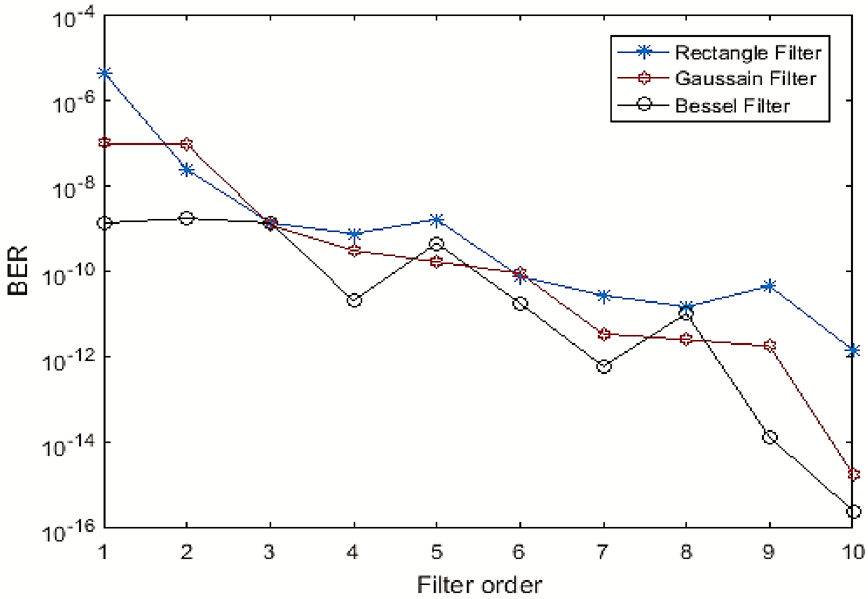

Figure 4.9: Effects of filter order on BER performance

The BER increased with the related filter order. Different types of filter and filter factors were investigated to measure the BER and proper communication signal quality. Initially, Blue LED was considered for measuring the filtering effect.

WDM VLC system uses multi-colors version as Red, Green, Blue, Yellow, and Amber (RGBYA) with a different full width half maximum of those LEDs. Different color LEDs emits different spectral power and using five different wavelengths for the conventional WDM-VLC model, and total data rate achieved 1.97 Gb/s. Related BER for those channels have shown in Table 4.2. CWDM-VLC model has specific channel spacing between different color LEDs. Using full visible spectrum, a total 20 channel system was designed and measured the performance. BER analyzer was used to calculate the BER, the Q factor, and the data rate, which is summarized in Table 3.

Table 4.2: Total data rate of conventional WDM-VLC systems

Peak Wavelength	BER	Data rate (Mb/s)
460	3.29×10^{-6}	250
525	2.35×10^{-8}	430
560	1.91×10^{-9}	510
610	1.15×10^{-8}	480
645	9.88×10^{-8}	300

Initially, 10 channels are used for communication and other 10 channels keep on just for illumination. The total data rate of 3.2 Gb/s was achieved for 10 channels CWDM-VLC system. This data rate is relatively good with OOK modulation, maintaining the bit error rate is below the FEC limit 3.8×10^{-3}. The variety of data rate depends on the

Table 4.3: Total data rate from 10 channels of CWDM-VLC systems

Peak Wavelength	BER	Data rate (Mb/s)
390	1.50×10^{-3}	120
430	1.93×10^{-3}	180
470	1.04×10^{-8}	250
510	3.77×10^{-6}	300
550	1.32×10^{-7}	570
590	2.21×10^{-8}	590
630	1.73×10^{-8}	430
670	3.06×10^{-5}	300
710	7.45×10^{-4}	260
750	5.51×10^{-3}	200

SPD of a different wavelength. Table 4.4 shows the total aggregate data rate for 20 channels with full utilization of 400nm visible spectrum by the CWDM-VLC model.

The data rate that could be achieved is 7.20 Gb/s, maintaining high power LED's configuration in the model. Within this visible range maximum of 20 channels can fit in the LED-based VLC model. Each channel has a different BER and data rate, because of the LED spectra and transmitted powers.

Table 4.4: Total data rate from 20 channels of CWDM-VLC systems

Peak Wavelength	**BER**	**Data rate (Mb/s)**
390	3.29×10^{-3}	120
410	2.35×10^{-5}	150
430	1.91×10^{-5}	200
450	3.85×10^{-6}	250
470	7.88×10^{-4}	260
490	7.81×10^{-4}	270
510	1.09×10^{-4}	310
530	5.75×10^{-6}	510
550	5.74×10^{-5}	610
570	5.79×10^{-6}	600
590	9.87×10^{-8}	620
610	1.26×10^{-6}	580
630	5.29×10^{-4}	510
650	8.31×10^{-6}	490
670	1.59×10^{-6}	440
690	1.05×10^{-4}	350
710	2.32×10^{-5}	280
730	2.21×10^{-6}	250
750	6.28×10^{-4}	220
770	3.28×10^{-4}	180

The results for conventional WDM-VLC and CWDM-VLC (10 channels and 20 channels) systems are presented in Figure 4.10. This figure clearly shows the ability the 20 channel CWDM-VLC model has in increasing the data rate.

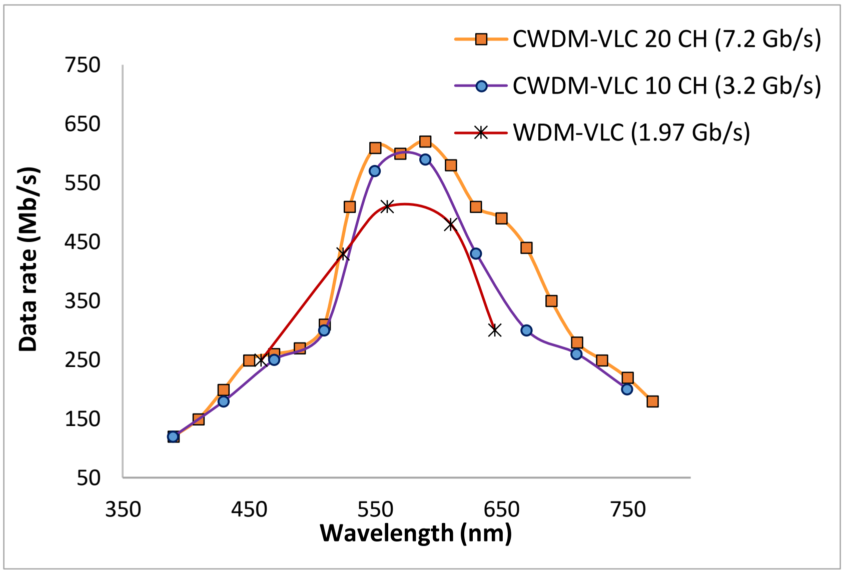

Figure 4.10: Data rate comparison among WDM, CWDM-VLC (10 Ch &20 Ch)

For the CWDM VLC model, 20 LEDs optical power was detected, and maximum power differences between high and low-intensity levels were around 12 dB, as shown in Figure 4.11.

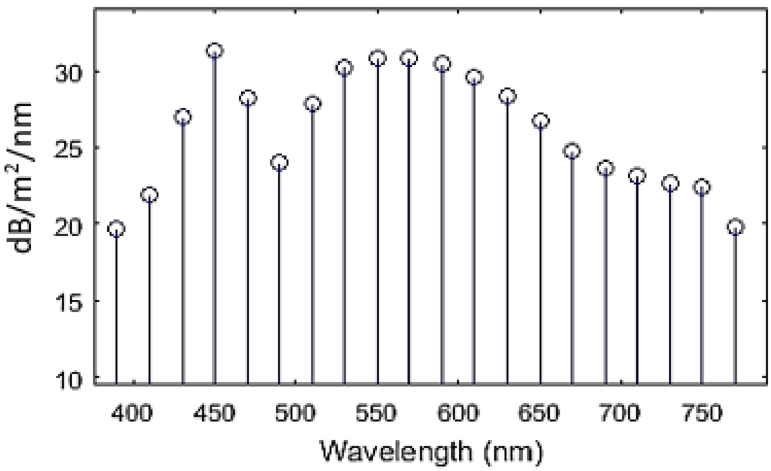

Figure 4.11: Optical power level of the 20 channels CWDM

4.7 Summary

In this Chapter, a new CWDM-VLC system has been proposed for the first time with the optimum number of channels to get the maximum data rate. The results indicate that narrower emission spectra increased system performance by reducing channel overlapping and crosstalk because narrower emission spectra permit less ambient light and interference from the adjacent channel. Moreover, with the OOK modulation scheme, the data rate achieved was 7.19 Gb/s using the total 20 channel CWDM grid with acceptable BER and 3 m distance between transmitter and receiver. Besides, three different optical filters (Gaussian, Bessel, and Rectangular) are analyzed at the receiver. The amount of light received by the filters can be controlled using filter order to get better BER. For comparison purposes, the data rate and total output power of 10 and 20 channels CWDM-VLC system were investigated within the indoor environment. The system can have up to 10-20 channels, and channel spacing and filter space can be modified to increase the data rate. If the spectra of each channel are optimized using suitable filters and higher-order modulation techniques, the system's total data rate may increase further in the future.

There could be concerns about whether it is possible to fabricate LEDs in the channels required in the CWDM-VLC systems. This concern is addressed in detail in the next Chapter.

FDTD ANALYSIS OF GaN/InGaN BASED MQW LEDs

5.1 Introduction

A new CWDM-VLC system has been proposed for the first time with the optimum number of VLC channels to get the maximum data rate in the previous chapter. The results indicate that narrower emission spectra increased system performance by reducing channel overlapping and crosstalk because narrower emission spectra permit less ambient light and interference from the adjacent channel.

In this chapter, the optical properties of highly polarized InGaN/GaN-based multiple quantum well (MQW) LEDs coupled with and without nano-lens on the top layer of LED structure has been investigate. Previous works have used either MQW or nano lens, but this work examines the effect of combining these two to get desired peak wavelengths for implementing coarse wavelength division multiplexing (CWDM)-visible-light communication (VLC) grid. Using FDTD method, three different peak wavelength LED 510nm, 530nm, and 550nm was produced and compare the performance with recombination lifetime, light extraction efficiency (LEE), and beam divergence of the LEDs. The outcome of changing the thickness of QWs within a fixed active area and remaining constant of each layer thickness of QWs in the adjustable active area has been investigated. A parabolic nano-lens array attached to the LED's top layer reduces the narrow half-width half maximum (HWHM) to increase the LED bandwidth. The performance with the nano lens array and without lens for both conditions have been also measured. Far-field emission pattern is very important to produce narrowband LED for high-speed VLC application, and SiO_2 lenses are used on the top layer to reduce field divergence of 20 nm. The proof-of-concept of a nano parabolic lens to control the light extraction angle to maintain the CWDM-VLC grid modeling was presented (Rahman & Parthiban, 2020).

The rest of the chapter is organized as follows. Initially, the techniques to enhance the efficiency of GaN based QWs LED in Section 5.2. Therefore, Section 5.3 presents background of the simulation and comparison among the previous LEDs modeling work and, FDTD analysis for LED modeling was studied in Sections 5.4 and 5.5 respectively. The methodology of this research work and MQW LED structure was explained in Sections 5.6 and 5.7. Based on the simulation work, in detail results and discussion was deliberated in Section 5.8. To conclude, a summary of the chapter and key outcomes is presented in Section 5.9.

5.2 Techniques to Enhance the Efficiency of GaN LED

Group III-nitride materials GaN/InGaN LEDs can be used in different solid-state lighting applications, such as color displays, car headlight, street lighting, backlighting, smart lighting and VLC applications. Conventional GaN-based quantum well (QW) LEDs are developed using the surface of polar c-plane (0001) orientation. However, it undergoes from strong quantum confined stark effect (QCSE) because of its significant internal polarization field effects, which degrade emission efficiency and quantum efficiency. With the polarization effect, the carrier lifetime of QW structured LEDs can be decreased, which is a key parameter for achieving high modulation bandwidth for LEDs. The amount of inserted charges (electrons and holes) and the total excited photons determine the performance of the GaN LED. The efficiency of GaN LEDs can be improved by increasing charge injection, reducing recombination time, increasing IQE, and increasing LEE (B. Park et al., 2014).

Different methods have been introduced to improve the light efficiency of GaN LEDs with modeling work, such as external surface roughing by chemical etching (Zhao & Zhao, 2012) antireflection coating (Y. M. Song et al., 2010), using high-refractive-index material(Chung et al., 2012), flip-chip LEDs, metallic grating, placing a photonic crystal on GaN layer (Liu et al., 2015), micro or nanostructure improvement, sub-wavelength structure changing on the top layer of GaN (Son et al., 2015), reducing Fresnel reflection, patterning sapphire substrates (Pan et al., 2013), and reducing far-field divergence by implementing nano lens (Demory et al., 2018). Figure 5.1 explains four primary techniques to enhance the efficiency of GaN LEDs such as in Fig 5.1 a) surface grating on the structure b) Pyramid structure on top &

sapphire layer, c) SiN Lens on the top layer, and d) Nanotube structure on the LED's top layer.

5.3 Background of Simulation

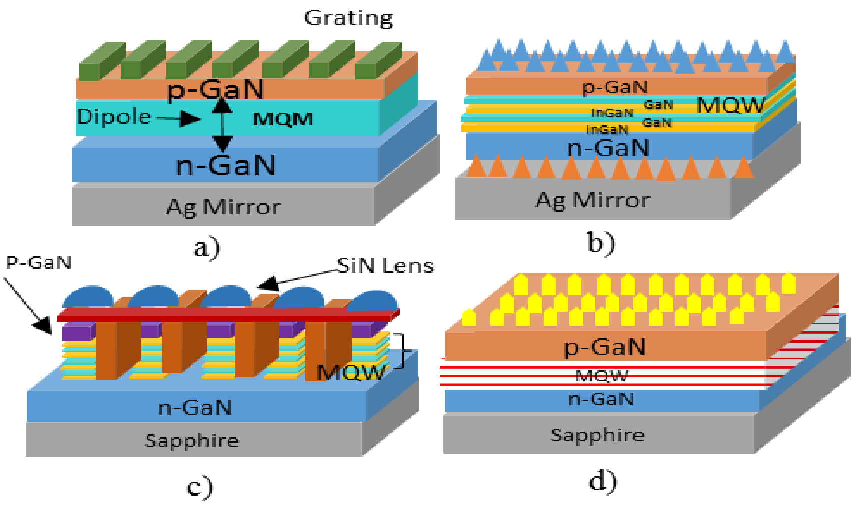

Figure 5.1: Primary techniques to improve the bandwidth of GaN/InGaN MQW LED a) Polarized surface grating structure b) Pyramid structure on top & sapphire layer c) SiN Lens on the top layer and d) Nanotube on top layer LED

FDTD is a numerical analysis tool for designing computational electrodynamics and it covers a wide frequency range for nonlinear material properties. FDTD method belongs to grid-based differential numerical modeling and it has the ability to model light propagation, reflection, scattering, diffraction, and the device polarity. GaN based LED emits light mainly in TE mode (H. Chen et al., 2016). The simulation was done using a point dipole as a light source where the light comes out from the quantum well region, and it emits most of the light in TE polarization mode due to piezoelectric effects. A single dipole was used as a light source which was placed in the central point of the MQW and emission spectrum set to Gaussian shape in the frequency axis. The peak wavelength and FWHM of the spectrum was set to 510nm and 20 nm, respectively. Boundary conditions are necessary because the entire simulation region needs to be fixed to control computational resources and simulation time. In the simulation, two kinds of boundary conditions need to be used, which are perfectly matched layer (PML) and periodic boundary conditions. PML boundary condition was used as a numerical absorbing layer, which prevents the reflecting electromagnetic field within the simulation region (Zhao et al., 2012). A power monitor box was used to calculate the LEE improvement, and it was placed on a dipole and at half of the distance from the top layer of p-GaN. Near field transmission function was taken from the air above the structure, and far-field function used to get far-field power radiation. Light extraction efficiency was measured by the total transmitted power from the cavity over total radiated power from the dipole in the simulation. The dispersion was taken lowest value in this simulation because of the relative change of the refractive indices of GaN.

The theoretical background used in this simulation is explained in this section. American physicist, Edward Mills Purcell, explained that spontaneous emission from the materials can be improved by changing its dielectric status where F_P is the ratio between total emission rate in the cavity structure and total emission rates in bulk materials. In the FDTD simulation, F_P is the ratio between the released power from the dipole in the cavity and the output power of dipole considered in the material, which can be explained by this equation (Son et al., 2015).

$$F_p = \frac{3}{4\pi^2}\left(\frac{\lambda_c}{n}\right)^3\left(\frac{Q}{V}\right) = \frac{R_L}{R_0} \tag{5.1}$$

where λc is the central wavelength in vacuum, n is the refractive index of the selected material, quality factor is defined by Q, and V is mode volume. R_L is the light extraction rate using nano lens structure, and R_0 is the natural emission rate for bulk material without a lens. Relating with the F_P and LEE, It can be defined the IQE and EQE of multi-layer QWs with metallic nano lenses as (H. Chen et al., 2016)

$$IQE_L = \frac{F_p IQE_0}{F_p IQE_0 - IQE_0 + 1} \tag{5.2}$$

Modulation speed is limited for QW LEDs, due to the strong cavity influence. However, for a strong cavity effect in the simulated structure, the Q factor affects the device's photon lifetime and modulation speed. For the carrier lifetime τ_c, inside the MQW can be estimated by (Son et al., 2015).

$$\frac{1}{\tau_c} = \frac{F_p}{\tau_r} + \frac{1}{\tau_{nr}} \tag{5.3}$$

where τ_r is radiative carrier lifetime, τ_{nr} is the non-radiative recombination time, and τ_c is the actual carrier recombination time. LED modulation bandwidth is one of the main barrier for high-speed VLC system, and this bandwidth is related to the recombination time, which can be measured by

$$f_{3dB} = \frac{1}{2\pi\tau_c} \tag{5.4}$$

where τc is the recombination lifetime of the photons from the dipole. LEE is the ratio of power extracted from the structure and concerning total power emitted power from the dipole source(Choi et al., 2006)

$$LEE = \frac{P_{out}}{P_{Souce}} \tag{5.5}$$

For the standard composition of indium with GaN composite, light polarization (TM polarized) is comparatively weaker than TE polarized light, and here the composition of GaN is chosen for radiating light at the desired wavelength of 510 nm. For QWs LED on c-plane with medium polarized radiation, a classical dipole source is simulated in the middle of the quantum wells.

5.4 Comparison of LEDs Modeling Work

Some of the benchmarking papers that explore LED performance using FDTD analysis and compared with this research are tabulated in Table 5.1. Hao-Yu-lan et.al. discussed the effect of a single quantum well and triple QWs in the active region of the energy bandgap and modulation bandwidth achieved 1.6 times higher by single QW (Lan et al., 2018). Therefore, the 3dB modulation bandwidth of the LED 3.6 GHz was achieved using the optical pumping method. QW's effect on emission efficiency was measured by rigorous coupled-wave analysis (RCWA) by D. Fattal.et.al (Fattal et al., 2008). Peng Zhao.et.al. has been demonstrated Ultra-thin InGaN QWs(1nm) and GaN layer (3nm) on c-plane (0001) to handle QCSE of the LED by K. Rajabi et.al and achieved a lower recombination time of 1.42ns which increased LED bandwidth up to 536 MHz (Rajabi et al., 2018). Hong Chen.et.al investigated all optical properties of InGaN LEDs which is attached with the metallic grating structure on the

Table 5.1: Summary of LED Design based on Higher Modulation Bandwidth

Ref	Methods	Parameters	Materials	Structure	Modulation Bandwidth	FWHM/ Peak λ	MQW effects	Nano lens
(Demory et al., 2018)	integrating parabolic nanolenses for HWHM reduction	Far-field emission divergence, lens collimation	InGaN /GaN, Silicon nitride (SiN), spin-on-glass (SOG), SiN	Nano pillars µLEDs with Nano lens	N/A	√ (12.4°) Peak 495 nm	×	√
(Fattal et al., 2008)	Optical pumping (Modelling work)	Intensity power, recombination time	$GaAs_{0.885}P_{0.115}$ QW, Ag, $AL_{0.35}Ga_{0.65}As$	metallic grating	3.6 GHz	× Peak 780 nm	×	×
(H. Chen et al., 2016)	Polarization control	LEE, IQE, EQE, Purcell factor, Modulation frequency	GaN/InGaN	Metallic grating on the top surface	5.4 GHz	× Peak 470 nm	×	×
(Zhao et al., 2012)	Changing current densities	power dissipation and efficiency	AlGaN QWs based UV LED	Metal ring on the top layer (ITO)	1.5 GHz	√ (10nm) Peak 250 nm	×	×
(Lan et al., 2018)	Increasing current densities	Effects of QW numbers on modulation bandwidth, Optical power	GaN blue micro-LED	Single and triple QWs based epitaxial structure	752 MHz	× Peak 440 nm	√	×
(Rajabi et al., 2018)	Reduce the quantum-confined Stark effect (QCSE)	Recombination rate, the thickness of QWs, EQE	Ultra-thick InGaN /GaN	Semi-polar substrates	536 MHz	× Peak 399 nm	√	×
(Zhu et al., 2015)	Surface plasmon (SP) coupling with QW	IQE, Photon emission rate	18 pairs InGaN/ GaN, Ag Nps, SOG, HfO_2,	Nano rod array	15.1MHz (Nano rod) 29.8 MHz (Ag Nps)	× Peak 525 nm	√	×
This Research	MQWs efferects, Nanolence used for narrow band	Narrow spectrum, recombination time, LEE	10 pairs InGaN/ GaN, SiO_2 Nano lens	MWQs LED with Nano lens	6.15 GHz	√ Peak 510 nm	√	√

top layer. They obtained a maximum 5.4 GHz modulation frequency and enhanced quantum efficiency by tuning polarized emission control, and surface Plasmon (H. Chen et al., 2016). Moreover, ZnO nanorod structures were used on top of the p-layer to enhance the light extraction and demonstrated 6.7 times better performance than available green LEDs. To reduce the micro-LED line width for micro pixel application, a parabolic nano lens array attached to the nanopillar array and HWHM reduced ~2x times from 23.8° to 12.4° by Brandon Demory et.al. (Demory et al., 2018).

5.5 Finite-Difference Time-Domain (FDTD) Method

Finite-Difference Time-Domain (FDTD) is a state-of-the-art method for modeling micro or nano scale optical materials solving Maxwell’s equations without any physical estimate. Being a time and space division problem, it offers the solution for all types of problems in electromagnetics and photonics. FDTD solves Maxwell's curl equations for semiconductor materials:

$$\frac{\delta \vec{D}}{\delta t} = \nabla \times \vec{H} \tag{5.6}$$

$$\vec{D}(\omega) = \varepsilon_0 \varepsilon_r(\omega) \vec{E}(\omega)$$

$$\frac{\delta \vec{H}}{\delta t} = -\frac{1}{\mu_0} \nabla \times \vec{E} \tag{5.7}$$

where H is magnetic, E is electric, and D are the displacement fields. $\epsilon_r(\omega)$ is a dielectric constant. This method can calculate the effects of light scattering, absorption, reflection, transmission using Fast Fourier Transform (FFT), and the Discrete Fourier Transform (DFT). Especially in the LED structure, to measure total light propagation, effects of refraction in device materials, total internal reflection, FDTD method is being used (Gedney, 2011). To see the difference between the epoxy/GaN/sapphire LED and the epoxy/GaN/SiC LED in the light propagation, three-dimensional (3D) and two-dimensional (2D) FDTD methods are used (R. Zheng & Taguchi, 2003).

5.6 Methodology

The methodology implemented in this work for FDTD analysis of InGaN/GaN based MQW LED and its optical properties of the LED such as LEE, FWHM of LED, recombination time, far-field divergence and quantum efficiency. The working process has been explained in Figure 5.2. InGaN/GaN based a MQW LED was designed with peak wavelength 510 nm, 530 nm, and 550 nm where FWHM of the LED was 20nm which essential for the implementation CWDM-VLC system.

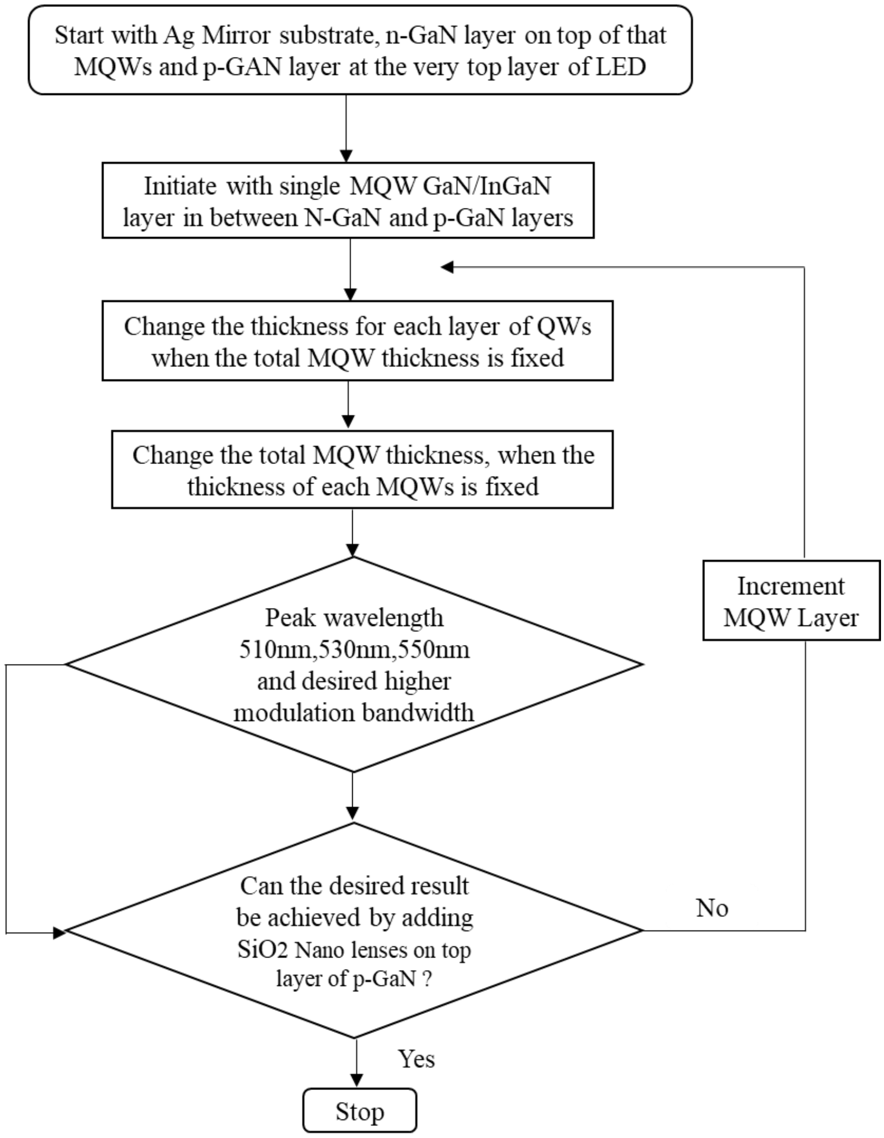

Figure 5.2: Methodology flow chart

The simulation and comparison of the previous modeling work's theoretical background have been explained in sections 5.3 and 5.5. Therefore, the effects of using a nano lens and without nano lens were observed for two conditions: (i) when the total MQW thickness is fixed with adjustable thickness for each layer of QWs, and (ii) when the thickness of each MQWs is fixed with adjustable total MQW thickness. Finally, desired consecutive three LEDs with 20 nm FWHM was designed for the CWDM-VLC system.

5.7 MQW LED Structure

MQWs LED is made by GaN/InGaN composite materials that help to improve the LED's luminescence. QWs are used to trap the injected charge carriers inside it, and with the increasing number of QWs, more charge carriers can be trapped to emit more photons (Łopuszyński & Majewski, 2012). QW layered GaN/InGaN LED (4000 nm, 4000 nm, and 50 nm as for length, width, and thickness when each layer's thickness is fixed) is set with a 30nm Ag mirror. Ag mirror is used just as a sapphire layer to reduce the Fresnel reflection from the cavity, and a built-in palik model was chosen for it. The thickness of the n-GaN and p-GaN layer is 250 nm and 200 nm, respectively. Nanostructure SiO_2 (Glass) lenses are set on the top layer of p-GaN with radius 500nm and 50 nm thickness. SiO_2-Quartz was chosen as the lens material with the refractive index of 1.458 (extracted from refractiveindex.info) and 3D span x 1000, y 1000, and z 3650. N-contact consists of Al (Aluminium palik) pad with dimensions 800 nm, 600 nm, and 75nm (for x,y, and z axis). P-contact Au (gold) pad with thickness 62.5nm is used on the top layer of MQW. To measure the output power from the cavity, power transmission 3D box (span x 4000, y 3000, z 1000) is used. To measure the source dipole's power, a 3D transmission box (50x50x10) nm was used from the analysis group. The light emission was simulated as a linear dipole inside the InGaN active region 250 nm below the p-GaN. Refractive indices of vacuum, InGaN and GaN were fixed as 1, 2.521 and 2.47, respectively. InGaN/GaN based five and nine MQWs were introduced between the n-GaN and the p-GaN layer, shown in Figure 5.3(a) and (b). Figure 5.3 (a) shows the structure with nano lens array, and

Figure 5.3 (b) shows the same set up with 9 MQWs without nano lens. A classical dipole simulates the light source, and its orientation represents the QW's polarized radiation (Lin et al., 2013). Figure 5.3(c) shows the light extraction with the nano lens,

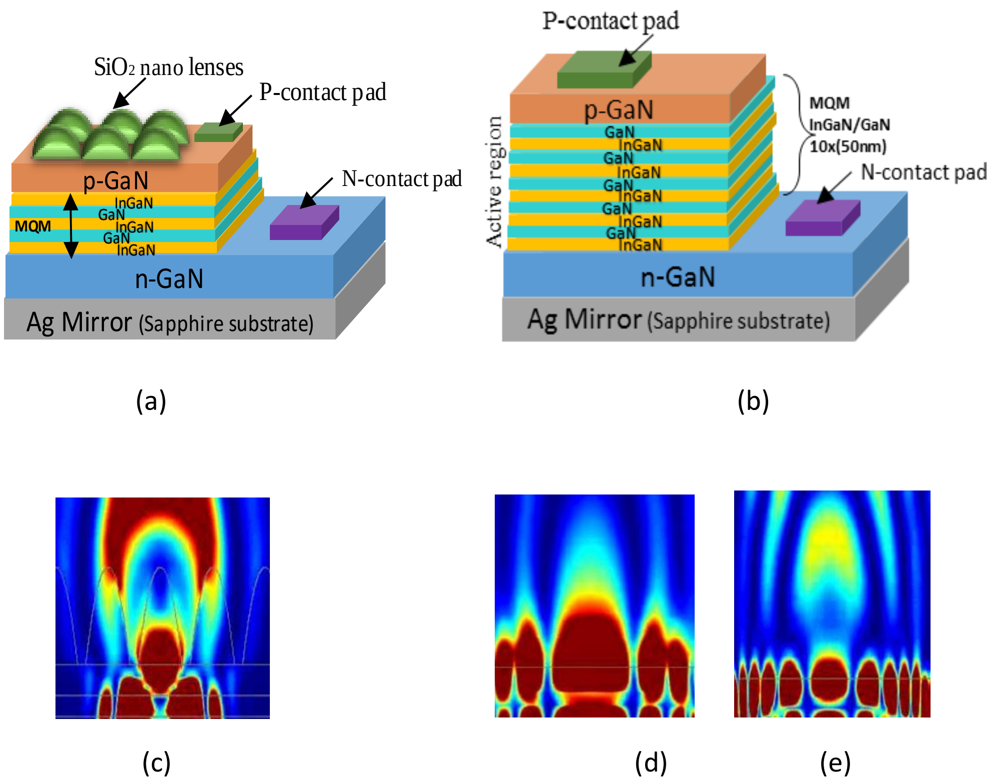

Figure 5.3: (a) 5 MQWs based GaN/InGaN micro LED with nano lens (b) 10 MQWs based LED structure (c) light extraction from nano lens LED (d) light extraction using 5 QWs without nano lens (e) light extraction using 10 QWs

and that structure produces a narrow spectrum. This dipole spectrum is centered at a wavelength of 510 nm, and span is 20 nm from 500 to 520 nm. Figure 5.3(d) and 5.3 (e) show the light extraction from 5 QWs, and 9 QWs, respectively, without nano lens and a perfectly matched layer (PML) has been used to enclose the entire simulated cavity to absorb outgoing electromagnetic waves avoiding non-physical reflections.

5.8 Results and Discussion

Figure 5.4(a) shows the approximate line width of 510nm peak wavelength LED. Figure 5.4 (b) shows electric field intensity in the near field, and xy-view of intensity level is 6.4 x 10^{-3} cd. Figure 5.4 (c) shows the far-field distribution from the top view of the cavity. In this case, the direction of propagation is visible. The source is a highly focused beam with plane waves at many angles but centered at 30 degrees. The box monitor measures the amount of power emitted by the dipole and the power emitted to the far-field. In the simulation, the dipole is located in the middle of the QWs and maintain a peak wavelength at 510 nm. The maximum modulation bandwidth achieved was 6.15 GHz with a nano lens. Lower recombination carrier lifetime leads to faster switching capability and increases spontaneous emission rate from the LED.

The same procedure was repeated to design another two LED, which has peak wavelengths 530 nm and 550nm to check the feasibility to implement CWDM based VLC grid. For 530nm, 7 MQWs were used, and xyz layer dimensions of nGaN were 4000nm,4000nm and 1000 nm, and of p-GaN were 3989, 3938, and 200. Nano lens

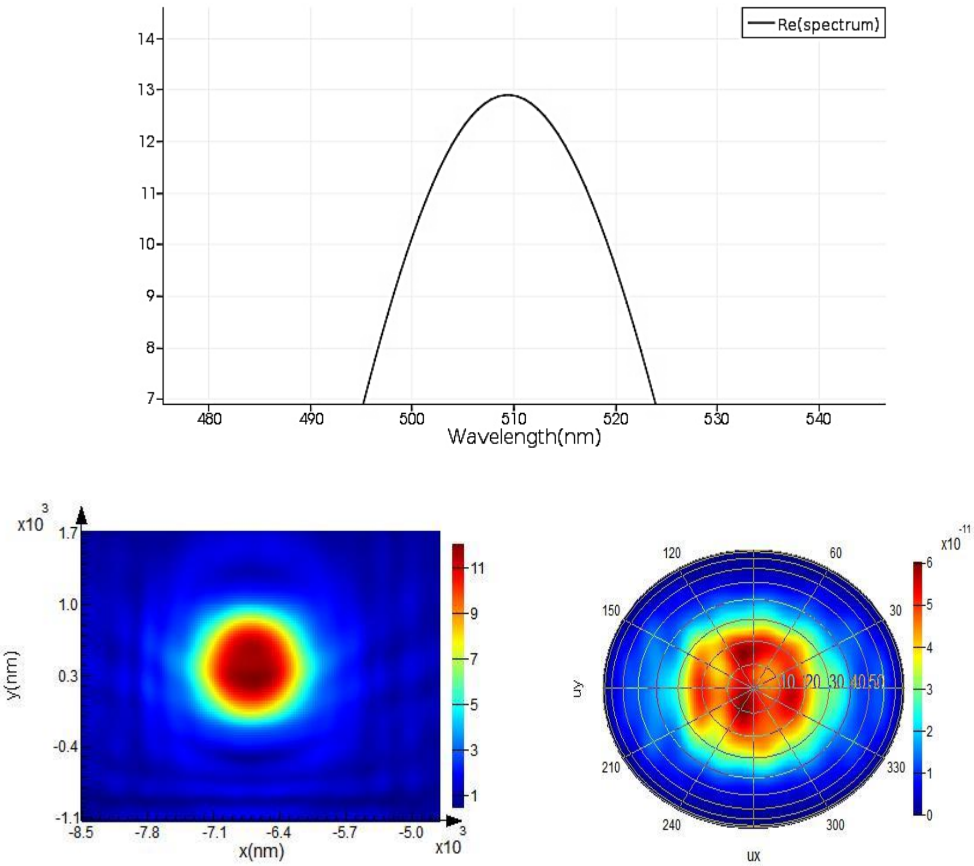

Figure 5.4: (a) LED narrow spectrum with SiO2 lenses (b) Electric field in near field and (c) Far-field pattern for nano lens LED.

radius was 500nm, and InGaN/GaN layer thickness was 50nm. The internal transmitted power from the dipole is 1.1 mW, and the output power of LED was 0.98

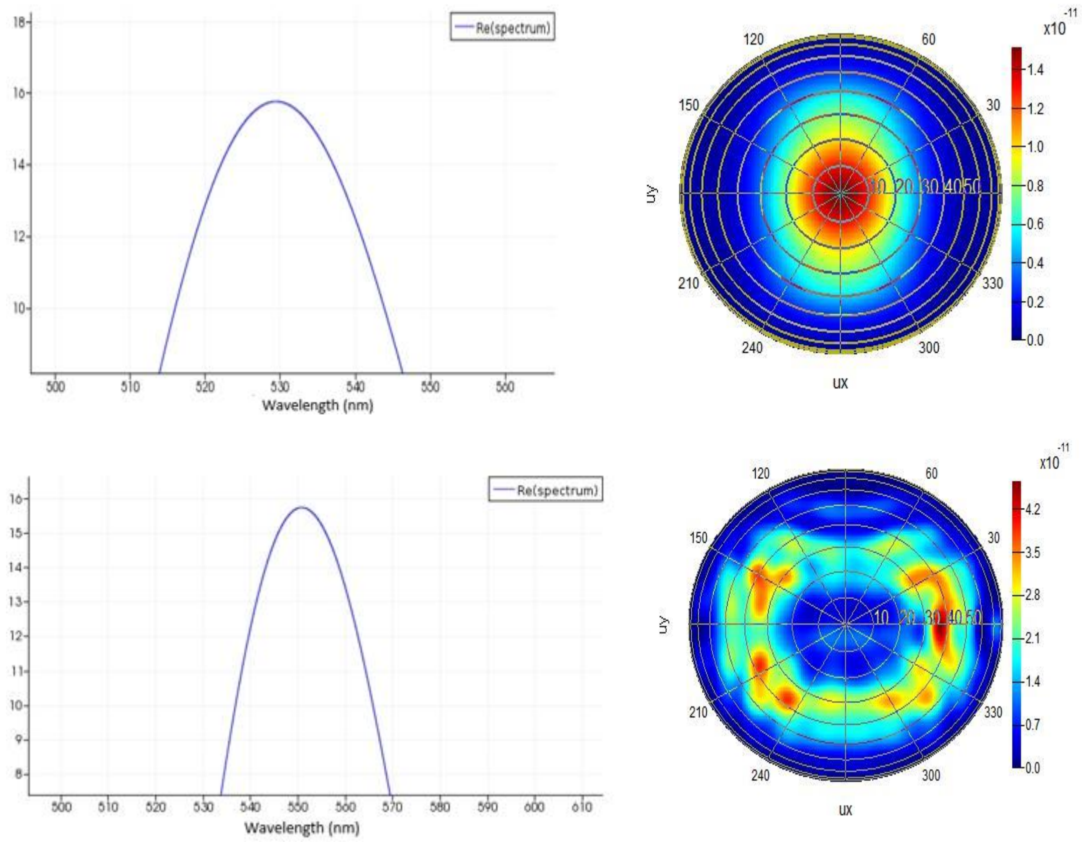

Figure 5.5: LED spectrum and related Far field divergence for peak wavelength 530nm (up), 550nm (down) for CWDM-VLC grid.

mW. For 550 nm peak wavelength, the LED structure required 9 MWQs with 150 nm GaN/InGaN layer concentration. The internal dipole transmitted power was 0.92 mW, and the LED's output transmitted power was 0.88 mW. The performances for 530nm and 550nm are shown in Figure 5.5. The lower electric field results in better recombination of electron and hole and better carrier confinement in the band gap structure and blue-LED peak spectrum shifting by decreasing thickness of the GaN or AlGaN (Lin et al., 2013).

To keep the same material quality, the single well is fixed 50 nm, and the thicknesses of total active region was changed according to the number of QWs, which are 250 nm for 5 QWs, 350nm for 7 QWs and 450nm for 9 QWs. The effects on recombination time with the QW structure change using nano lens and without nano lens have been explained in Figure 5.6. LED modulation bandwidth for both with and without a nano lens were observed. Modulation bandwidth 6.15GHz for the wavelength of 510nm, 2.27 GHz bandwidth for wavelength of 530nm and 0.18 GHz for wavelength 550nm LED where the number of MQW were 5 ,7, and 9 sequentially with a nano lens. Without nano lens bandwidth was 1.31 GHz, 0.11GHz, and 0.07GHz for 5, 7 and 9 MQWs. Therefore, to keep 20 nm FWHM, SiO_2 nano lens and without lens, results are shown in Figure 5.7, where FWHM has increased from 45 nm to 64 nm.

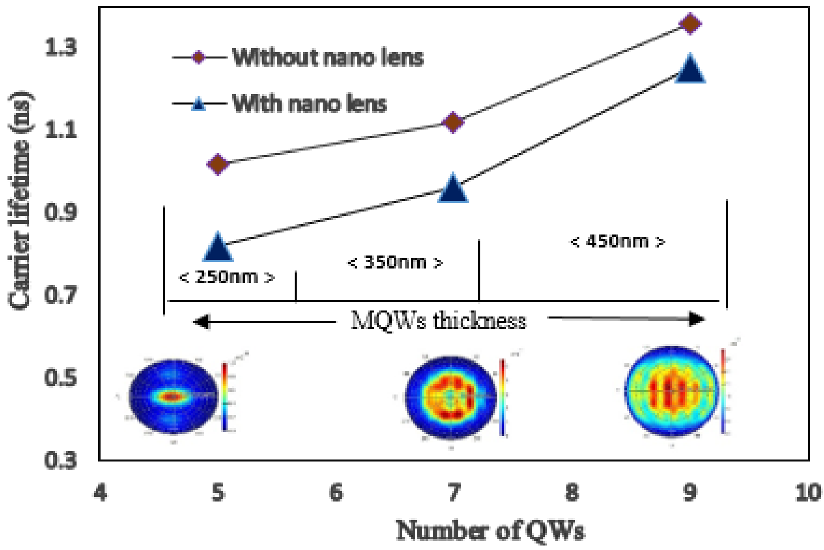

Figure 5.6: Carrier life time vs number of QWs

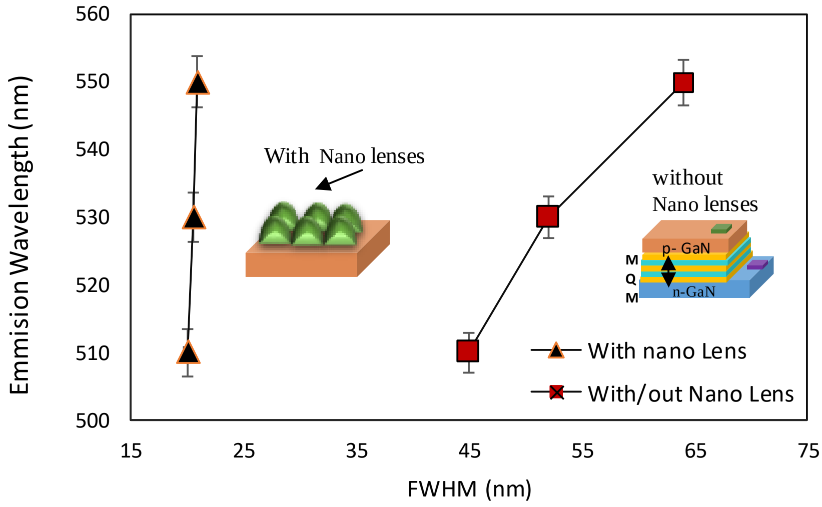

Figure 5.7: Emitted wavelength vs FWHM of the LEDs with and without nano lens

Moreover, another approach has been done to keep constant MQWs thickness about 300nm where each layer thickness changed from 50nm to 42.85nm and 33.33 nm with the increase of QWs and found that the peak wavelength was shifted which has shown in Figure 5.8.

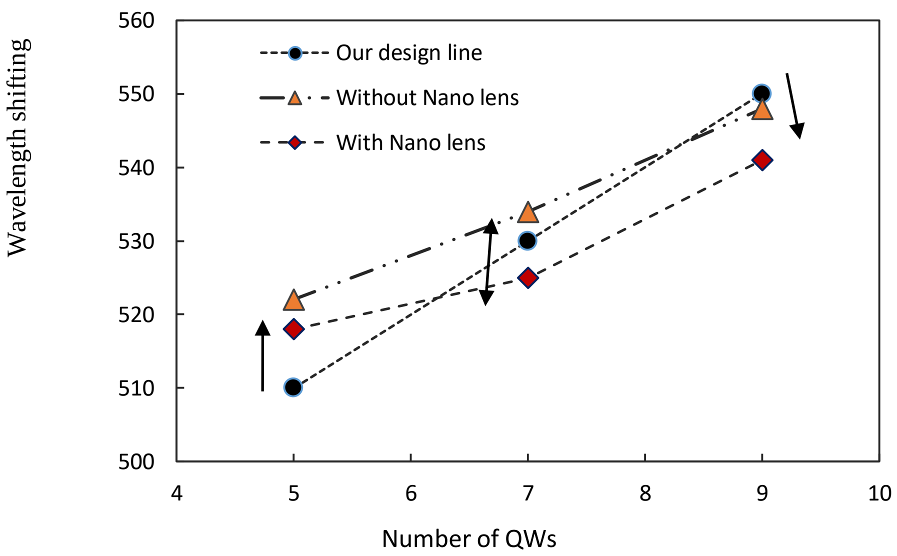

Figure 5.8: Wavelength shifting trend with MQWs

With this condition (fixed QW area), FWHM without nano lens is wider than with the nano lens, as shown in Figure 5.9. With the change of QW number with and without nano lens, the electron carrier lifetime measured in Figure 5.10 where the minimum value is 0.82ns using lens and maximum is 1.72 ns without a lens. New peak wavelength was 510nm, 518nm, and 522nm with nano lens and without nano lens. The 3dB bandwidth was maximum of 9.37GHZ, 6.14GHz, and 0.17GHz for three different QWs number using the nano lens. Without lens, the bandwidth was 2.27GHZ,0.35GHZ, and 0.086GHz simultaneously.

Remaining total area of QWs, In the FDTD simulation, dipole source is responsible for light emission in the QWs in xy plane temperature when re-growing n-GaN microstructure inner side of InGaN/GaN MQWs (Yang et al., 2016). In the FDTD simulation, dipole source is responsible for light emission in the QWs in xy plane (Shakya et al., 2005) and desired peak wavelength was set as a central wavelength in the spectrum of the dipole.

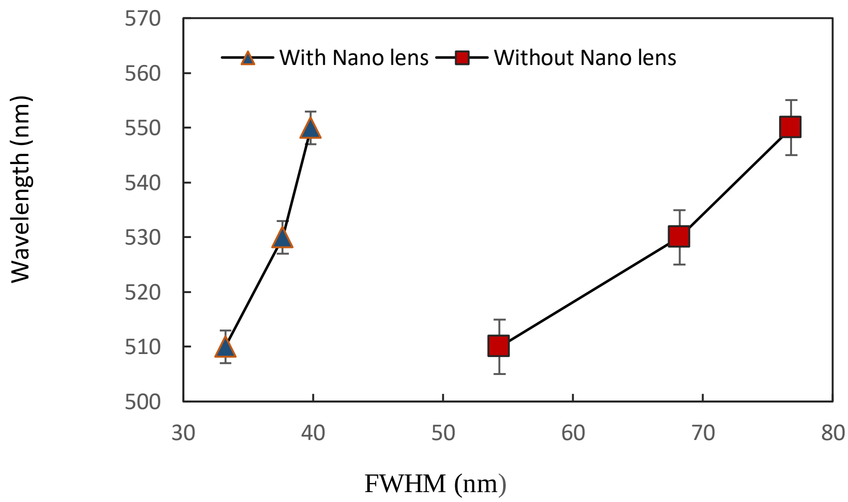

Figure 5.9: FWHM vs Wavelength with fixed QW area

The nano parabolic lens emission was simulated to capture the near-field emission in the air above and converted to control or collimate the far field pattern that is coming out from the dipole source located at the GaN/InGaN active region.

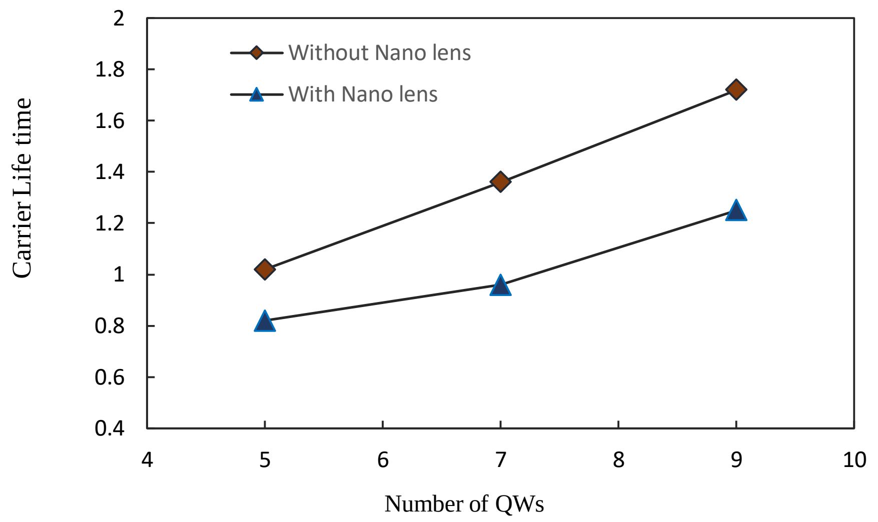

Figure 5.10: Carrier life time vs number of QWs (Thickness is fixed)

5.9 Summary

In this chapter, InGaN/GaN-based multiple quantum well (MQW) LEDs coupled with and without nano-lens on the top layer of LED structure has been designed and investigated. Previous works have used either MQW or nano lens, but this work examines the effect of combining these two to get desired peak wavelengths for implementing coarse wavelength division multiplexing (CWDM)-visible-light communication (VLC) grid. Using FDTD technique, three different peak wavelength LED have been produced at 510nm, 530nm, and 550nm and compared the performance. The single well is fixed 50 nm and the thicknesses of the total active region were changed according to the number of QW increases from 250 nm for 5 QWs, 350nm for 7 QWs, and 450nm for 9 QWs and the effects on recombination time with the change of QW structure using nano lens and without nano lens. Modulation bandwidth 6.15GHz, 2.27 GHz, and 0.18 GHz were for 5 ,7, and 9 QWs with a nano lens and desired wavelength 510nm,530nm and 550nm were achieved simultaneously. Without nano lens bandwidth was 1.31 GHz,0.11GHz and 0.07GHz for 5,7 and 9 MQWs. Another approach was used, where the MQWs thickness was kept at 300nm and each layer thickness was changed from with the increase of QWs. For this case, the peak wavelengths shifted. New peak wavelength was 510nm, 518nm, and 522nm with nano lens and without nano lens. The 3dB bandwidth was a maximum of 9.37GHZ, 6.14GHz and 0.17GHz for three different QWs numbers using a nano lens. Without a lens, the bandwidth was 2.27GHZ,0.35GHZ, and 0.086GHz simultaneously.

The concept was extended to other LED spectrum to establish that the general method can be developed to the CWDM-VLC grid. This method proposed an idea that can contribute to LEDs' design for high-speed VLC applications and solid-state lighting.

HYBRID ROF-VLC SYSTEM FOR 5G NETWORKS

6.1 Introduction

5G wireless technology utilizes RoF network for data transmission between center office (CO) and base stations (BSs) or customer end as a backhaul. There is a vast amount of available spectrum from 3-30 GHz and 30-300 GHz, known as super-high frequency (SHF) and extremely high-frequency millimeter wave (mmWave) ranges. The mmWave band normally refers to the frequency range from 5 GHz to 300 GHz with wavelength spacing from 1mm to 100mm (Sharma et al., 2020). The major challenges in RoF systems are an optical signal generation at mmWave range and connecting backhaul to an indoor customer unit in a spectrally efficient way.

Both mmWave and VLC have similar advantages considering high bandwidth (Feng et al., 2016), but both have a high dependency on line-of-sight (LoS) to achieve good performance. For indoor downlink communication, LED is one of the possible sources for VLC as a transmitter. Because, it can provide white light for illumination and high-speed data rate for transmission. A combination of multi-color red, green, blue, and yellow (RGBY) LEDs is mostly used for high speed data communication as a WDM-VLC system to increase channel number (Chaudhary et al., 2019). Recently, CWDM-VLC was proposed by (Rahman & Parthiban, 2020) to increase the higher data rate for indoor communication utilizing the full visible spectrum. In this chapter, a hybrid system combined with mmWave RoF and VLC has been proposed. The performance of VLC downlink is measured by different optical filters such as Bessel, Trapezoidal, Gaussian, and Fabry Perot. This results are presented based on the BER of the signal, the power level for different indoor link range, and beam divergence of VLC channels. A maximum data rate of 2.64 Gb/s and 6.58 Gb/s was achieved with 10 and 20 channels off the shelf LEDs using 16 QAM with a reasonable of BER $3.8\text{x}10^{-3}$. Moreover, compared to other works, 2.5 Gb/s VLC uplink data using OOK modulation was down converted at Central Office (CO) through mmWave based RoF backhaul successfully.

6.2 Hybrid VLC System

Different types of sources have been proposed to improve the uplink communication, i.e. Radio Frequency (RF)(Basnayaka & Haas, 2015), IR LED (850nm) (Alresheedi et al., 2017), Laser Diode (LD)(Janjua et al., 2015), and UV LED (375nm) (He et al., 2019).

Table 6.1: Comparison table for hybrid VLC system for indoor communication

Name, year	**Hybrid link**	**VLC range**	**Data rate**	**UP/DW link (VLC link type)**	**Modulation**
(Khalid et al., 2011)	1 km RoF	1- 3 m	54 Mb/s	UP+DW link	64 QAM
Simarpreet Kaur,2019 (Kaur et al., 2019)	50 km SMF	150 cm IR LED	1.87 Gb/s	UP ||DW link	OFDM-WDM
(R. Deng et al., 2016)	100 km SMF	6 m VLLC (LD)	2.65 Gb/s	Downlink	16QAM-OFDM
(Z. Huang et al., 2017)	430-m FSO	1.0-m VLC	450-Mb/s	Downlink	OOK
(Pavan & Jeyachitra, 2018)	30kmSMF +150m MMF	80 cm VLC	600Mb/s	Downlink	16/64QAM-OFDM
(Mandal et al., 2018)	50 km SMF	10m FSO/LD	2.5 Gb/s	UP ||DW link	OOK
(Chia-Ti Chen,2013)	20 km SMF	15m (LD)	2.5 Gb/s	UP ||DW link	16QAM-OFDM

Table 6.1 compares different existing works that use RoF-VLC hybrid network model. Using simulations, the highest data rate achieved is 600 Mb/s over 80cm VLC link, where they used 30 km SMF and 150 m MMF as a backhaul (Pavan & Jeyachitra, 2018). IR LED was used for uplink which was connected 50 km optical fiber link getting data rate 1.87 Gb/s. especially, WDM CO-OFDM-PON employed in this by bidirectinal VLC model (Kaur et al., 2019). Experimentally, a hybrid RoF-VLC system has been demonstrated to transmit 54 Mb/s over a visible distance range (3 m free space) (Khalid et al., 2011). The highest data rate achieved using LED-based VLC is 450 Mb/s over 1m indoor link (Z. Huang et al., 2017). A bidirectional WDM hybrid fiber-wired/fiber, wireless/fiber, VLC/fiber, IVLC transmission system based on quantum dash-laser diode (QD-LD) have been demonstrated with 10 Gb/s 10 GHz and 100GHz mmWave signal over 50-km SMF and 40 m optical free space downlink and 10 m free space considered for uplink with 2.5 Gb/s data rate (Mandal et al., 2018). A data rate of 2.5 Gb/s was achieved using 16 QAM-OFDM signals with two Laser Diodes (LD) both at transmitter and receiver ends with 20 km SMF and 15 m indoor VLC link range (C.-Y. Chen et al., 2013).WDM system was used in a hybrid

RoF-VLC link using passive optical network (WDM-PON) in (Zhong et al., 2015). They achieved data rates of 150 Mb/s with 2PAM and 600 Mb/ by 8PAM, respectively. Optical Wireless Communication (OWC) channel performance can be analyzed with different optical filters (e.i, Bessel, Trapezoidal, Gaussian and Fabry Perot optical filters) (Murugan & Sumathi, 2019).

A hybrid RoF-VLC system was propose using 5G mmWave wireless backhaul connected to an indoor CWDM-VLC grid to increase data-rate for the first time. BER performance has been improved using different optical filters (i.e., Bessel, Trapezoidal, and Rectangle). Millimeter-wave frequency reuse is also proposed for the first time for uplink communication.

6.3 Comparison Between mmWave and VLC

VLC and mmWave both have similar advantages such for wide spectrum (wider bandwidth), capability to transmit few gigabit/second data, higher security for LOS communication, lower interference, and license free etc. There are crucial factors that allow VLC to be more appropriate for indoor communication and to be a desirable complement of mmWave for 5G networks. The major differences between VLC and mmWave are shown in Table 6.1 captures (Feng et al., 2016). First, the VLC band has a higher spectrum at THz than the mmWave (GHz). Wavelength range in the VLC from 380nm to 780nm and a frequency range in the vicinity of 385 THz to 790 THz and which is completely license-free and low cost for implementation in the exiting setup. Secondly, VLC is based on the lighting infrastructure realized by white light-emitting diodes (LEDs), which will capture nearly 55 percent of indoor illuminations by 2020, and almost 100 percent by 2030 (Holland & Alliance, 2014). Considering exiting infrastructure VLC needs no additional costs and half of power consumption in indoor lighting.

In contrast, mmWave communication needs to be packed by CMOS chips and high-gain antennas at both the user end and the base station, mandating avoiding hardware complexity and costs. Both are subject to very strong penetration loss, which makes them rather comparable to each other in indoor arrangements.

Table 6.2: mmWave and VLC comparison

	Spectrum	**License**	**Safety**	**Power**	**Cost**	**Range**
mmWave	3-300GHz	Partly free	Medium	High	Medium	100-200m
VLC	385-790 THz	Free	High	Low	Low	<10m

6.4 mmWave Based Uplink Communication

In the existing VLC model, an indoor uplink's capacity is lower than its downlink; it can cause a problem for sending request and subsequent acknowledgments. Most of the literature highlight three different possible instruments such as RF communication, infrared (IR) LED and LD for uplink transmissions in indoor VLC (Alresheedi et al., 2017), (Janjua et al., 2015). Furthermore, suppose a large number of users are lodged in a single room and visible light uses as a transmitter for the uplink which will affect the indoor lighting with discomfort to people's eyes in the room. Compared to visible light based uplink schemes, radio frequency-based uplink transmission is more viable because of its wide applications (Cossu, Corsini, et al., 2014). Among radio frequency spectrum, mmWave has great prospect to implement as an uplink communication in VLC because it operates in a different spectrum from VLC, which prevents co-channel interference and has longer bandwidth capacity for frequency re-use as uplink. Though mmWave signal was used in fiber link, it also can use in wireless environment with lower electromagnetic interference because of its small size of antennas and less expensive radio frequency devices.

6.5 Optically mmWave Signal Generation

To simplify the hybrid network and remove VLC uplink complexity, a new method of full duplex transmission using the concept of frequency re-use. A configuration is depicted in Figure 6.1 consists a triple tone mmWave generation. Three independent continuous wave (CW) laser diodes (LDs) produce light waves at λ1, λ2 and λ3, set to 1550.2, 1550.016 and 1549.715 nm. The frequency spacing of 22.5 GHz exists between λ1 and λ2 and 37.5 GHz offset between λ2 and λ3. The optical light from the first laser is modulated by the random sequence of data mapped with NRZ OOK modulation using an MZM. The modulator's output is shown in Figure 6.1(a), which illustrates the data on top of the optical carrier. The other two CW lasers are un-modulated and coupled with the modulated tone to produce a triple tone spectrum, as shown in Figure 6.1(b).

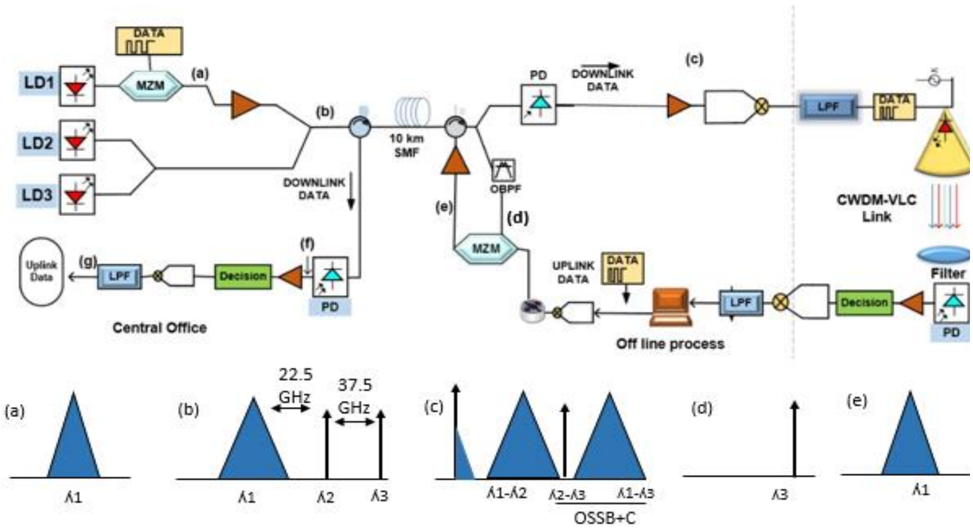

Figure 6.1: Triple tone mmWave hybrid system for wavelength reuse

The signal then enters an optical circulator port 1 with low insertion loss and high isolation loss between port 1-3. After the emission of light from port 2 the light passes through 20 km standard single-mode fiber (SMF) and arrives at the receiver end in a similar circulator. The light exits from port 3 and is divided by an optical coupler. One output of the coupler is connected to a PIN PD with responsivity of 0.8 A/W. The output of the PD is shown in subset Figure 6.1(c). where the electrical self homodyning method is used to down-convert to the baseband signal. The desired mmWave signal at 60 GHz with modulated data is produced by the biting modulated light wave (λ1) and free-running tone of λ3. Another mmWave signal with an unmodulated tone at 37.5 GHz and a baseband replica that is also produced for frequency reuse. At this point, an electrical BPF selects the tones at 60 GHz transfer to VLC access point (VAP) through an LPF filter for adjustment with LED driver to drive this signal into LED for indoor VLC (CU). Other output 37.5 GHz signal goes to an optical bandpass filter (OBPF) for carefully chosen out to be used as VLC uplink which is shown in inset Figure 6.1 (d). This tone is amplified and used as the carrier for the uplink data. Once again, the uplink optical transmission is in an optical suppressed carrier OSSB. The modulated signal is then sent back through SMF via port 3-1 of the circulator and passes through port 2-3 in CO.

6.6 Hybrid System Architecture

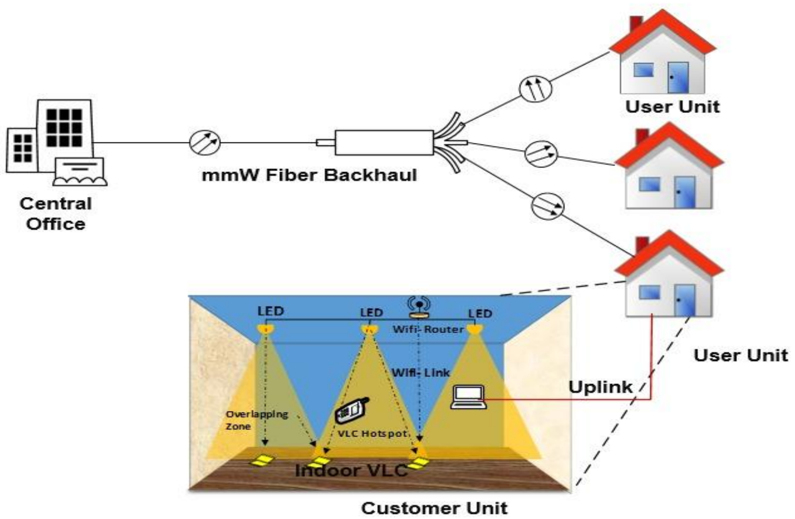

Figure 6.2: Proposed hybrid 5G mmWave -WDM-VLC model fiber backhaul from CO to VAP and CWDM-LED network for indoor.

Considering a successful and efficient wireless broadband network, the challenges would be generating 5G mmWave signal in the RoF system and distribution to the VLC access point for the indoor communication link. Figure 6.2 shows the overview of hybrid RoF-VLC system with 5G mmWave backhaul. In the central office (CO), an array of laser modules produce optical tones separated by specific frequencies, corresponding to the desired triple tone mmWave signal based on optical heterodyning. Three independent continuous wave (CW) LDs produce three different light waves. Out of these tones, one is modulated using a standard Mach-Zehnder modulator (MZM) with electrically coded data. CO is connected to the VLC customer unit using 20 km fiber link, and a photodetector receives mmWave signal with a baseband signal. With the help of a BPF, the desired mmWave signal and baseband signal are separated. Electrical self homodyning is used in order to convert the signal to baseband down. After detecting baseband signal, it goes to an indoor VLC access point and converted to visible light signal through LED. A VLC transmitter's structure consists of CWDM techniques to increase more data channels for high-speed indoor communication, and PD received this light signal at the VLC receiver. After receiving downlink data, it retransmits back to RoF backhaul through the mmWave 5G signal as a VLC uplink, and finally, the uplink data is received at CO.

6.7 Integration of CWDM-VLC at Customer End

The proposed method for CU in this project is shown in Figure 6.3. In this model, the downlink data is first received at the PD (VLC access point). Self homodyning is an electrical detection method that produces the baseband data illustrated in Figure 6.3(b), and this received baseband signal transmits to the LED through bias tee and this multi colors LED combined with CWDM-VLC system gives superior performance for indoor link. It uses 10/20 different wavelengths as a separate channel. This visible light signal passes through the optical wireless channel, and channel range is set to 3 m as standard indoor length and different channel parameters to get optimum performance and fiber to VLC link quality. Four different optical filters, such as Gaussian, Bessel, Trapezoidal, and Rectangle, are used to increase the transmission bandwidth and indoor link performance.

The other output of the power divider is connected to another OBPF, which filters out the free-running tone of $\lambda 2 - \lambda 3$ which is shown in Figure 6.3(c). This tone is

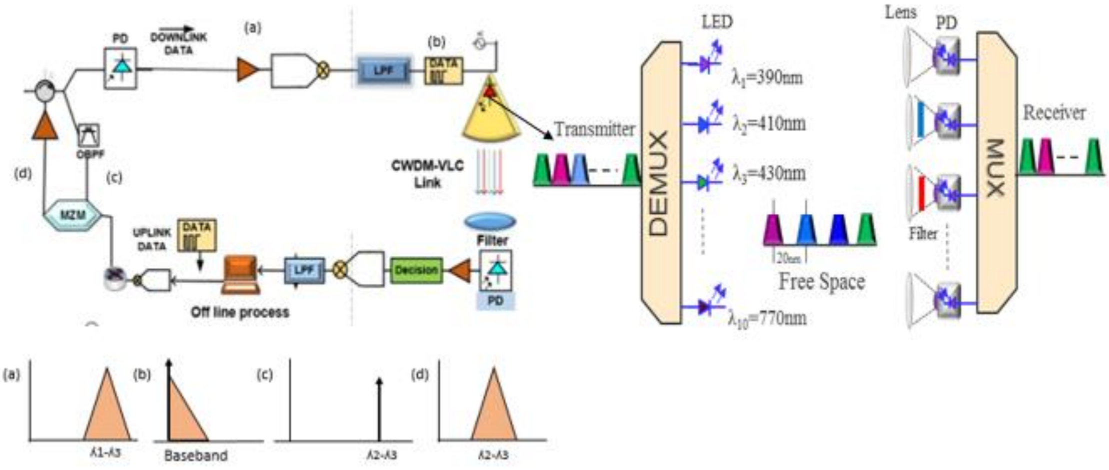

Figure 6.3: Integration of CWDM-VLC at Customer unit

unmodulated and can be used as an uplink transmitter. Therefore, it is used as a carrier of an electrical mixer determined by 2.5 Gb/s NRZ signal, as shown in Figure 6.3(d). The up-converted signal is amplified and passed through port 1-2 of the circulator and sent to RoF backhaul for transmission. A hybrid VLC system has been designed based on the principle of mmWave based VLC uplink and CWDM based VLC downlink. With the mmWave uplink, the bidirectional VLC system performs better.

6.8 Mathematical Model

This system model is explained through mathematical equations below. The electric fields of three independent laser signals have shown as,

$$E_1 \exp j(2\pi f_1 t + \varphi_1) \tag{6.1}$$

$$E_2 \exp j(2\pi f_2 t + \varphi_2) \tag{6.2}$$

$$E_3 \exp j(2\pi f_3 t + \varphi_3) \tag{6.3}$$

where E is the peak amplitude of the electric field of each laser. f_1, f_2 and f_3 are optical frequencies, and ϕ_1, ϕ_2 and ϕ_3 are distinct phase characteristics of three lasers. In this scheme, the optical signal from LD_1 is modulated (Figure 6.1), which is achieved by applying Taylor series expansion and combined with two unmodulated signals from LD_2 and LD_3, which can be represented by

$$A(t) = A_1(t) + A_2(t) + A_3(t) \tag{6.4}$$

$$A_1(t) = \exp j(2\pi f_1 t + \varphi_1)[1 + jmcos(2\pi f_m t)]$$

$$A_2(t) = \exp j(2\pi f_1 t + \varphi_1) + A_2(t) + A_3(t)$$

$$A_3(t) = \exp j(2\pi f_1 t + \varphi_1) + A_2(t) + A_3(t)$$

After passing through SMF, the overall signal is called $A_f(t)$. This received signal gets distorted by the SMF and is shown as

$$A_f(t) = A_{f_1}(t) + A_{f_2}(t) + A_{f_3}(t) \tag{6.5}$$

$$A_{f_1}(t) = [\exp j(2\pi f_1 t + \emptyset_1 + \varphi_0) + \frac{m}{2}\exp j(2\pi(f_1 + f_m)t + \emptyset_1 + \varphi_1) + \frac{m}{2}\exp j(2\pi(f_1 + f_m)t + \emptyset_1 + \varphi_2)] \tag{6.6}$$

$$A_{f_2}(t) = \exp j(2\pi f_2 t + \emptyset_2 + \varphi_3) \tag{6.7}$$

$$A_{f_3}(t) = \exp j(2\pi f_3 t + \emptyset_3 + \varphi_4) \tag{6.8}$$

where $\varphi 0$, $\varphi 1$, $\varphi 2$, $\varphi 3$ and $\varphi 4$ are spectral phase delays suffered by SMF transmission. The signal is then received at the CU, the optical signal is received and undergo various structural procedures. Since a wavelength re-use structure is used, the optical light signal from equation 6.8 is separated from the signal using an optical bandpass filter for uplink carrier usage. Other two signals are detected by PD and sent through down-conversion path this path uses the same self homodyning method as CU to produce baseband data.

The down-converted uplink data is used as the modulation data and is fed to a MZM which uses the signal at Equation (6.8) as optical carrier. Using Taylor series expansion, the outcome of the MZM ($B_1(t)$) can be expressed as

$$B_1(t) = \exp j(2\pi f_3 t + \emptyset_3)\,[1 + j\frac{N}{2}\exp(2\pi f_n t)]$$

$= \exp j(2\pi f_3 t + \emptyset_3)\,[1 + \frac{N}{2} \exp j2\pi f_n t + expj - 2\pi f_n t)]$

$= \exp j(2\pi f_3 t + \emptyset_3) + \frac{N}{4} \exp j(2\pi f_n t + 2\pi f_3 t + \emptyset_3) + expj(2\pi f_3 t + \emptyset_3 - 2\pi f_n t)]$

$$= \exp j(2\pi f_3 t + \emptyset_3) + \frac{N}{4} \exp j(2\pi t(f_n + f_3) + \emptyset_3) + \frac{N}{4} expj(2\pi t(f_3 - f_n) + \emptyset_3)] \quad (6.9)$$

which shown the optical signal at center frequency of f_3 with data bandwidth of f_n, carrying the laser phase of $\phi 3$. This signal is sent back through the SMF to the CO. After transmission, the signal can be expressed as

$$B_{f_1}(t) = \exp j(2\pi f_3 t + \emptyset_3 + \varphi_8) + \frac{N}{2} \exp \mathrm{j}(2\pi(f_3 + f_n t) + \emptyset_3 + \varphi_9) + \frac{N}{2} \exp \mathrm{j}(2\pi(f_3 + f_n)t + \emptyset_3 + \varphi_{10})] \quad (6.10)$$

where $\varphi 8$, $\varphi 9$ and $\varphi 10$ are the phase noise induced by fiber dispersion. At CO, the optical signal is detected using a direct PD which outputs

$$i_p(t) = R \times B_{f_1}(t) \times B^*{}_{f_1}(t) \quad (6.11)$$

where R is responsivity of the PD and $B^*{}_{f_1}(t)$ is the complex conjugate of e.q 6.10.

At the VLC access point, optical self-heterodyning produces signal at baseband which is known as baseband replica shown as

$$i_p(t) = R \times [(A_{f_1}(t) + A_{f_2}(t) + A_3(t)) \times ((A^*{}_{f_1}(t) + (A^*{}_{f_2}(t) + (A^*{}_{f_3}(t))] \quad (6.12)$$

Here $A^*{}_{f_1}(t)$, $(A^*{}_{f_2}(t)$, $(A^*{}_{f_3}(t)$ are complex conjugates of the equations (6.6-6.8) and R is the responsivity of PD. At the Customer Unit (CU), the received mmWave signal arrives with desired data carrying tone and mixed with itself as a self-homodyne detection method to make baseband and which as shown below

$$mcos\{2\pi(f_d)t + \varphi_d\} \quad (6.13)$$

Which has a center frequency of f_{d} and has a phase noise of φ_d. This signal is used for indoor communication through LEDs which has Lambertian radiant intensity, which can be explained as

$$R_i(\emptyset) = (m_l + 1)cos^m(\emptyset)/2\pi \quad (6.14)$$

$$m_l = -ln2/ln(\cos(\emptyset_{\frac{1}{2}})) \tag{6.15}$$

where $\emptyset$ is irradiance angle, *ml* is the Lambertian emission, that relates to the LED's semi-angle at half power $\emptyset_{\frac{1}{2}}$ as shown in Equation (9). The horizontal luminance Ehor at point (x, y) is given by

$$E_{hor} = I(0)cos^{ml}(\emptyset)/r^2\cos(\varphi) \tag{6.16}$$

where r is the line-of-side (LOS) distance in the free space between the LED and photodiode (PD). Modulated output signal power from LED, $P_0(t)$, can be described as

$$P_0(t) = P_{LED}[1 + m_i x(t)] \tag{6.17}$$

where P_{LED} is the launched optical power of LEDs, m_i is the modulation index, and $x(t)$ is the non-return-to-zero (NRZ) on-off-keying (OOK) signal. The modulated signal depends on the electron lifetime, RC constant, and the materials of the diode. 3dB bandwidth of the LED can measure using the following equation (Chun et al., 2016).

$$f_{3dB} = \frac{\sqrt{3}}{2\pi(\tau_n + \tau_{rc})} \tag{6.18}$$

where τ_n is an electron lifetime, and τ_{rc} is the RC constant of parasitic capacitance. The light signal passes through the wireless free space channel, and the DC gain of this channel is measured by (H. Huang et al., 2015).

$$H(0) = \frac{(m_l+1)Acos^{ml}(\theta)\cos(\varphi)T_S(\psi)}{2\pi r^2}[\varphi \leq \psi FOV] \tag{6.19}$$

where *A* is the physical surface area of the photodiode (PD), *r* is the distance between the LED and PD, $T_s(\psi)$ is the gain of the optical filter at the receiver, ψ is the angle of incidence, and ψ_{FOV} is the field of view (FOV) of PD. Optical filters are important for higher bandwidth and rejecting the ambient light. For the Gaussian filter, the frequency transfer function can be given as:

$$H(f) = \alpha e^{-ln(\sqrt{2})(\frac{f-f_c}{\frac{B}{2}})^2} \tag{6.20}$$

where *H(f)* is the filter function, α is the insertion loss, *d* is the parameter depth, f_c is filter's center frequency, *B* is the filter bandwidth, and *f* is the frequency. Therefore, the transfer function used for a rectangular optical filter is

$$H(f) = \begin{Bmatrix} \propto, (f_c - \frac{B}{2} < f < f_c + \frac{B}{2}) \\ d \end{Bmatrix} \tag{6.21}$$

For the Bessel filter, the transfer function is

$$H(f) = \alpha \frac{d_0}{B_N(s)} \tag{6.22}$$

where *N* is the parameter order, and d_0 is a normalizing constant, and $B_N(s)$ is the filtering order, which can be defined as:

$$B_N(s) = \sum_{k=0}^{N} d_k S^k \tag{6.23}$$

where $$d_k = \frac{(2N-k)!}{2^{N-K}.k!(N-k)!} \tag{6.24}$$

and $$S = j\left(\frac{2(f-f_c).W_b}{B}\right) \tag{6.25}$$

Here, *B* is the filter bandwidth, and W_b denotes the normalized 3 dB bandwidth (for $N \geq 10$). Bandpass filters are used to transmit electromagnetic radiation within a selected spectral region, and filter order defines the amount of light passing through the filters.

6.9 Simulation Setup

Three independent CW LDs used to produce 3 different light waves at LD1 are 1550.2 nm, LD2 is 1550.016 nm and LD3 is 1549.715 nm to generate a triple tone. The frequency spacing has been set 22.5 GHz between LD1 and LD2 and 37.5 GHz offset between LD2 and LD3. The optical signal from the first laser is modulated by NRZ OOK and 16 QAM or 4 bits per symbol. In that case of 16 QAM, gray code differential coding is applied to the input binary bit sequence for better BER. The other two CW lasers are un-modulated and coupled with the modulated tone to produce a triple tone spectrum by optical heterodyning. The desired mmWave signal at 60 GHz with modulated data is produced by the biting modulated light wave (LD1) and free-running tone of LD3. Another mmWave signal with an unmodulated tone at a frequency difference of 37.5 GHz and a baseband replica that is also produced. Then the signal goes to 20 km long standard single-mode fiber (SMF) through an optical circulator. Then light signal arrives at the customer end, entering into a similar circulator. The light exits from the circulator and is divided by an optical coupler. One output of the coupler is connected to a PIN PD and using electrical self homodyning to down-convert the signal to baseband. At this point, an electrical BPF selects the tones at 37.5 GHz and 60 GHz to transfer through an LPF filter for adjustment with an LED driver to drive this signal into LED for indoor VLC (CU). Another output goes to an optical bandpass filter (OBPF) for the signal to be carefully chosen out to be used as the mmWave signal theme OSSB+C for the VLC uplink, which is explained in Figure 6.4.

The received baseband signal transmits to the LED through bias tee and this multi colors LED combined with CWDM-VLC system gives superior performance for an indoor link.

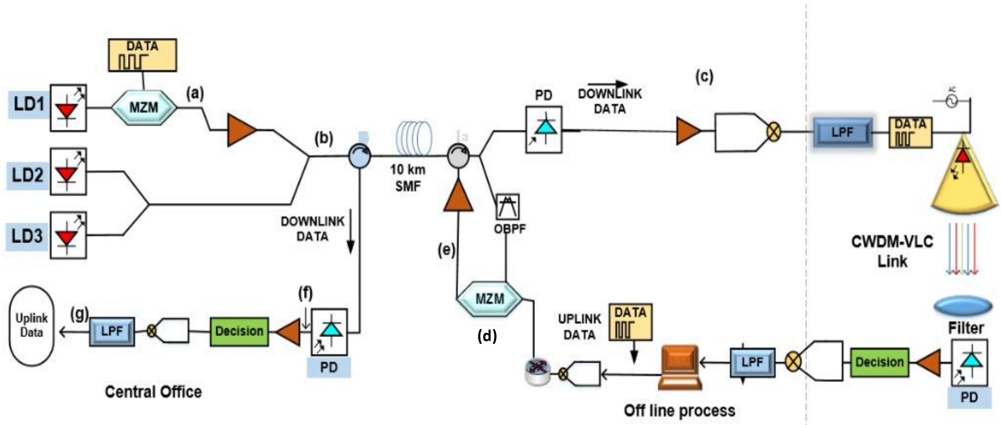

Figure 6.4: Layout of central office and customer unit of proposed RoF-VLC system ((a) MZM modulated signal from LD1, (b) triple tone spectrum from combined three lasers, (c) received 60GHz modulated data signal, (d) VLC uplink data, (e) VLC uplink signal combined with mmWave signal, (f) signal at circulator after fiber backbone link (g) received signal from CU at the CO

It uses 10/20 different wavelengths as a separate channel. This visible light signal passes through the optical wireless channel where channel range is set to 3 m as standard indoor length. Each LED has 20 nm of FWHM to make whole visible spectral slicing into 20 channels considering the CWDM grid. Four different optical filters such as Gaussian, Bessel, Trapezoidal, and Rectangle are used to increase the modulation bandwidth of LEDs and the performance-wise Bessel filter is used for the final indoor link. After receiving the downlink data, the user sends the uplink data to the central office through the same RoF backbone link with another mmWave frequency. With the mmWave uplink, the bidirectional VLC system performs better. All numerical parameters associated to the system permanence for this proposed hybrid RoF- VLC model have been tabulated in Table 6.3.

Table 6.3. Simulation Parameters

Component	Parameter	Value
Global Parameter	Bit rate	2.5 Gb/s
	Samples per bit	64 samples
	Time window	5.12e-006s
	Sequence length	64 bits
Customer Unit (CU)	Wavelength	
Transmitter (LED)	10 CHs	390, 430,470,510,550, 590,630,670,710,750
	20 CHs	390,410, 430,450, 470, 490,510,530, 550,570, 590,610,630, 650,670, 690,710,730, 750,770
	Carrier lifetime	3.95e-09s
	RC content	3.95e-09s
	Modulation BW	50MHz
	Slope efficiency	0.8W/A
Free space Channel	Beam divergence	1-10(mard)
	Tx aperture dia	10mm
	Rx aperture dia	25mm
	Range	1m-10m
Receiver APD	Responsivity	0.65A/W
	Bandwidth	2.5GHz
	Dark current	10 nA
	Load resistance	50 Ohm
Base Station (BS)		
SMF	Length	20 km
	Ref Wavelength	1550.2nm
	Attenuation	0.2dB/km
Central Office (CO)		
CO LDs	LDs frequencies	1550.2, 1550.016, 1549.715
	Prefix points	8
	Modulation type	16 QAM
	Gray code	Yes

6.10 Results and Discussion

Results are obtained from the proposed RoF-mmWave-VLC hybrid system, and this model which is tested with several iterations to achieve the best results. mmWave based optical fiber backhaul is considered, which is connected to an indoor visible light access point (VAP) $9m^2$ (3m×3m) room condition. mmWave generation is based on a multi-tone optical ROF methodology at CO. In the first phase of the result, apply the proposed method of mmWave signal generation. Figure 6.5 (a) shows transmitter modulated data on the LD1 at a wavelength of 1550.2 nm using a single drive MZM.

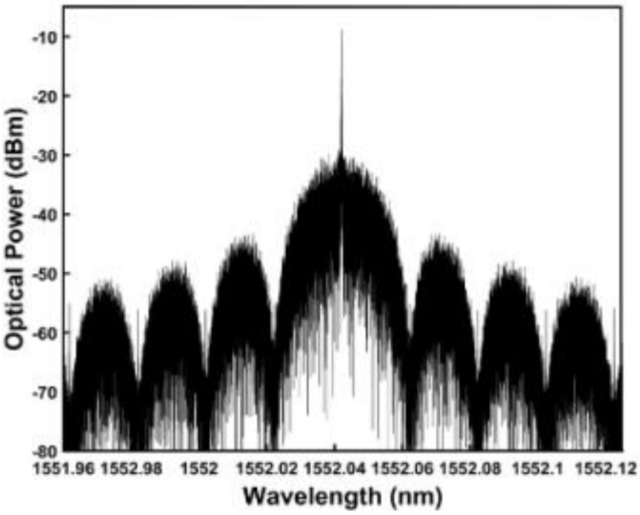

(a)

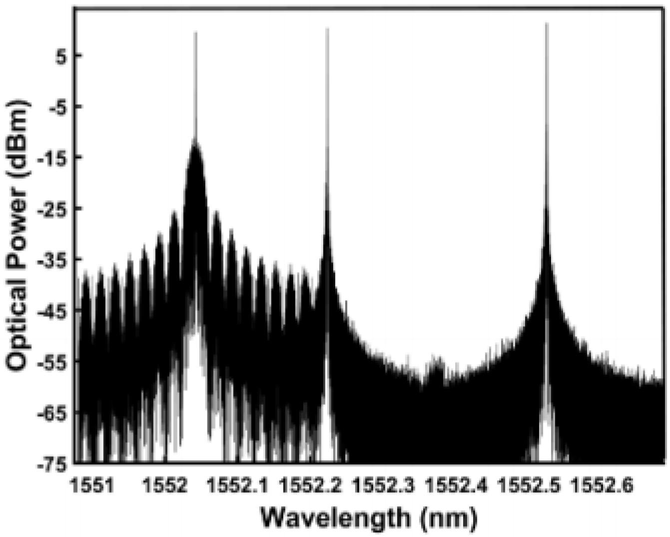

(b)

Figure 6.5 (a) Transmitted laser spectrum, (b) Optical Spectrum of the triple tone signal.

This modulated optical signal is then coupled with the other two un-modulated signals at 1550.014 nm and 1549.715 nm, which is shown in Figure 6.5 (b) constituting a triple tone optical spectrum. All three tones are adjusted to transmit -10 dBm power. Due to short-haul connection, not much optical power is required, and avoiding fiber non-linearity is also important. As expected, when optical signals at different wavelengths are detected, the resulting spectrum generates several tones. These include a mmWave signal which carries the baseband data at 60 GHz, an unmodulated tone at 37.5 GHz, and another data-carrying signal at 22.5 GHz. An electrical BPF

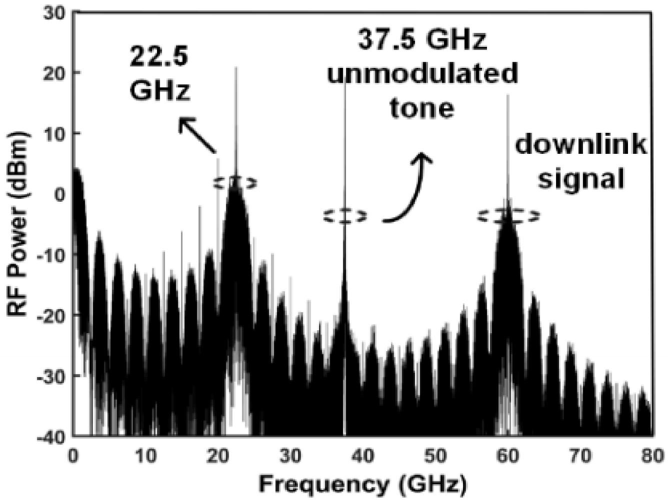

Figure 6.6: Generated mmWave signal at 60 GHz, 22.5GHz and 37.5 GHz

selects the tones at 37.5 GHz and 60 GHz to transfer to CU from Figure 6.6. This optical signal is filtered from the receiving signal using an OBPF of Bessel type with center wavelength of 1552.524 nm wavelength reuse to be used for uplink transmission. The electrical amplifier of gain 30 dB is used to boost the power. At this point, an electrical BPF selects the tones at 37.5 GHz and 60 GHz to transfer through an LPF filter for adjustment with an LED driver to drive this signal into LED for indoor VLC (CU). Figure 6.7 (a) shows the baseband signal at the customer unit with 2.5 GHz which will transmit to an LED driver at the customer unit for an indoor VLC access point (VLC-AP). The initial LED bandwidth was 50 MHz for the end-user

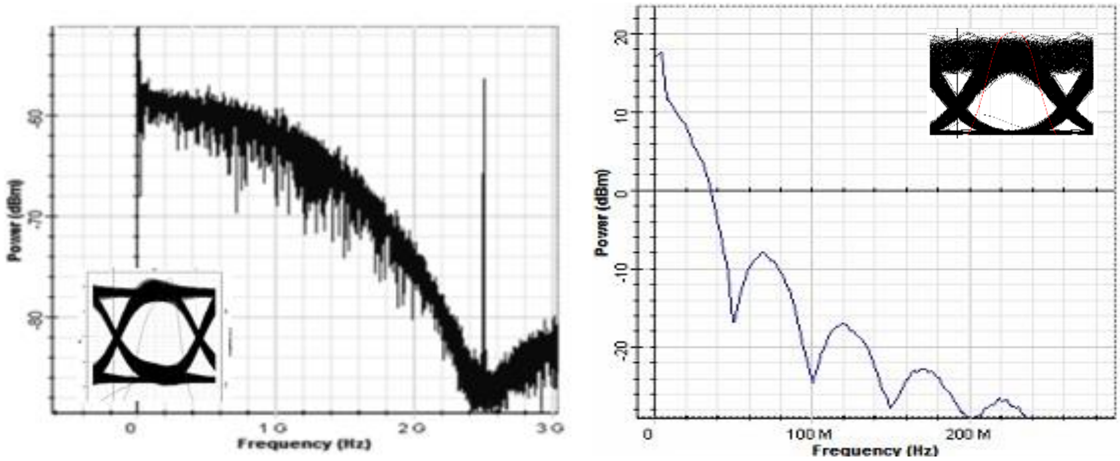

Figure 6.7(a): Indoor baseband signal 1 GHz, (b): Downlink: 50 MHz LED bandwidth

controlled by the driver, shown in Figure 6.7 (b). LED bandwidth can be extended up to 70 MHz using Bessel, Trapezoidal, Rectangular, and 100 MHz using Gaussian optical filter. Each LED can transmit up to 80 Mbps data using Bessel, Trapezoidal, Rectangular and 100 Mbps with a Gaussian filter to maintain FEC limit $3.8\text{x}10^{-3}$ using OOK modulation scheme from Figure 6.8.

Transmitted original data bit from CO, received OOK bit stream at VLC receiver, and 16QAM constellation diagram at the user receiver point has been shown in Figure 6.8 (inside).

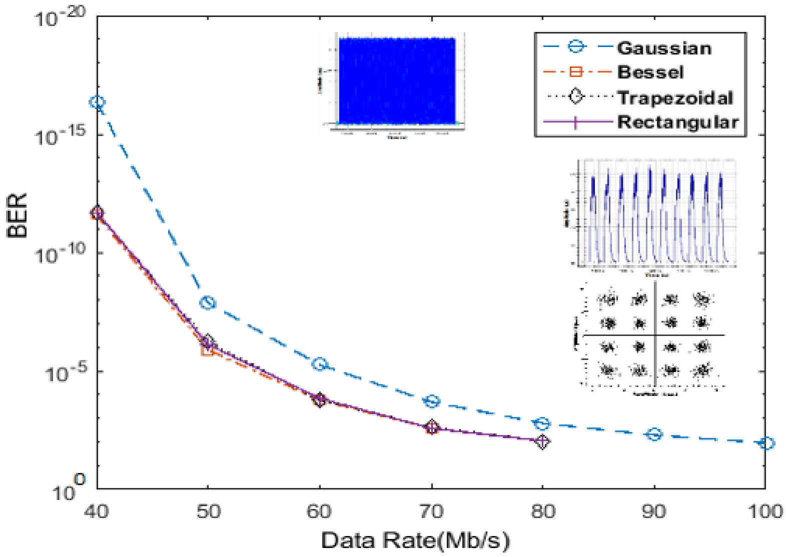

Figure 6.8: BER vs Maximum data rate with different optical filters

To decrease the signal BER, beam divergence of the free space channel is set to 1 mard, shown in Figure 6.9. Lowest BER 10^{-26} have achieved, which can increase the data rate at the receiver end. Beam divergence is a part of FSO link, and it is an angular measurement of LED collimator even in the transmitter aperture.

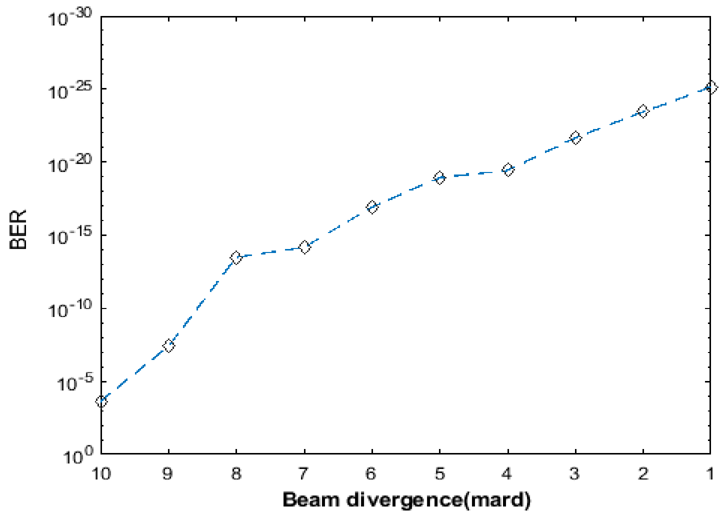

Figure 6.9. Maximum BER versus beam divergence for short range applications.

The total optical power distribution was measured from each VLC access point within 9 m^2 room size, and it was 2.9 mW explained in Figure 6. 10. Illumination contrast, which is well enough to accommodate proper lighting. VLC model has specific channel spacing between different color LEDs. Using full visible spectrum, a total 20 channel system was designed and measured the performance. BER analyzer was used to calculate the BER, the Q factor, and the data rate for 10 channels by OOK, which is summarized in Table 6.4.

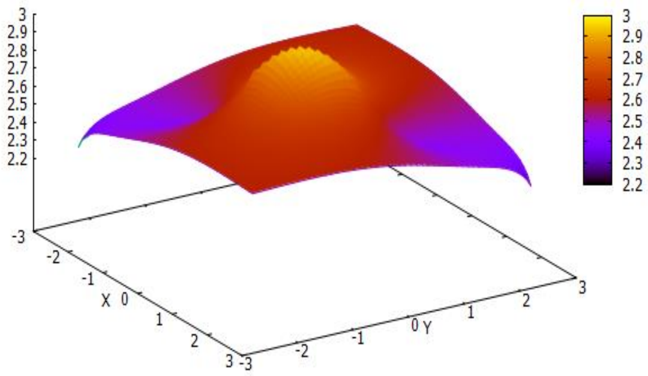

Figure 6.10: Optical power level at VAP in the 9 m^2 room

Table 6.4: Total data rate from 10 channels of CWDM-VLC systems

Peak Wavelength	BER	Data rate (Mb/s)
390	1.50 x10^{-3}	55
430	1.93 x10^{-3}	60
470	1.04 x10^{-8}	70
510	3.77 x10^{-6}	65
550	1.32 x10^{-7}	85
590	2.21 x10^{-8}	90
630	1.73 x10^{-8}	70
670	3.06 x10^{-5}	60
710	7.45 x10^{-4}	55
750	5.51 x10^{-3}	50

Initially, 10 channels are used for communication and other 10 channels keep on just for illumination. The total data rate of 660 Mb/s by OOK and 3.2 Gb/s by 16 QAM was achieved for 10 channels CWDM-VLC system. This data rate is relatively good with OOK modulation, maintaining the BER below the FEC limit 3.8x10^{-3}. Table 6.5 shows the total aggregate data rate by OOK for 20 channels with full utilization of 400 nm visible spectrum by the CWDM-VLC model. The data rate that could be achieved 6.58 Gb/s by 16QAM, maintaining high power LED's configuration in the model.

Table 6.5: Total data rate from 20 channels of CWDM-VLC systems

Peak Wavelength	BER	Data rate (Mb/s)
390	3.29×10^{-3}	55
410	2.35×10^{-5}	65
430	1.91×10^{-5}	80
450	3.85×10^{-6}	90
470	7.88×10^{-4}	100
490	7.81×10^{-4}	110
510	1.09×10^{-4}	95
530	5.75×10^{-6}	90
550	5.74×10^{-5}	95
570	5.79×10^{-6}	100
590	9.87×10^{-8}	105
610	1.26×10^{-6}	80
630	5.29×10^{-4}	10
650	8.31×10^{-6}	90
670	1.59×10^{-6}	100
690	1.05×10^{-4}	90
710	2.32×10^{-5}	80
730	2.21×10^{-6}	75
750	6.28×10^{-4}	75
770	3.28×10^{-4}	60

For uplink, users send 2.5 Gb/s data from indoor receiver point to the central office through unused mmWave frequency and the same ROF link. Figure 6.11 shows the baseband signal transmitted from the customer unit, which is 2.5 GHz, and using OOK modulation 2.5 Gb/s data received at the CO. This signal is modulated with another single drive MZM to carry the uplink data that is returned from CU. After 20 km of optical fiber transmission and photo detection at CO, the resulting RF spectrum shows a signal power of -20 dBm in Figure 6.11 (a), and signal side mode suppression ratio (SMSR) is 26 dBm. Transmitted bit and received bit for uplink transmission is included in Figure 6.11 (b) where BER was recorded 10^{-17}. The 2.5 Gb/s uplink data with NRZ pattern is also added to the input. As a result of multiplication, the mixer's output would be an active mmWave signal 37.5 GHz carrying 2.5 Gb/s OOK data.

This signal is then amplified with 30 dB electrical amplifier to mitigate losses in the mixer and sent to down-converts at CO.

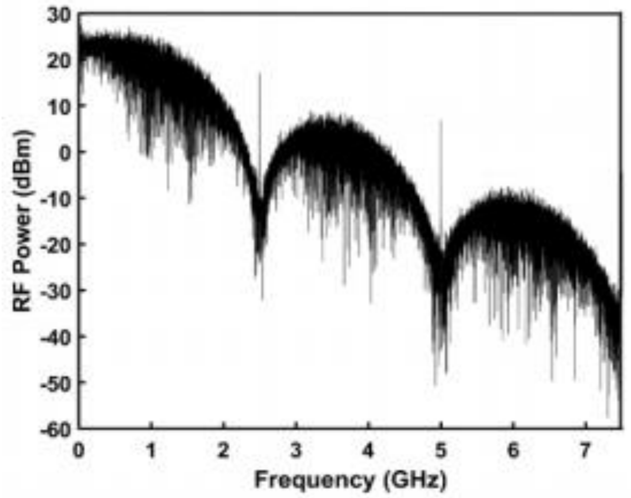

(a)

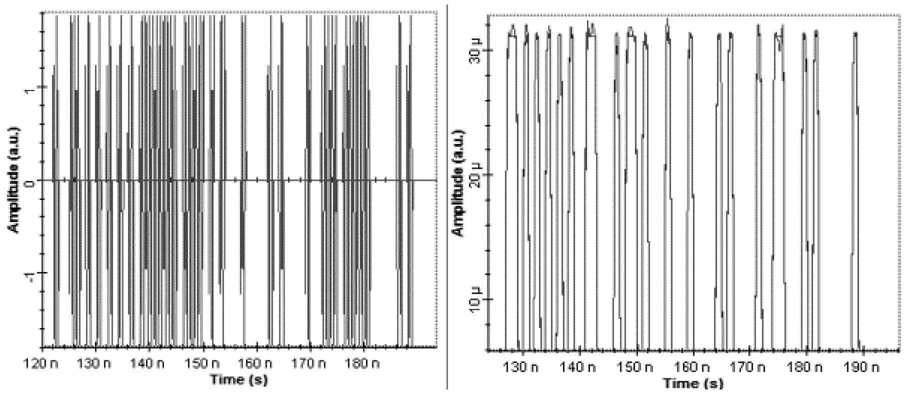

(b)

Figure 6.11: (a) Received 1 GHz RF spectrum for uplink signal at the CO (b) transmitted bit from the indoor user and received bit.

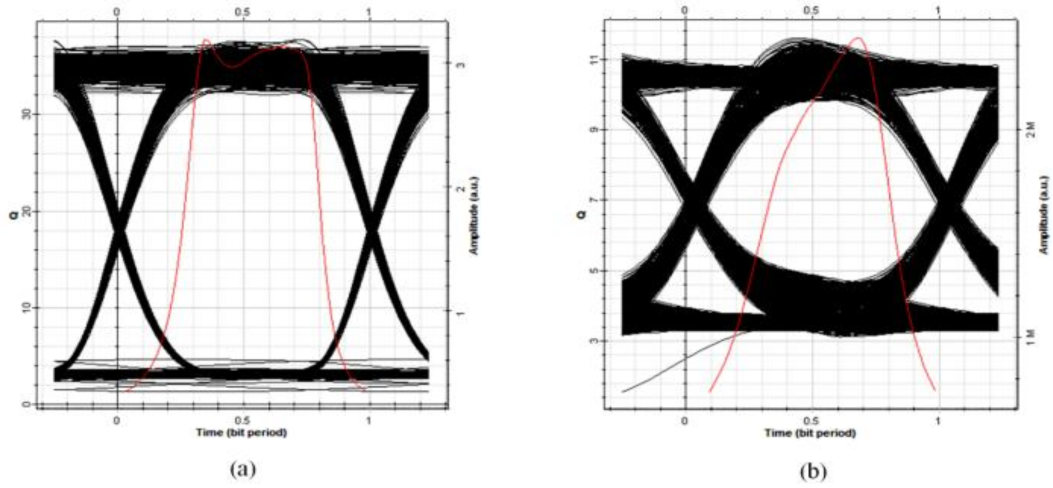

Figure 6.12: The Eye diagram of (a) downlink and (b) uplink data

The eye diagram of this uplink received signal is shown in Figure 6.12 (b), indicating good opening and clear height exhibiting BER of 10^{-18} and shows robust communication link. Uplink signal is showing slight distortion because of two-way channel optical channel noise.

6.11 Summary

mmWave and visible light communication are two promising technologies for future 5G network implementation in outdoor and indoor communications. This chapter focuses on mmWave signal generation and is based on radio over fiber (ROF) backhaul connectivity to VLC link for indoor communication. Heterodyning of optical carriers was used for the generation of 5G mmWave signal with link range, beam divergence, received power, and BER of the signal analyzed at the VLC receiver point. CWDM-VLC model was used to increase the data rate of LED access point at the indoor visible link with acceptable BER. BER performance was measured using different optical filters, and Gaussian optical filter performed better than others (i.e Bessel, Trapezoidal, and Rectangle). To improve the VLC uplink performance, mmWave signal was used for uplink to send data from the customer end through RoF backhaul to the central office. The results show reasonable system performance and similar data rate for downlink and uplink in this hybrid system. Moreover, a novel method of remote uplink mmWave generation was proposed in this work. It is evident that performance of downstream link is more than uplink only when 16 QAM is used. mmWave based wired system uplink exhibits better performance than optical wireless communication with OOK system with 2.5 Gb/s data rate and acceptable BER of 10^{-17} for hybrid VLC network.

CONCLUSION

7.1 Introduction

In the last two decades, enormous growth in wireless communication along with increasing demands of wireless data traffic is shrinking the availability of RF spectrum. This has increased the interest in complementary optical wireless communication technologies. VLC is an emerging technology for indoor wireless communication, which can be integrated with the existing lighting infrastructure. However, there are many constrains in implementing high speed VLC systems. Several techniques have been proposed to increase the VLC data rate. In this thesis, some of these techniques have been investigated and new techniques are proposed for this purpose.

7.2 Key Contributions

This section highlights the key contributions of this research. All major contributions and working procedures are explained in Figure 7.1. RGB-LEDs can increase the aggregate data rate using the wavelength division multiplexing (WDM) method. In this work, initially, the WDM VLC system was designed and experimentally verified with different modulation schemes such as NRZ-OOK and 16 (QAM) using Red, Green, Blue, Amber (RGBA) LEDs. This system could operate at maximum data rates up to 260 Mb/s using OOK and 1.04 Gb/s using 16QAM in the experimental setup. On the other hand, this simulation model could achieve a maximum data rate of 290 Mb/s using OOK and 1.16 Gb/s using 16 QAM. For the first time Coarse Wavelength Division Multiplexed (CWDM)-VLC system has been proposed to increase the number of channels. The maximum data rate achieved was 7.19 Gb/s using 20 channels and 3.2 Gb/s using 10 channels with acceptable BER and 3 m distance between transmitter and receiver.

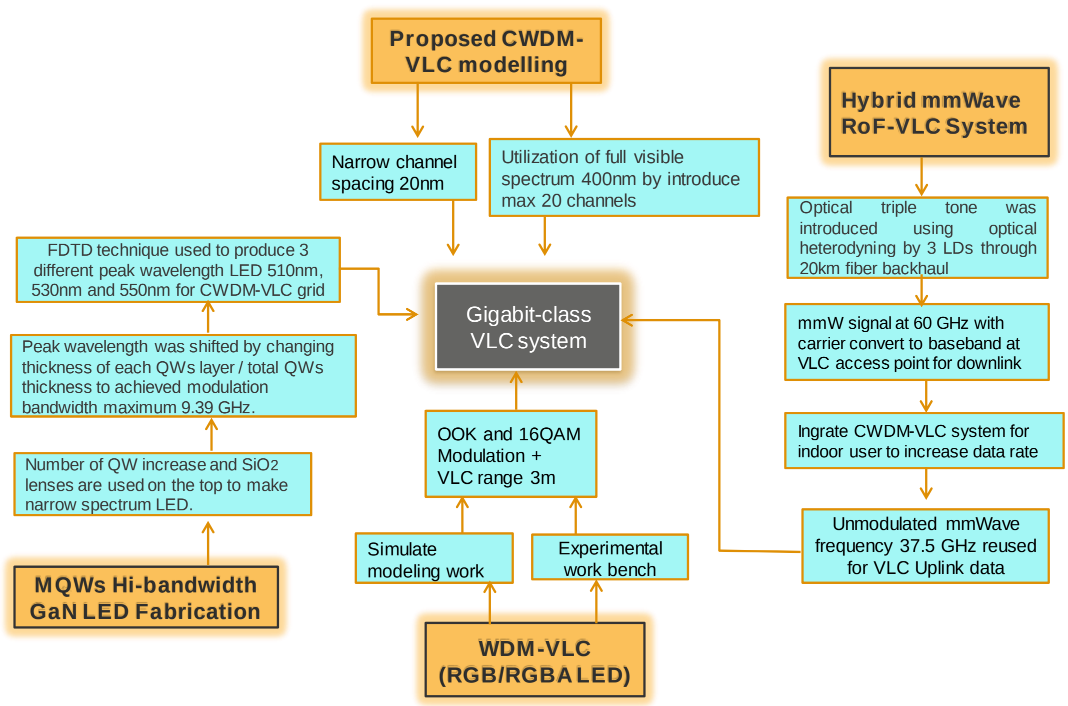

Figure 7.1: Major contributions and working flow chart of the research

Modulation bandwidth limitation is one of the main challenges for high-speed VLC. InGaN/GaN based high bandwidth multiple quantum well (MQW) LED can be a solution to tackle this problem. Here the feasibility of developing the narrowband high bandwidth LEDs based on CWDM-VLC grid has been investigated. To achieve this, InGaN/GaN-based multiple quantum well (MQW) LEDs coupled with the nano-lens structures were designed and investigated through simulation. With this, LEDs with a maximum modulation bandwidth of 6.15 GHz was designed at the peak wavelength of 510nm and using band structural engineering, another two LEDs with 530nm and 550nm has been produced.

In the existing VLC architecture, the indoor uplink communication performance is very much lower than the downlink. To improve the uplink communication speed, a hybrid Radio over VLC (RoF-VLC) communication model was proposed combined with 5G-mmWave and CWDM-VLC for multi-user indoor environment. This hybrid set up achieved data-rates of up to 2.64 Gb/s and 6.58 Gb/s for 10 and 20 channel

CWDM-VLC system using off the shelf LEDs. The uplink data rate achieved was 2.5 Gb/s using mmWave communication.

7.3 Future Research Direction

This section gives a brief overview regarding the different research directions for further advancement of this project

7.3.1 Performance enhancement of Multi-Channel WDM-VLC Schemes

Current VLC system has a limitation in terms of distance between transmitter and receiver. Three or more channels of the RGB links could be segmented into multiple channel VLC system enabling greater number of parallel channels to increase the aggregate data rate and distance. Proper equalization techniques and adaptive higher order modulation schemes can also be used to increase data rate. Optical lenses and filters could be used at the receiver side to identify particular channels. In addition, large FOV concentrator could be used to increase the received signal strength into the small photo detector area and collect large visible light.

7.3.2 Fabrication of GaN/InGaN Based High bandwidth LED

Modulation bandwidth restriction is one of the main challenges for commercial LEDs. Recent micro LEDs offer much higher bandwidth, better contrast, response times and energy efficiency. GaN/InGaN based MQWs LED is a good candidate for high speed VLC application, but a proper procedure is needed for fabrication using adjustable QW thickness, polarization control in the active area and applying nano lens on the top layer of LED to collimate the light extraction for better VLC performance.

7.3.3 Implementation of CWDM-VLC System

Experimental implementation of CWDM-VLC conceptual model can be a big achievement for future high speed VLC research.

7.3.4 Hybrid RoF-VLC System using mmWave uplink Communication

Similarly, to the above proposal, experimental implementation of the RoF-VLC system proposed in this thesis can be a major step towards integrating VLC with 5G networks.

BIBLIOGRAPHY

Ahsan, M. S., Hossain, M. R., Mehbuba, S., Islam, K. M. S., Amin, M. Z., & Sohn, I.-B. (2016). Efficiency improvement of organic light emitting diodes (OLEDs) using micro/nano-structures. *2016 3rd International Conference on Electrical Engineering and Information Communication Technology (ICEEICT)*, 1–6.

Al-kinani, A., Wang, C., Haas, H., & Yang, Y. (2016). *Characterization and Modeling of Visible Light Communication Channels*. 1–5.

Al-Rubaye, S., Al-Dulaimi, A. A., & Al-Raweshidy, H. S. (2009). Next Generation Optical Access Network Using CWDM Technology. *IJCNS*, *2*(7), 636–640.

Alatawi, A. A., Holguin-Lerma, J. A., Kang, C. H., Shen, C., Subedi, R. C., Albadri, A. M., Alyamani, A. Y., Ng, T. K., & Ooi, B. S. (2018). High-power blue superluminescent diode for high CRI lighting and high-speed visible light communication. *Optics Express*, *26*(20), 26355–26364.

Alresheedi, M. T., Hussein, A. T., & Elmirghani, J. M. H. (2017). Uplink design in VLC systems with IR sources and beam steering. *IET Communications*, *11*(3), 311–317.

Armstrong, J., & Schmidt, B. J. C. (2008). Comparison of asymmetrically clipped optical OFDM and DC-biased optical OFDM in AWGN. *IEEE Communications Letters*, *12*(5), 343–345.

Arnon, S. (2010). Underwater optical wireless communication network. *Optical Engineering*, *49*(1), 15001.

Barry, J. R., Kahn, J. M., Krause, W. J., Lee, E. A., & Messerschmitt, D. G. (1993). *Simulation of Multipath Impulse Response for Indoor Wireless Optical Channels*. *1*(3).

Basnayaka, D. A., & Haas, H. (2015). Hybrid RF and VLC systems: Improving user data rate performance of VLC systems. *2015 IEEE 81st Vehicular Technology Conference (VTC Spring)*, 1–5.

BBC. (2015). *Li-fi 100 times faster than wi-fi*. http://www.bbc.com/news/technology-34942685

Beshr, M., Andonovic, I., & Hussien, M. (2012). The impact of sunlight on the performance of visible light communication systems over the year. *Unmanned/Unattended Sensors and Sensor Networks IX*, *8540*, 85400F.

Bian, R., Tavakkolnia, I., & Haas, H. (2019). 15.73 Gb/s visible light communication with off-the-shelf LEDs. *Journal of Lightwave Technology*, *37*(10), 2418–2424.

Bian, R., Tavakkolnia, I., & Haas, H. (2018). 10.2 Gb/s visible light communication with off-the-shelf LEDs. *2018 European Conference on Optical Communication (ECOC)*, 1–3.

Borogovac, T., Rahaim, M. B., Tuganbayeva, M., & Little, T. D. C. (2011). “Lights-off” visible light communications. *2011 IEEE GLOBECOM Workshops (GC Wkshps)*, 797–801.

Boucouvalas, A. C., Chatzimisios, P., Ghassemlooy, Z., Uysal, M., & Yiannopoulos, K. (2015). Standards for indoor optical wireless communications. *IEEE Communications Magazine*, *53*(3), 24–31.

Bui, T.-C., Singh, R., O’Farrell, T., & Biagi, M. (2018). Performance evaluation of generalized optical spatial modulation with dimming support. *2018 IEEE Globecom Workshops (GC Wkshps)*, 1–6.

Burchardt, H., Serafimovski, N., Tsonev, D., & Haas, H. (n.d.). *VLC : Beyond Point-to-Point Communication*. 1–24.

Burton, A., Bentley, E., Le Minh, H., Ghassemlooy, Z., Aslam, N., & Liaw, S.-K. (2014). Experimental demonstration of a 10BASE-T Ethernet visible light communications system using white phosphor light-emitting diodes. *IET Circuits, Devices & Systems*, *8*(4), 322–330.

Burton, A., Le Minh, H., Ghassemlooy, Z., Bentley, E., & Botella, C. (2014). Experimental Demonstration of 50-Mb/s Visible Light Communications Using 4$\,\times\, $4 MIMO. *IEEE Photonics Technology Letters*, *26*(9), 945–948.

Butala, P. M., Elgala, H., & Little, T. D. C. (2014). Performance of optical spatial modulation and spatial multiplexing with imaging receiver. *2014 IEEE Wireless Communications and Networking Conference (WCNC)*, 394–399.

Căilean, A.-M., & Dimian, M. (2017). Current challenges for visible light communications usage in vehicle applications: A survey. *IEEE Communications Surveys & Tutorials*, *19*(4), 2681–2703.

Castro, I., Lamar, D. G., Arias, M., Hernando, M. M., & Sebastian, J. (2017). Multicell three-phase AC–DC driver for HB-LED lighting applications. *IEEE Transactions on Industry Applications*, *53*(4), 3803–3813.

Chau, Y. A., & Yu, S.-H. (2001). Space modulation on wireless fading channels. *IEEE 54th Vehicular Technology Conference. VTC Fall 2001. Proceedings (Cat. No. 01CH37211)*, *3*, 1668–1671.

Chaudhary, S., Tang, X., Ghassemlooy, Z., Lin, B., Wei, X., & Liaw, S.-K. (2019). A 3× 25 Mbps WDM-Ro-VLC System for Amateur Radio Applications. *2019 2nd West Asian Colloquium on Optical Wireless Communications (WACOWC)*, 6–10.

Chen, C.-Y., Wu, P.-Y., Lu, H.-H., Lin, Y.-P., Wen, J.-Y., & Hu, F.-C. (2013). Bidirectional 16-QAM OFDM in-building network over SMF and free-space VLC transport. *Optics Letters*, *38*(13), 2345–2347.

Chen, C., Basnayaka, D., Purwita, A. A., Wu, X., & Haas, H. (2019). Physical Layer

Performance Evaluation of Wireless Infrared-based LiFi Uplink. *ArXiv Preprint ArXiv:1904.13163*.

Chen, H., Fu, H., Lu, Z., Huang, X., & Zhao, Y. (2016). Optical properties of highly polarized InGaN light-emitting diodes modified by plasmonic metallic grating. *Optics Express*, *24*(10), A856–A867.

Chen, S., Zhao, J., & Peng, Y. (2014). The development of TD-SCDMA 3G to TD-LTE-advanced 4G from 1998 to 2013. *IEEE Wireless Communications*, *21*(6), 167–176.

Chi, N., Zhang, M., Zhou, Y., & Zhao, J. (2016). 3.375-Gb/s RGB-LED based WDM visible light communication system employing PAM-8 modulation with phase shifted Manchester coding. *Optics Express*, *24*(19), 21663–21673.

Chi, N., Zhou, Y., Liang, S., Wang, F., Li, J., & Wang, Y. (2018). Enabling technologies for high-speed visible light communication employing CAP modulation. *Journal of Lightwave Technology*, *36*(2), 510–518.

Choi, W. J., Park, Q. H., Kim, D., Jeon, H., Sone, C., & Park, Y. (2006). FDTD simulation for light extraction in a GaN-based LED. *Journal of the Korean Physical Society*, *49*(3), 877–880.

Chun, H., Chiang, C.-J., & O'Brien, D. C. (2012). Visible light communication using OLEDs: Illumination and channel modeling. *2012 International Workshop on Optical Wireless Communications (IWOW)*, 1–3.

Chun, H., Rajbhandari, S., Faulkner, G., Tsonev, D., Xie, E., McKendry, J. J. D., Gu, E., Dawson, M. D., O'Brien, D. C., & Haas, H. (2016). LED based wavelength division multiplexed 10 Gb/s visible light communications. *Journal of Lightwave Technology*, *34*(13), 3047–3052.

Chung, P. T., Yang, C. T., Wang, S. H., Chen, C. W., Chiang, A. S. T., & Liu, C.-Y. (2012). ZrO2/epoxy nanocomposite for LED encapsulation. *Materials Chemistry and Physics*, *136*(2–3), 868–876.

Collins, S., Mulyawan, R., Rajbhandari, S., Chu, H., Faulkner, G. E., O'Brien, D. C., Manousiadis, P. P., Vithanage, D. A., Turnbull, G. A., & Samuel, I. D. W. (2015). A simple wide field of view concentrator for free space visible light communications. *2015 IEEE Summer Topicals Meeting Series (SUM)*, 43–44.

Cossu, G., Ali, W., Corsini, R., & Ciaramella, E. (2015). Gigabit-class optical wireless communication system at indoor distances (1.5–4 m). *Optics Express*, *23*(12), 15700–15705.

Cossu, G., Corsini, R., & Ciaramella, E. (2014). High-speed bi-directional optical wireless system in non-directed line-of-sight configuration. *Journal of Lightwave Technology*, *32*(10), 2035–2040.

Cossu, G., Presi, M., Corsini, R., Choudhury, P., Khalid, A. M., & Ciaramella, E. (2011). A visible light localization aided optical wireless system. *2011 IEEE GLOBECOM Workshops (GC Wkshps)*, 802–807.

Cossu, G., Wajahat, A., Corsini, R., & Ciaramella, E. (2014). 5.6 Gbit/s downlink and 1.5 Gbit/s uplink optical wireless transmission at indoor distances (≥ 1.5 m). *2014 The European Conference on Optical Communication (ECOC)*, 1–3.

Cui, L., Tang, Y., Jia, H., Luo, J., & Gnade, B. (2016). Analysis of the multichannel WDM-VLC communication system. *Journal of Lightwave Technology*, *34*(24), 5627–5634.

D'Andrade, B. W., & Forrest, S. R. (2004). White organic light-emitting devices for solid-state lighting. *Advanced Materials*, *16*(18), 1585–1595.

Damen, O., & Othman, G. R.-B. (2019). On the Performance of Spatial Modulations Over Multimode Optical Fiber Transmission Channels. *IEEE Transactions on Communications*, *67*(5), 3470–3481.

Demory, B., Chung, K., Katcher, A., Sui, J., Deng, H., & Ku, P.-C. (2018). Integrated parabolic nanolenses on MicroLED color pixels. *Nanotechnology*, *29*(16), 165201.

Deng, P., & Kavehrad, M. (2016). Adaptive real-time software defined MIMO visible light communications using spatial multiplexing and spatial diversity. *2016 IEEE International Conference on Wireless for Space and Extreme Environments (WiSEE)*, 111–116.

Deng, R., He, J., Zhou, Z., Shi, J., Hou, M., & Chen, L. (2016). Experimental demonstration of software-configurable asynchronous real-time OFDM signal transmission in a hybrid fiber-VLLC system. *IEEE Photonics Journal*, *9*(1), 1–8.

Dhoble, S. J., & Nair, G. B. (2020). *The Fundamentals and Applications of Light-Emitting Diodes: The Revolution in the Lighting Industry*. Woodhead Publishing.

Di Renzo, M., Haas, H., Ghrayeb, A., Sugiura, S., & Hanzo, L. (2013). Spatial modulation for generalized MIMO: Challenges, opportunities, and implementation. *Proceedings of the IEEE*, *102*(1), 56–103.

Dietz, P., Yerazunis, W., & Leigh, D. (2003). Very low-cost sensing and communication using bidirectional LEDs. *International Conference on Ubiquitous Computing*, 175–191.

Dimitrov, S., Sinanovic, S., & Haas, H. (2012). Clipping noise in OFDM-based optical wireless communication systems. *IEEE Transactions on Communications*, *60*(4), 1072–1081.

Din, I., & Kim, H. (2014). *Energy-Efficient Brightness Control and Data Transmission for Visible Light Communication*. *26*(8), 781–784.

Drost, R. J., & Sadler, B. M. (2010). Constellation design for color-shift keying using billiards algorithms. *2010 IEEE Globecom Workshops*, 980–984.

Du, C., Huang, X., Jiang, C., Pu, X., Zhao, Z., Jing, L., Hu, W., & Wang, Z. L. (2016). Tuning carrier lifetime in InGaN/GaN LEDs via strain compensation for high-speed visible light communication. *Scientific Reports*, *6*(1), 1–10.

Fahs, B., Chowdhury, A. J., & Hella, M. M. (2016). A 12-m 2.5-Gb/s lighting compatible integrated receiver for OOK visible light communication links. *Journal of Lightwave Technology*, *34*(16), 3768–3775.

Fath, T., & Haas, H. (2012). Performance comparison of MIMO techniques for optical wireless communications in indoor environments. *IEEE Transactions on Communications*, *61*(2), 733–742.

Fattal, D., Fiorentino, M., Tan, M., Houng, D., Wang, S. Y., & Beausoleil, R. G. (2008). Design of an efficient light-emitting diode with 10 GHz modulation bandwidth. *Applied Physics Letters*, *93*(24), 243501.

Feng, L., Hu, R. Q., Wang, J., Xu, P., & Qian, Y. (2016). Applying VLC in 5G networks: Architectures and key technologies. *IEEE Network*, *30*(6), 77–83.

Ferreira, R. X. G., Xie, E., McKendry, J. J. D., Rajbhandari, S., Chun, H., Faulkner, G., Watson, S., Kelly, A. E., Gu, E., & Penty, R. V. (2016). High bandwidth GaN-based micro-LEDs for multi-Gb/s visible light communications. *IEEE Photonics Technology Letters*, *28*(19), 2023–2026.

Fuada, S., Putra, A. P., & Adiono, T. (2017). *Analysis of Received Power Characteristics of Commercial Photodiodes in Indoor Los Channel Visible Light Communication*. *August*. https://doi.org/10.14569/IJACSA.2017.080722

Fujimoto, N., & Yamamoto, S. (2014). The fastest visible light transmissions of 662 Mb/s by a blue LED, 600 Mb/s by a red LED, and 520 Mb/s by a green LED based on simple OOK-NRZ modulation of a commercially available RGB-type white LED using pre-emphasis and post-equalizing techniques. *2014 The European Conference on Optical Communication (ECOC)*, 1–3.

Galkin, I., Milashevski, I., & Teteryonok, O. (2011). Comparative study of steady-state performance of LED drivers at different modulation techniques. *2011 7th International Conference-Workshop Compatibility and Power Electronics (CPE)*, 382–387.

Galli, S., Scaglione, A., & Wang, Z. (2011). For the grid and through the grid: The role of power line communications in the smart grid. *Proceedings of the IEEE*, *99*(6), 998–1027.

Gao, Q., Wang, R., Xu, Z., & Hua, Y. (2015). DC-informative joint color-frequency modulation for visible light communications. *Journal of Lightwave Technology*, *33*(11), 2181–2188.

Gedney, S. D. (2011). Introduction to the finite-difference time-domain (FDTD) method for electromagnetics. *Synthesis Lectures on Computational Electromagnetics*, *6*(1), 1–250.

Ghassemlooy, Z., Popoola, W., & Rajbhandari, S. (2019). *Optical wireless communications: system and channel modelling with Matlab®*. CRC press.

Group, I. 1901 W. (2010). *Ieee standard for broadband over power line networks: Medium access control and physical layer specifications*. Tech. Report.

Group, O. research. (2019). *OPTICWISE*. http://opticwise.uop.gr

Grubor, J., Randel, S., Langer, K.-D., & Walewski, J. W. (2008). Bandwidth-efficient indoor optical wireless communications with white light-emitting diodes. *2008 6th International Symposium on Communication Systems, Networks and Digital Signal Processing*, 165–169.

Guan, W., Chen, X., Li, J., Wen, S., Xie, C., & Chen, B. (2018). High Speed Novel Hybrid Modulation Technique of Visible Light Communication Based on Artificial Neural Network Equalizer. *2018 IEEE 3rd Optoelectronics Global Conference (OGC)*, 9–16.

Guidehouseinsights. (2017). *Navigate Research*.

Haas, H., Yin, L., Wang, Y., & Chen, C. (2016). What is LiFi? *Journal of Lightwave Technology*, *34*(6), 1533–1544. http://jlt.osa.org/abstract.cfm?URI=jlt-34-6-1533

Hanzo, L., Haas, H., Imre, S., O'Brien, D., Rupp, M., & Gyongyosi, L. (2012). Wireless myths, realities, and futures: from 3G/4G to optical and quantum wireless. *Proceedings of the IEEE*, *100*(Special Centennial Issue), 1853–1888.

Hao, H., Du, Z., Luo, W., & Ruan, W. (2019). Design of an optical receiving antenna with high gain and large field of view for indoor visible light communication. *Optoelectronics Letters*, *15*(5), 321–329.

He, X., Xie, E., Islim, M. S., Purwita, A. A., McKendry, J. J. D., Gu, E., Haas, H., & Dawson, M. D. (2019). 1 Gbps free-space deep-ultraviolet communications based on III-nitride micro-LEDs emitting at 262 nm. *Photonics Research*, *7*(7), B41–B47.

Ho, K.-T., Chen, R., Liu, G., Shen, C., Holguin-Lerma, J., Al-Saggaf, A. A., Ng, T. K., Alouini, M.-S., He, J.-H., & Ooi, B. S. (2018). 3.2 gigabit-per-second visible light communication link with InGaN/GaN MQW micro-photodetector. *Optics Express*, *26*(3), 3037–3045.

Holland, C., & Alliance, N. E. E. (2014). Are LEDs the next CFL: a diffusion of innovation analysis. *ACEEE Summer Study on Energy Efficiency in Buildings*, 9–184.

Hsu, C.-W., Lu, I.-C., Liu, Y.-L., Yeh, C.-H., & Chow, C.-W. (2016). Demonstration of high speed imaging 3× 3 MIMO-OFDM visible light communication system. *2016 IEEE Photonics Conference (IPC)*, 729–730.

Hu, P., Pathak, P. H., Das, A. K., Yang, Z., & Mohapatra, P. (2016). PLiFi: Hybrid WiFi-VLC networking using power lines. *Proceedings of the 3rd Workshop on Visible Light Communication Systems*, 31–36.

Huang, H., Tang, Y., Cui, L., Zhu, Q., & Luo, J. (2015). Capacity analyze of WDM indoor visible light communication based on LED for standard illumination. *2015 International Conference on Optical Instruments and Technology: Optoelectronic Devices and Optical Signal Processing*, *9619*, 96190U.

Huang, J., Padmanabhan, K., & Collins, O. M. (2011). The sampling theorem with constant amplitude variable width pulses. *IEEE Transactions on Circuits and Systems I: Regular Papers*, *58*(6), 1178–1190.

Huang, X., Shi, J., Li, J., Wang, Y., & Chi, N. (2015). A Gb/s VLC transmission using hardware preequalization circuit. *IEEE Photonics Technology Letters*, *27*(18), 1915–1918.

Huang, X., Wang, Z., Shi, J., Wang, Y., & Chi, N. (2015). 1.6 Gbit/s phosphorescent white LED based VLC transmission using a cascaded pre-equalization circuit and a differential outputs PIN receiver. *Optics Express*, *23*(17), 22034–22042.

Huang, Z., Wang, Z., Huang, M., Li, W., Lin, T., He, P., & Ji, Y. (2017). Hybrid optical wireless network for future SAGO-integrated communication based on FSO/VLC heterogeneous interconnection. *IEEE Photonics Journal*, *9*(2), 1–10.

Hussein, A. T., & Elmirghani, J. M. H. (2015). 10 Gbps mobile visible light communication system employing angle diversity, imaging receivers, and relay nodes. *Journal of Optical Communications and Networking*, *7*(8), 718–735.

Hussein, H. S., & Hagag, M. (2019). Optical MIMO-OFDM with fully generalized index-spatial LED modulation. *IEEE Communications Letters*, *23*(9), 1556–1559.

Ijaz, M., Tsonev, D., McKendry, J. J. D., Xie, E., Rajbhandari, S., Chun, H., Faulkner, G., Gu, E., Dawson, M. D., & O'Brien, D. (2015). Experimental proof-of-concept of optical spatial modulation OFDM using micro LEDs. *2015 IEEE International Conference on Communication Workshop (ICCW)*, 1338–1343.

Islim, M. S., Ferreira, R. X., He, X., Xie, E., Videv, S., Viola, S., Watson, S., Bamiedakis, N., Penty, R. V, White, I. H., Kelly, A. E., Gu, E., Haas, H., & Dawson, M. D. (2017). Towards 10Gb/s orthogonal frequency division multiplexing-based visible light communication using a GaN violet micro-LED. *Photonics Research*, *5*(2), A35–A43. https://doi.org/10.1364/PRJ.5.000A35

Islim, M. S., & Haas, H. (2019). Modulation techniques for li-fi. *ZTE Communications*, *14*(2), 29–40.

ITU. (2020). *CWDM wavelength Grid*. https://en.wikipedia.org/wiki/Fiber-optic_communication#Transmission_windows, 2019.

Janjua, B., Oubei, H. M., Retamal, J. R. D., Ng, T. K., Tsai, C.-T., Wang, H.-Y., Chi, Y.-C., Kuo, H.-C., Lin, G.-R., & He, J.-H. (2015). Going beyond 4 Gbps data rate by employing RGB laser diodes for visible light communication. *Optics Express*, *23*(14), 18746–18753.

Jastrow, C., Munter, K., Piesiewicz, R., Kurner, T., Koch, M., & Kleine-Ostmann, T. (2008). 300 GHz transmission system. *Electronics Letters*, *44*(3), 213–214.

Javaudin, J.-P., Bellec, M., Varoutas, D., & Suraci, V. (2008). OMEGA ICT project: Towards convergent Gigabit home networks. *2008 IEEE 19th International Symposium on Personal, Indoor and Mobile Radio Communications*, 1–5.

Jha, M. K., Kumar, N., & Lakshmi, Y. V. S. (2019). Generalized Spatial Modulation for Multi-User in Visible Light Communication. *2019 28th Wireless and Optical Communications Conference (WOCC)*, 1–5.

Jiang, F., Deng, H., Xiao, W., Tao, S., & Zhu, K. (2015). An ICA based MIMO-OFDM VLC scheme. *Optics Communications*, *347*, 37–43.

Jovicic, A., Li, J., & Richardson, T. (2013). Visible light communication: opportunities, challenges and the path to market. *IEEE Communications Magazine*, *51*(12), 26–32.

Kadam, K., & Dhage, M. R. (2016). Visible light communication for IoT. *2016 2nd International Conference on Applied and Theoretical Computing and Communication Technology (ICATccT)*, 275–278.

Kahn, J. M., & Barry, J. R. (1997). Wireless infrared communications. *Proceedings of the IEEE*, *85*(2), 265–298.

Kashani, M. A., & Kavehrad, M. (2014). On the performance of single-and multi-carrie modulation schemes for indoor visible light communication systems. *2014 IEEE Global Communications Conference*, 2084–2089.

Kashef, M., Ismail, M., Abdallah, M., Qaraqe, K. A., & Serpedin, E. (2016). Energy efficient resource allocation for mixed RF/VLC heterogeneous wireless networks. *IEEE Journal on Selected Areas in Communications*, *34*(4), 883–893.

Kaur, S., Kumar, M., & Verma, A. (2019). An Integrated High-Speed Full Duplex Coherent OFDM-PON and Visible-Light Communication System. *Journal of Optical Communications*, *1*(ahead-of-print).

Khalid, A. M., Cossu, G., Corsini, R., Presi, M., & Ciaramella, E. (2011). Demonstrating a hybrid radio-over-fibre and visible light communication system. *Electronics Letters*, *47*(20), 1136–1137.

Khreishah, A., Shao, S., Gharaibeh, A., Ayyash, M., Elgala, H., & Ansari, N. (2018). A hybrid RF-VLC system for energy efficient wireless access. *IEEE Transactions on Green Communications and Networking*, *2*(4), 932–944.

Kim, D. Y., Han, N., Jeong, H., Kim, J., Hwang, S., Song, K., Choi, S.-Y., & Kim, J. K. (2017). Pressure-dependent growth of wafer-scale few-layer h-BN by metal–organic chemical vapor deposition. *Crystal Growth & Design*, *17*(5), 2569–2575.

Kim, J., Moon, S., Kim, Y., & Hong, S. (2019). Optical Spatial Modulation with Polar Coordinate for Optical Wireless Communication System. *2019 Eleventh International Conference on Ubiquitous and Future Networks (ICUFN)*, 653–655.

Koester, R., Sager, D., Quitsch, W.-A., Pfingsten, O., Poloczek, A., Blumenthal, S., Keller, G., Prost, W., Bacher, G., & Tegude, F.-J. (2015). High-speed GaN/GaInN nanowire array light-emitting diode on silicon (111). *Nano Letters*, *15*(4), 2318–2323.

Komine, T., & Nakagawa, M. (2004). Fundamental analysis for visible-light communication system using LED lights. *IEEE Transactions on Consumer Electronics*, *50*(1), 100–107.

Lan, H.-Y., Tseng, I.-C., Kao, H.-Y., Lin, Y.-H., Lin, G.-R., & Wu, C.-H. (2018). 752-MHz modulation bandwidth of high-speed blue micro light-emitting diodes. *IEEE Journal of Quantum Electronics*, *54*(5), 1–6.

Le Minh, H., O'Brien, D., Faulkner, G., Zeng, L., Lee, K., Jung, D., & Oh, Y. (2008). 80 Mbit/s visible light communications using pre-equalized white LED. *2008 34th European Conference on Optical Communication*, 1–2.

Le Minh, H., O'Brien, D., Faulkner, G., Zeng, L., Lee, K., Jung, D., Oh, Y., & Won, E. T. (2009). 100-Mb/s NRZ visible light communications using a postequalized white LED. *IEEE Photonics Technology Letters*, *21*(15), 1063–1065.

Lee, C., Zhang, C., Cantore, M., Farrell, R. M., Oh, S. H., Margalith, T., Speck, J. S., Nakamura, S., Bowers, J. E., & DenBaars, S. P. (2015). 4 Gbps direct modulation of 450 nm GaN laser for high-speed visible light communication. *Optics Express*, *23*(12), 16232–16237.

Lee, K., Park, H., & Barry, J. R. (2011). Indoor channel characteristics for visible light communications. *IEEE Communications Letters*, *15*(2), 217–219.

Lee, S. H., Jung, S.-Y., & Kwon, J. K. (2015). Modulation and coding for dimmable visible light communication. *IEEE Communications Magazine*, *53*(2), 136–143.

Li, G., Hu, F., Zhao, Y., & Chi, N. (2019). Enhanced performance of a phosphorescent white LED CAP 64QAM VLC system utilizing deep neural network (DNN) post equalization. *2019 IEEE/CIC International Conference on Communications in China (ICCC)*, 173–176.

Li, H., Chen, X., Guo, J., Tang, D., Huang, B., & Chen, H. (2014). 200 Mb/s visible optical wireless transmission based on NRZ-OOK modulation of phosphorescent white LED and a pre-emphasis circuit. *Chinese Optics Letters*, *12*(10), 100604.

Li, Shuai, Pandharipande, A., & Willems, F. M. J. (2016). Two-way visible light communication and illumination with LEDs. *IEEE Transactions on Communications*, *65*(2), 740–750.

Li, Shunfeng, & Waag, A. (2012). GaN based nanorods for solid state lighting. *Journal of Applied Physics*, *111*(7), 5.

Liang, X., Yuan, M., Wang, J., Ding, Z., Jiang, M., & Zhao, C. (2017). Constellation design enhancement for color-shift keying modulation of quadrichromatic LEDs in visible light communications. *Journal of Lightwave Technology*, *35*(17), 3650–3663.

Liao, C.-L., Chang, Y.-F., Ho, C.-L., & Wu, M.-C. (2013). High-speed GaN-based blue light-emitting diodes with gallium-doped ZnO current spreading layer. *IEEE Electron Device Letters*, *34*(5), 611–613.

Liao, C.-L., Ho, C.-L., Chang, Y.-F., Wu, C.-H., & Wu, M.-C. (2014). High-speed light-emitting diodes emitting at 500 nm with 463-MHz modulation bandwidth. *IEEE Electron Device Letters*, *35*(5), 563–565.

Lifi Application. (2020). *LIfi Application*. https://www.lifitn.com/blog/2018/8/30/5-applicationsof-li-fi-technology

Lin, G.-B., Kim, D.-Y., Shan, Q., Cho, J., Schubert, E. F., Shim, H., Sone, C., & Kim, J. K. (2013). Effect of quantum barrier thickness in the multiple-quantum-well active region of GaInN/GaN light-emitting diodes. *IEEE Photonics Journal*, *5*(4), 1600207.

Liu, M., Li, K., Kong, F., Zhao, J., Yue, Q., & Yu, X. (2015). Enhanced light-extraction efficiency of GaN-based light-emitting diodes with hybrid Photonic Crystals. *Optical and Quantum Electronics*, *47*(8), 2593–2604.

Liverman, S., Wang, Q., Chu, Y.-J., Borah, A., Wang, S., Natarajan, A., Wang, A. X., & Nguyen, T. (2018). WiFO: A hybrid communication network based on integrated free-space optical and WiFi femtocells. *Computer Communications*, *132*, 74–83.

Łopuszyński, M., & Majewski, J. A. (2012). Ordering in ternary nitride semiconducting alloys. *Physical Review B*, *85*(3), 35211.

Luo, J., Fan, L., & Li, H. (2017). Indoor positioning systems based on visible light communication: State of the art. *IEEE Communications Surveys & Tutorials*, *19*(4), 2871–2893.

M. Beshr, C. Michie, and I. Andonovic. (2015). *Evaluation of Visible Light Communication System Performance in the Presence of Sunlight Irradiance*. 2–5.

Maaskant, P. P., Shams, H., Akhter, M., Henry, W., Kappers, M. J., Zhu, D., Humphreys, C. J., & Corbett, B. (2013). High-speed substrate-emitting micro-light-emitting diodes for applications requiring high radiance. *Applied Physics Express*, *6*(2), 22102.

Mandal, G. C., Mukherjee, R., Das, B., & Patra, A. S. (2018). A full-duplex WDM hybrid fiber-wired/fiber-wireless/fiber-VLC/fiber-IVLC transmission system based on a self-injection locked quantum dash laser and a RSOA. *Optics Communications*, *427*, 202–208.

Manousiadis, P., Chun, H., Rajbhandari, S., Mulyawan, R., Vithanage, D. A., Faulkner, G., Tsonev, D., McKendry, J. J. D., Ijaz, M., & Xie, E. (2015). Demonstration of 2.3 Gb/s RGB white-light VLC using polymer based colour-converters and GaN micro-LEDs. *2015 IEEE Summer Topicals Meeting Series (SUM)*, 222–223.

Marshoud, H., Muhaidat, S., Sofotasios, P. C., Imran, M., Sharif, B. S., & Karagiannidis, G. K. (2018). *Optical Asymmetric Modulation for VLC Systems*.

Milnes, A. G. (2012). *Heterojunctions and metal semiconductor junctions*. Elsevier.

Miramirkhani, F., & Uysal, M. (2015). Channel modeling and characterization for visible light communications. *IEEE Photonics Journal*, *7*(6), 1–16.

Murugan, K. H. S., & Sumathi, M. (2019). Design and Analysis of 5G Optical Communication System for Various Filtering Operations using Wireless Optical Transmission. *Results in Physics*, *12*, 460–468.

Nakamura, S. (1997). Present performance of InGaN-based blue/green/yellow LEDs. *Light-Emitting Diodes: Research, Manufacturing, and Applications*, *3002*, 26–35.

Nakamura, S., Iwasa, N., & Senoh, M. (1994). *Method of manufacturing p-type compound semiconductor*. Google Patents.

Naribole, S., Chen, S., Heng, E., & Knightly, E. (2017). LiRa: A WLAN architecture for visible light communication with a Wi-Fi uplink. *2017 14th Annual IEEE International Conference on Sensing, Communication, and Networking (SECON)*, 1–9.

Ndjiongue, A. R., Ferreira, H. C., Song, J., Yang, F., & Cheng, L. (2017). Hybrid PLC-VLC channel model and spectral estimation using a nonparametric approach. *Transactions on Emerging Telecommunications Technologies, 28*(12), e3224.

Nebeling, M. (2002). CWDM: lower cost for more capacity in the short-haul. *Fiber Network Engineering: Livermore, CA, USA*.

Noshad, M., & Brandt-Pearce, M. (2013). Application of expurgated PPM to indoor visible light communications—part II: access networks. *Journal of Lightwave Technology*, *32*(5), 883–890.

Noshad, M., & Brandt-Pearce, M. (2016). Hadamard-coded modulation for visible light communications. *IEEE Transactions on Communications*, *64*(3), 1167–1175.

O'Brien, D. (2009). Multi-input multi-output (MIMO) indoor optical wireless communications. *2009 Conference Record of the Forty-Third Asilomar Conference on Signals, Systems and Computers*, 1636–1639.

O'Brien, D., Le Minh, H., Zeng, L., Faulkner, G., Lee, K., Jung, D., Oh, Y., & Won, E. T. (2008). Indoor visible light communications: challenges and prospects. *Free-Space Laser Communications VIII*, *7091*, 709106.

Oh, H. S., Joo, J. H., Lee, J. H., Baek, J. H., Seo, J. W., & Kwak, J. S. (2008). Structural optimization of high-power algainp resonant cavity light-emitting diodes for visible light communications. *Japanese Journal of Applied Physics*, *47*(8R), 6214.

Olanrewaju, H. G., Thompson, J., & Popoola, W. O. (2018). Performance of optical spatial modulation in indoor multipath channel. *IEEE Transactions on Wireless Communications*, *17*(9), 6042–6052.

OPTICWISE. (2010). *OWC research group*. http://opticwise.uop.gr/,

Oubei, H. M., Duran, J. R., Janjua, B., Wang, H.-Y., Tsai, C.-T., Chi, Y.-C., Ng, T.

K., Kuo, H.-C., He, J.-H., & Alouini, M.-S. (2015). 4.8 Gbit/s 16-QAM-OFDM transmission based on compact 450-nm laser for underwater wireless optical communication. *Optics Express*, *23*(18), 23302–23309.

Pan, J.-W., Tsai, P.-J., Chang, K.-D., & Chang, Y.-Y. (2013). Light extraction efficiency analysis of GaN-based light-emitting diodes with nanopatterned sapphire substrates. *Applied Optics*, *52*(7), 1358–1367.

Pang, G., Kwan, T., Liu, H., & Chan, C.-H. (2002). LED wireless. *IEEE Industry Applications Magazine*, *8*(1), 21–28.

Park, B., Noh, H., Yu, Y. M., & Jang, J.-W. (2014). Finite-difference time-domain analysis on light extraction in a GaN light-emitting diode by empirically capable dielectric nano-features. *Journal of Applied Physics*, *116*(18), 184302.

Park, S. B., Jung, D. K., Shin, H. S., Shin, D. J., Hyun, Y. J., Lee, K., & Oh, Y. J. (2007). Information broadcasting system based on visible light signboard. *Proc. Wireless Opt. Commun*, 311–313.

Pavan, T. V. S., & Jeyachitra, R. K. (2018). Integration of Visible Light Communication and Fiber Communication System. *2018 International Conference on Wireless Communications, Signal Processing and Networking (WiSPNET)*, 1–6.

Penning, J., Stober, K., Taylor, V., & Yamada, M. (2016). *Energy savings forecast of solid-state lighting in general illumination applications*. Navigant Consulting Inc., Washington, DC (United States).

Pessa, M., Guina, M., Dumitrescu, M., Hirvonen, I., Saarinen, M., Toikkanen, L., & Xiang, N. (2002). Resonant cavity light emitting diode for a polymer optical fibre system. *Semiconductor Science and Technology*, *17*(6), R1.

Philips Hue, C. L. (2017). *Philips Corporation*.

Popoola, W. O., Poves, E., & Haas, H. (2013). Error performance of generalised space shift keying for indoor visible light communications. *IEEE Transactions on Communications*, *61*(5), 1968–1976.

PureLifi. (2019). *Purelifi*. https://purelifi.com/consumer-ready-gigabit-lifi-to-bedemonstrated-at-mobile-world-congress/

Rahaim, M. B., Vegni, A. M., & Little, T. D. C. (2011). A hybrid radio frequency and broadcast visible light communication system. *2011 IEEE GLOBECOM Workshops (GC Wkshps)*, 792–796.

Rahman, M. T., & Parthiban, R. (2020). Modeling and analysis of multi-channel gigabit class CWDM-VLC system. *Optics Communications*, *460*, 125141.

Rajabi, K., Wang, J., Jin, J., Xing, Y., Wang, L., Han, Y., Sun, C., Hao, Z., Luo, Y., & Qian, K. (2018). Improving modulation bandwidth of c-plane GaN-based light-emitting diodes by an ultra-thin quantum wells design. *Optics Express*, *26*(19), 24985–24991.

Rajagopal, S., Roberts, R. D., & Lim, S.-K. (2012). IEEE 802.15. 7 visible light communication: modulation schemes and dimming support. *IEEE Communications Magazine*, *50*(3), 72–82.

Rajbhandari, S., Chun, H., Faulkner, G., Haas, H., Xie, E., McKendry, J. J. D., Herrnsdorf, J., Gu, E., Dawson, M. D., & O'Brien, D. (2019). Neural network-based joint spatial and temporal equalization for MIMO-VLC system. *IEEE Photonics Technology Letters*, *31*(11), 821–824.

Rajbhandari, S., McKendry, J. J. D., Herrnsdorf, J., Chun, H., Faulkner, G., Haas, H., Watson, I. M., O'Brien, D., & Dawson, M. D. (2017). A review of gallium nitride LEDs for multi-gigabit-per-second visible light data communications. *Semiconductor Science and Technology*, *32*(2), 23001.

Rangan, S., Rappaport, T. S., & Erkip, E. (2014). Millimeter-wave cellular wireless networks: Potentials and challenges. *Proceedings of the IEEE*, *102*(3), 366–385.

Rao, H., Ding, K., Song, J., Xie, L., Wang, W., Wan, X., Zhou, L., & Liao, J. (2012). Self-adaptive phosphor coating technology for white LED packaging. *Frontiers of Optoelectronics*, *5*(2), 147–152.

Rashidi, A., Monavarian, M., Aragon, A., Rishinaramangalam, A., & Feezell, D. (2018). Nonpolar ${m} $-Plane InGaN/GaN Micro-Scale Light-Emitting Diode With 1.5 GHz Modulation Bandwidth. *IEEE Electron Device Letters*, *39*(4), 520–523.

Rea, M. S. (2000). *The IESNA lighting handbook: reference & application*.

Rihawi, Z. S., Mutalip, Z. A., Green, R. J., Higgins, M. D., & Leeson, M. S. (2016). Free-space optical communications in vehicular networks using rectangular guiding models. *IEEE Photonics Technology Letters*, *28*(13), 1430–1433.

Schmid, S., Corbellini, G., Mangold, S., & Gross, T. R. (2013). LED-to-LED visible light communication networks. *Proceedings of the Fourteenth ACM International Symposium on Mobile Ad Hoc Networking and Computing*, 1–10.

Schmid, S., Ziegler, J., Corbellini, G., Gross, T. R., & Mangold, S. (2014). Using consumer LED light bulbs for low-cost visible light communication systems. *Proceedings of the 1st ACM MobiCom Workshop on Visible Light Communication Systems*, 9–14.

Schmid, S., Ziegler, J., Gross, T. R., Hitz, M., Psarra, A., Corbellini, G., & Mangold, S. (2014). (In) visible light communication: Combining illumination and communication. In *ACM SIGGRAPH 2014 Emerging Technologies* (p. 1).

Schubert, E. F., Wang, Y., Cho, A. Y., Tu, L., & Zydzik, G. J. (1992). Resonant cavity light-emitting diode. *Applied Physics Letters*, *60*(8), 921–923.

Shakya, J., Knabe, K., Kim, K. H., Li, J., Lin, J. Y., & Jiang, H. X. (2005). Polarization of III-nitride blue and ultraviolet light-emitting diodes. *Applied Physics Letters*, *86*(9), 91107.

Shao, S., Khreishah, A., Ayyash, M., Rahaim, M. B., Elgala, H., Jungnickel, V., Schulz, D., Little, T. D. C., Hilt, J., & Freund, R. (2015). Design and analysis of a visible-light-communication enhanced WiFi system. *Journal of Optical Communications and Networking*, *7*(10), 960–973.

Sharma, A., Chaudhary, S., Thakur, D., & Dhasratan, V. (2020). A cost-effective high-speed radio over fibre system for millimeter wave applications. *Journal of Optical Communications*, *41*(2), 177–180.

Shen, C., Lee, C., Ng, T. K., Nakamura, S., Speck, J. S., DenBaars, S. P., Alyamani, A. Y., El-Desouki, M. M., & Ooi, B. S. (2016). High-speed 405-nm superluminescent diode (SLD) with 807-MHz modulation bandwidth. *Optics Express*, *24*(18), 20281–20286.

Sheu, J.-S., Li, B.-J., & Lain, J.-K. (2017). LED non-linearity mitigation techniques for optical OFDM-based visible light communications. *IET Optoelectronics*, *11*(6), 259–264.

Shi, M., Wang, C., Li, G., Liu, Y., Wang, K., & Chi, N. (2019). A 5Gb/s 2×2 MIMO Real-time Visible Light Communication System based on silicon substrate LEDs. *2019 Global LIFI Congress (GLC)*, 1–5.

Signifi. (2019). *Signify*.

Singh, Ravi. (2020). *A Review Paper on Li-Fi (Light Fidelity) Technology*. EasyChair.

Singh, Ravinder, O'Farrell, T., & David, J. P. R. (2013). Performance evaluation of IEEE 802.15. 7 CSK physical layer. *2013 IEEE Globecom Workshops (GC Wkshps)*, 1064–1069.

Sivabalan, A., & John, J. (2003). Modeling and simulation of indoor optical wireless channels: a review. *TENCON 2003. Conference on Convergent Technologies for Asia-Pacific Region*, *3*, 1082–1085.

Son, T., Shin, D. S., Mageshwari, K., Kim, K.-K., & Park, J. (2015). Improved light extraction efficiency and leakage characteristics in light-emitting diodes by nanorod arrays formed on hexagonal pits. *Materials Science in Semiconductor Processing*, *29*, 380–385.

Song, J., Liu, S., Zhou, G., Yu, B., Ding, W., Yang, F., Zhang, H., Zhang, X., & Amara, A. (2016). A cost-effective approach for ubiquitous broadband access based on hybrid PLC-VLC system. *2016 IEEE International Symposium on Circuits and Systems (ISCAS)*, 2815–2818.

Song, Y. M., Choi, E. S., Park, G. C., Park, C. Y., Jang, S. J., & Lee, Y. T. (2010). Disordered antireflective nanostructures on GaN-based light-emitting diodes using Ag nanoparticles for improved light extraction efficiency. *Applied Physics Letters*, *97*(9), 93110.

Steigerwald, D. A., Bhat, J. C., Collins, D., Fletcher, R. M., Holcomb, M. O., Ludowise, M. J., Martin, P. S., & Rudaz, S. L. (2002). Illumination with solid state lighting technology. *IEEE Journal of Selected Topics in Quantum Electronics*, *8*(2), 310–320.

Takase, D., & Ohtsuki, T. (2004). Optical wireless MIMO communications

(OMIMO). *IEEE Global Telecommunications Conference, 2004. GLOBECOM'04.*, *2*, 928–932.

Tanaka, Y., Haruyama, S., & Nakagawa, M. (2000). Wireless optical transmissions with white colored LED for wireless home links. *11th IEEE International Symposium on Personal Indoor and Mobile Radio Communications. PIMRC 2000. Proceedings (Cat. No. 00TH8525)*, *2*, 1325–1329.

Tanaka, Y., Komine, T., Haruyama, S., & Nakagawa, M. (2003). Indoor visible light data transmission system utilizing white LED lights. *IEICE Transactions on Communications*, *86*(8), 2440–2454.

Tang, S., Kalavally, V., Ng, K. Y., & Parkkinen, J. (2017). Development of a prototype smart home intelligent lighting control architecture using sensors onboard a mobile computing system. *Energy and Buildings*, *138*, 368–376.

Tsonev, D., Chun, H., Rajbhandari, S., McKendry, J. J. D., Videv, S., Gu, E., Haji, M., Watson, S., Kelly, A. E., & Faulkner, G. (2014). A 3-Gb/s Single-LED OFDM-Based Wireless VLC Link Using a Gallium Nitride $\mu {\rm LED} $. *IEEE Photonics Technology Letters*, *26*(7), 637–640.

Tzikas, A. E., Sahinis, A., Trevlakis, S. E., Tegos, S. A., Diamantoulakis, P. D., & Karagiannidis, G. K. (2019). 3-Color Shift Keying for Indoor Visible Light Communications. *IEEE Communications Letters*, *23*(12), 2271–2274.

VLNComm. (n.d.). VLC Internet. In *2018*. t p. www.vlncomm.com, 26/05/2019

Vučić, J., Kottke, C., Habel, K., & Langer, K.-D. (2011). 803 Mbit/s visible light WDM link based on DMT modulation of a single RGB LED luminary. *2011 Optical Fiber Communication Conference and Exposition and the National Fiber Optic Engineers Conference*, 1–3.

Vucic, J., Kottke, C., Nerreter, S., Habel, K., Buttner, A., Langer, K.-D., & Walewski, J. W. (2009). 125 Mbit/s over 5 m wireless distance by use of OOK-modulated phosphorescent white LEDs. *2009 35th European Conference on Optical Communication*, 1–2.

Wang, C.-X., Haider, F., Gao, X., You, X.-H., Yang, Y., Yuan, D., Aggoune, H. M., Haas, H., Fletcher, S., & Hepsaydir, E. (2014). Cellular architecture and key technologies for 5G wireless communication networks. *IEEE Communications Magazine*, *52*(2), 122–130.

Wang, F., Liu, Y., Shi, M., Chen, H., & Chi, N. (2019). 3.075 Gb/s underwater visible light communication utilizing hardware pre-equalizer with multiple feature points. *Optical Engineering*, *58*(5), 56117.

Wang, T. Q., He, C., & Armstrong, J. (2016). Performance analysis of aperture-based receivers for MIMO IM/DD visible light communications. *Journal of Lightwave Technology*, *35*(9), 1513–1523.

Wang, Yiguang, Chi, N., Wang, Y., Tao, L., & Shi, J. (2014). Network architecture of a high-speed visible light communication local area network. *IEEE Photonics Technology Letters*, *27*(2), 197–200.

Wang, Yiguang, Huang, X., Tao, L., Shi, J., & Chi, N. (2015). 4.5-Gb/s RGB-LED based WDM visible light communication system employing CAP modulation and RLS based adaptive equalization. *Optics Express*, *23*(10), 13626–13633.

Wang, Yiguang, Tao, L., Huang, X., Shi, J., & Chi, N. (2015). 8-Gb/s RGBY LED-based WDM VLC system employing high-order CAP modulation and hybrid post equalizer. *IEEE Photonics Journal*, *7*(6), 1–7.

Wang, Yiguang, Wang, Y., & Chi, N. (2014). Experimental verification of performance improvement for a gigabit wavelength division multiplexing visible light communication system utilizing asymmetrically clipped optical orthogonal frequency division multiplexing. *Photonics Research*, *2*(5), 138–142.

Wang, Yuanquan, Li, R., Wang, Y., & Zhang, Z. (2014). 3.25-Gbps visible light communication system based on single carrier frequency domain equalization utilizing an RGB LED. *OFC 2014*, 1–3.

Wang, Yuanquan, Wang, Y., Chi, N., Yu, J., & Shang, H. (2013). Demonstration of 575-Mb/s downlink and 225-Mb/s uplink bi-directional SCM-WDM visible light communication using RGB LED and phosphor-based LED. *Optics Express*, *21*(1), 1203–1208.

Wikipedia. (2020). *Fiber-optic communication*. https://en.wikipedia.org/wiki/Fiber-optic_communication#Transmission_windows, 2019

Wu, F.-M., Lin, C.-T., Wei, C.-C., Chen, C.-W., Chen, Z.-Y., & Huang, H.-T. (2013). 3.22-Gb/s WDM visible light communication of a single RGB LED employing carrier-less amplitude and phase modulation. *2013 Optical Fiber Communication Conference and Exposition and the National Fiber Optic Engineers Conference (OFC/NFOEC)*, 1–3.

Wu, L., Cheng, J., Zhang, Z., Dang, J., & Liu, H. (2019). Low-complexity spatial modulation for IM/DD optical wireless communications. *IEEE Photonics Technology Letters*, *31*(6), 475–478.

Wu, Xingbang, Hu, F., & Liang, S. (2018). High Speed Geometrically Shaped 8-QAM modulation based Underwater Visible Light Communication System. *Conference on Lasers and Electro-Optics/Pacific Rim*, Th4I-6.

Wu, Xiping, & Haas, H. (2019). Handover skipping for LiFi. *IEEE Access*, *7*, 38369–38378.

Wun, J.-M., Lin, C.-W., Chen, W., Sheu, J.-K., Lin, C.-L., Li, Y.-L., Bowers, J. E., Shi, J.-W., Vinogradov, J., & Kruglov, R. (2012). GaN-based miniaturized cyan light-emitting diodes on a patterned sapphire substrate with improved fiber coupling for very high-speed plastic optical fiber communication. *IEEE Photonics Journal*, *4*(5), 1520–1529.

Yan, Y., Ding, W., Yang, H., & Song, J. (2015). The video transmission platform for The PLC and VLC integrated system. *2015 IEEE International Symposium on Broadband Multimedia Systems and Broadcasting*, 1–5.

Yang, G. F., Zhang, Q., Wang, J., Lu, Y. N., Chen, P., Wu, Z. L., Gao, S. M., & Chen,

G. Q. (2016). InGaN/GaN multiple quantum wells on selectively grown GaN microfacets and the applications for phosphor-free white light-emitting diodes. *Reviews in Physics*, *1*, 101–119.

Yeh, C.-H., Wei, L.-Y., & Chow, C.-W. (2017). Using a single VCSEL source employing OFDM downstream signal and remodulated OOK upstream signal for bi-directional visible light communications. *Scientific Reports*, *7*(1), 1–6.

Yesilkaya, A., Bian, R., Tavakkolnia, I., & Haas, H. (2019). OFDM-based optical spatial modulation. *IEEE Journal of Selected Topics in Signal Processing*, *13*(6), 1433–1444.

Zafar, F., Karunatilaka, D., & Parthiban, R. (2015). Dimming schemes for visible light communication: the state of research. *IEEE Wireless Communications*, *22*(2), 29–35.

Zeng, L., O'Brien, D. C., Le Minh, H., Faulkner, G. E., Lee, K., Jung, D., Oh, Y., & Won, E. T. (2009). High data rate multiple input multiple output (MIMO) optical wireless communications using white LED lighting. *IEEE Journal on Selected Areas in Communications*, *27*(9), 1654–1662.

Zhang, D.-F., Yu, H.-Y., & Zhu, Y.-J. (2020). A multi-user joint constellation design of color-shift keying for VLC downlink broadcast channels. *Optics Communications*, 126001.

Zhang, M., Shi, M., Wang, F., Zhao, J., Zhou, Y., Wang, Z., & Chi, N. (2017). 4.05-Gb/s RGB LED-based VLC system utilizing PS-Manchester coded Nyquist PAM-8 modulation and hybrid time-frequency domain equalization. *Optical Fiber Communication Conference*, W2A-42.

Zhao, P., Han, L., McGoogan, M. R., & Zhao, H. (2012). Analysis of TM mode light extraction efficiency enhancement for deep ultraviolet AlGaN quantum wells light-emitting diodes with III-nitride micro-domes. *Optical Materials Express*, *2*(10), 1397–1406.

Zhao, P., & Zhao, H. (2012). Analysis of light extraction efficiency enhancement for thin-film-flip-chip InGaN quantum wells light-emitting diodes with GaN micro-domes. *Optics Express*, *20*(105), A765–A776.

Zheng, D., Zhang, H., Pan, C., & Song, J. (2019). Scaling QAM Technique for LED-based Visible Light Communication System with Signal-related Noise. *2019 IEEE International Conference on Electrical Engineering and Photonics (EExPolytech)*, 157–160.

Zheng, R., & Taguchi, T. (2003). Optical design of large-area GaN-based LEDs. *Light-Emitting Diodes: Research, Manufacturing, and Applications VII*, *4996*, 105–112.

Zhong, W.-D., Chen, C., & Wu, D. (2015). Seamless integration of indoor VLC with WDM-PON based on hierarchically modulated constant envelope OFDM. *2015 17th International Conference on Transparent Optical Networks (ICTON)*, 1–4.

Zhou, Y., Liang, S., Chen, S., Huang, X., & Chi, N. (2016). 2.08 Gbit/s visible light communication utilizing power exponential pre-equalization. *2016 25th Wireless and Optical Communication Conference (WOCC)*, 1–3.

Zhou, Y., Zhao, J., Zhang, M., Shi, J., & Chi, N. (2016). 2.32 Gbit/s phosphorescent white LED visible light communication aided by two-staged linear software equalizer. *2016 10th International Symposium on Communication Systems, Networks and Digital Signal Processing (CSNDSP)*, 1–4.

Zhou, Y., Zhu, X., Hu, F., Shi, J., Wang, F., Zou, P., Liu, J., Jiang, F., & Chi, N. (2019). Common-anode LED on a Si substrate for beyond 15 Gbit/s underwater visible light communication. *Photonics Research*, *7*(9), 1019–1029.

Zhu, S.-C., Yu, Z.-G., Zhao, L.-X., Wang, J.-X., & Li, J.-M. (2015). Enhancement of the modulation bandwidth for GaN-based light-emitting diode by surface plasmons. *Optics Express*, *23*(11), 13752–13760.

Zhu, S.-C., Zhao, L.-X., Yang, C., Cao, H.-C., Yu, Z.-G., & Liu, L. (2017). GaN-based flip-chip parallel micro LED array for visible light communication. *International Conference on Optoelectronics and Microelectronics Technology and Application*, *10244*, 102441Y.